R-06-15

Rock mechanics modelling of rock mass properties – summary of primary data

Preliminary site description Laxemar subarea – version 1.2

Flavio Lanaro, Berg Bygg Konsult AB

Johan Öhman and Anders Fredriksson
Golder Associates AB

May 2006

Svensk Kärnbränslehantering AB
Swedish Nuclear Fuel
and Waste Management Co
Box 5864
SE-102 40 Stockholm Sweden
Tel 08-459 84 00
+46 8 459 84 00
Fax 08-661 57 19
+46 8 661 57 19

ISSN 1402-3091
SKB Rapport R-06-15

Rock mechanics modelling of rock mass properties – summary of primary data

Preliminary site description Laxemar subarea – version 1.2

Flavio Lanaro, Berg Bygg Konsult AB

Johan Öhman and Anders Fredriksson
Golder Associates AB

May 2006

Abstract

The results presented in this report are the summary of the primary data for the Laxemar Site Descriptive Modelling version 1.2. At this stage, laboratory tests on intact rock and fracture samples from borehole KSH01A, KSH02A, KAV01 (already considered in Simpevarp SDM version 1.2) and borehole KLX02 and KLX04 were available.

Concerning the mechanical properties of the intact rock, the rock type "granite to quartz monzodiorite" or "Ävrö granite" (code 501044) was tested for the first time within the frame of the site descriptive modelling. The average uniaxial compressive strength and Young's modulus of the granite to quartz to monzodiorite are 192 MPa and 72 GPa, respectively. The crack initiation stress is observed to be 0.5 times the uniaxial compressive strength for the same rock type. Non negligible differences are observed between the statistics of the mechanical properties of the granite to quartz monzodiorite in borehole KLX02 and KLX04.

The available data on rock fractures were analysed to determine the mechanical properties of the different fracture sets at the site (based on tilt test results) and to determine systematic differences between the results obtained with different sample preparation techniques (based on direct shear tests).

The tilt tests show that there are not significant differences of the mechanical properties due to the fracture orientation. Thus, all fracture sets seem to have the same strength and deformability. The average peak friction angle for the Coulomb's Criterion of the fracture sets varies between 33.6° and 34.1°, while the average cohesion ranges between 0.46 and 0.52 MPa, respectively. The average of the Coulomb's residual cohesion and friction angle vary in the ranges 28.0°–29.2° and 0.40–0.45 MPa, respectively. The only significant difference could be observed on the average cohesion between fracture set S_A and S_d.

The direct shear tests show that the mechanical properties obtained from the laboratory tests very much depend on the sample preparation technique and size of the steel ring holders. The tests performed with concrete mould or with large steel ring holders (SP results) present larger deformability compared to the tests performed with epoxy resin mould and small steel ring holders (NGI results). The normal and shear stiffness of the fractures obtained by NGI are on average 608 and 21 MPa/mm, while their standard deviation is 394 and 9 MPa/mm, respectively. For comparison, the normal and shear stiffness of the fractures obtained by SP are on average 135–237 and 29–41 MPa/mm, respectively. Due to the limitation in amount of data from direct shear tests, a determination of the properties for each fracture set was not possible.

Sammanfattning

De resultat som presenteras i denna rapport är en sammanfattning av primärdata för Laxemar platsbeskrivande modell version 1.2. Laboratorietester av intakt berg och sprickor innefattar prover från borrhål KSH01A, KSH02A, KAV01 (tidigare redovisade i Simpevarp modell version 1.2) samt borrhål KLX02 och KLX04.

Beträffande de mekaniska egenskaperna hos intakt berg testades bergarten ”granit till kvarts-monzodiorit” eller ”Ävrö granit” (kod 501044) för första gången inom ramen för Laxemars platsbeskrivande modellering. Medelvärden för den enaxiella tryckhållfastheten och elasticitets modulen hos granit till kvartsmonzodiorit är 192 MPa respektive 72 GPa. Den s k ”crack initiation stress” har observerats vara 0,5 gånger den enaxiella tryckhåll-fastheten för samma bergart. Man kan se icke-negligerbara skillnader i de bergmekaniska testresultaten för granit till kvartsmonzodiorit mellan borrhål KLX02 och borrhål KLX04.

Tillgänglig data från tester på bergsprickor har analyserats för att undersöka de mekaniska egenskaperna hos olika sprickgrupper i Laxemar/Simpevarp (baserat på tilttestresultat) och för att undersöka systematiska skillnader mellan uppnådda resultat vid olika typer av provpreparering (baserat på direkta skjuvtester).

Tilttesterna visar att det inte finns någon signifikant skillnad hos de mekaniska egenska-perna med avseende på sprickorientering. Sålunda verkar alla sprickgrupper oavsett ori-entering ha samma hållfasthet- och deformationsegenskaper. För Coulombs brottskriterium har sprickgruppernas maximala pikfriktionsvinkel medelvärden mellan 33,6° och 34,1° medan maximala pik-kohesionen har medelvärden mellan 0,46 och 0,52 MPa. Medelvärdet för de residuala friktionsvinkeln och kohesionen varierar mellan 28,0° och 29,2° respektive 0,40 och 0,45 MPa. Den enda signifikanta skillnaden mellan sprickgrupper observerades för kohesionen mellan sprickgrupp S_A och S_d.

Direkta skjuvtester visar att de mekaniska egenskaperna till stor del beror på prov-prepareringen och storleken på stålringshållarna. Tester gjorda med gjuten betong eller epoxy och stora stålringshållare (SP-resultat) ger lägre hållfasthet och större deformer-barhet, jämfört med tester gjorda med gjuten epoxy och små stålringshållare (NGI-resultat). Medelvärdet för sprickornas normal- och skjuvstyvhet är 608 respektive 21 MPa/mm och standardavvikelsen är 394 respektive 9 MPa/mm, för NGI-resultaten. Som jämförelse, normal- och skjuv-styvheten beräknat från SP-resultat har medelvärde varierande mellan 135 och 237, och respektive 29 och 41 MPa/mm. Den tillgängliga datamängden från direkta skjuvtester tillät inte en bestämning av egenskaperna för varje sprickgrupp.

Contents

1 Introduction

Table 1-1 lists the number of intact rock samples tested in laboratory for the determination of the strength and deformability. Uniaxial, triaxial and indirect tensile tests were performed on these samples. The results of the tests are summarised in Chapter 2. Table 1-2, on the other hand, lists the number of natural fracture samples tested in laboratory. The tests performed were direct shear and tilt tests. The results of the tests on fractures are summarised in Chapter 3. A map of the site with the location of the five boreholes where the samples were collected is shown in Figure 1-1.

Boreholes KSH01A, KSH02A and KAV01 are located in the Simpevarp site investigation area, and boreholes KLX02 and KLX04 are located at the Laxemar site.

Table 1-1. Summary of tests performed on intact rock samples from borehole KSH01A, KSH02A, KLX02 and KLX04.

Borehole	Rock type	Indirect tensile tests	Uniaxial tests	Triaxial tests
KSH01A	Quartz monzonite to monzodiorite[1)]	20 [2[2)]]	10	8 [3[2)], 1[3)]]
	Fine-grained dioritoid[1)]	20 [6[2)]]	10 [4[2)]]	4 [1[2)]]
KSH02A	Fine-grained dioritoid[1)]	12 [2[2)]]	5 [1[2)]]	5 [2[2)]]
KLX02	Granite to quartz monzodiorite	30	15	–
KLX04	Granite to quartz monzodiorite	30	15	14

[1)] Data already reported in Simpevarp SDM version 1.2 /SKB 2005/.
[2)] Samples with sealed fractures.
[3)] Samples with intrusion of fine to medium grained granite.

Table 1-2. Summary of the results of tests performed on fracture samples from borehole KSH01A, KSH02A, KAV01, KLX02, and KLX04.

Borehole	Tilt tests	Rock type	Direct shear tests	Code in Chapter 3
KSH01A	41	Fine-grained dioritoid Quartz monzonite to monzodiorite	6[1)] 1[1)]	Shear I and III
KSH02A	48	Fine-grained dioritoid	6[1)]	Shear I
KAV01	26	Granite to quartz monzodiorite	5[1)]	Shear I
KLX02	29[2)]	Granite to quartz monzodiorite	9[1)]	Shear II
KLX04	18	Granite to quartz monzodiorite	10[1)]	Shear II

[1)] 3 levels of normal stress: 0.5, 5 and 20 MPa.
[2)] 5 samples from depth > 1,000 m.

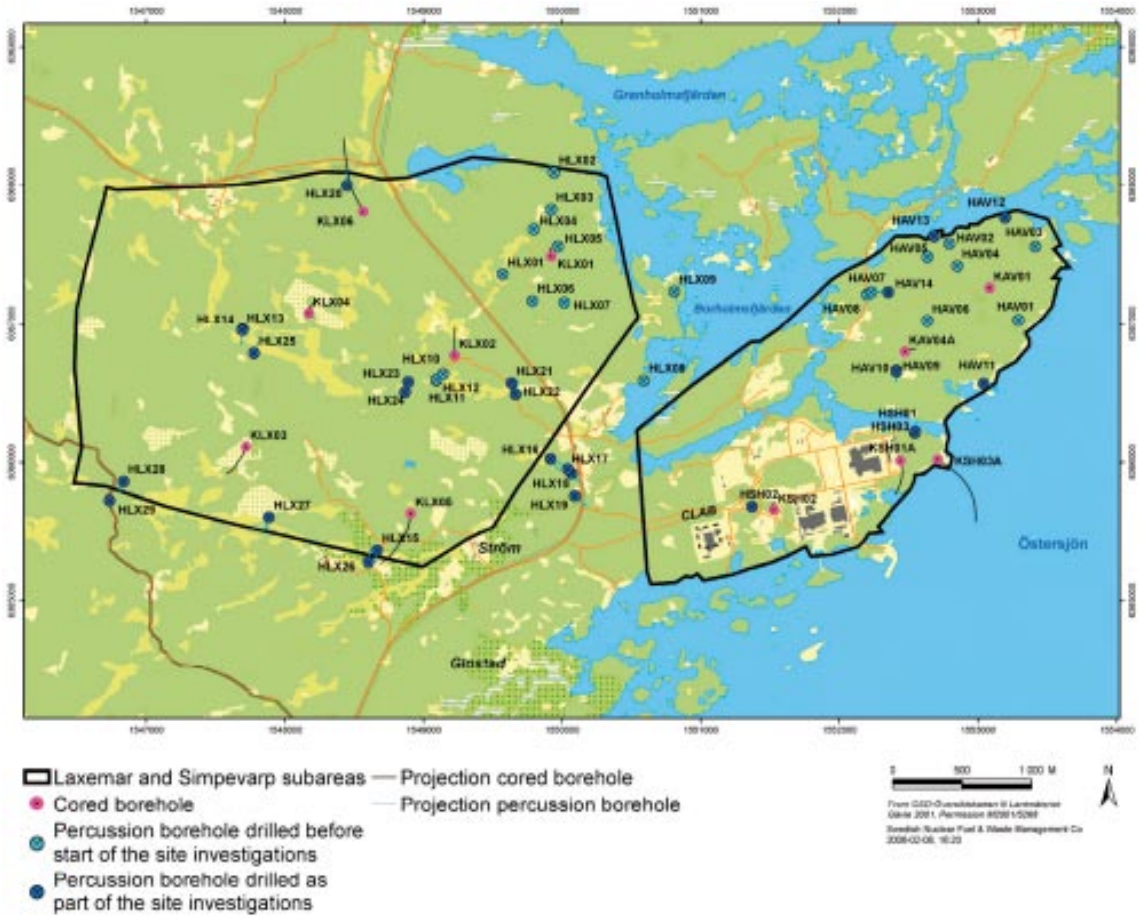

Figure 1-1. *Overview map of core-drilled and percussion-drilled boreholes in the Laxemar and Simpevarp subareas.*

2 Intact rock

In this Chapter, the results of the uniaxial compressive strength tests on intact rock samples are summarised independently and together with the results of the triaxial compressive strength tests. The rock types represented are: fine-grained dioritoid, quartz monzonite to monzodiorite and granite to quartz monzodiorite. The SICADA codes for these rock types are listed in Table 2-1.

The laboratory results are reported in:

- /Jacobsson 2004abcd/ for the uniaxial compression tests.
- /Jacobsson 2004fgh/ for the triaxial compression tests.
- /Jacobsson 2004ijkl/ for the indirect tensile tests.

In the following sections, only the updated set of mechanical properties for Laxemar Site Descriptive Model 1.2 compared to Simpevarp SDM 1.2 are provided. For all the properties that are unchanged, please refer to /SKB 2005/.

Table 2-1. List of the rock types and their SICADA code for the samples tested in laboratory for Laxemar SDM 1.2.

Rock type	SICADA code
Fine-grained dioritoid (metavolcanite, volcanite)	501030
Quartz monzonite to monzodiorite (equigranular to weakly porphyritic)	501036
Granite to quartz monzodiorite (generally porphyritic) – Ävrö granite	501044

2.1 Uniaxial compressive strength

Laboratory tests of uniaxial compressive strength UCSi were carried out at the SP Laboratory (Swedish National Testing and Research Institute) on samples from borehole KSH01A, KSH02A, KLX02 and KLX04 /Jacobsson 2004abcd/. The results are given per rock type by means of the mean value and the standard deviation in Table 2-2. The statistical description is completed with the minimum, maximum and most frequently occurring values.

In Figure 2-1, earlier results reported in Simpevarp SDM 1.1 /SKB 2004/ are also shown for comparison with the new frequency distributions of the uniaxial compressive strength in Figure 2-2.

It is worth it to notice that, compared to Simpevarp SDM 1.2, only samples of granite to monzodiorite were added to the sample set. For comparison, some statistics of the uniaxial compressive strength for borehole KLX02 and KLX04 are listed in Table 2-3. Considering the fact that many samples are available for each borehole (15), the difference between the

calculated statistics are significant (about 11% and 15% for the mean value and the standard deviation, respectively). In this table, the statistics for the samples containing sealed fractures are also reported.

Results were reported by the HUT Laboratory (Helsinki University of Technology) on 5 samples of quartz monzonite to monzodiorite taken from borehole KSH01A /Eloranta 2004a/. These results were not included in Table 2-2.

Table 2-2. Summary of the results of uniaxial compressive tests performed on intact rock samples from borehole KSH01A, KSH02A, KLX02 and KLX04.

Rock type	Number of samples	Minimum UCSi [MPa]	Mean UCSi [MPa]	Frequent UCSi [MPa]	Maximum UCSi [MPa]	UCSi Standard deviation [MPa]
Fine-grained dioritoid[1)]	10	109	205	230	264	51
Quartz monzonite to monzodiorite[1)]	10	118	161	164	193	24
Granite to quartz monzodiorite	29[2)]	151	192	195	239	21
Fine-grained dioritoid with sealed fractures	5	92	126	131	158	31

[1)] Data already reported in Simpevarp SDM version 1.2 /SKB 2005/.
[2)] Results are not reported in SICADA for 1 test on a sample from KLX02.

Table 2-3. Comparison of the uniaxial compressive strength obtained for samples from borehole KLX02 and KLX04.

Rock type	Number of samples	Minimum UCSi [MPa]	Mean UCSi [MPa]	Frequent UCSi [MPa]	Maximum UCSi [MPa]	UCSi's Standard deviation [MPa]
Granite to monzodiorite in KLX02	14[1)]	175.1	202.3	205.8	238.5	16.9
Granite to monzodiorite in KLX04	15	150.5	181.4	186.0	209.8	19.4

[1)] Results are not reported in SICADA for 1 test on a sample from KLX02.

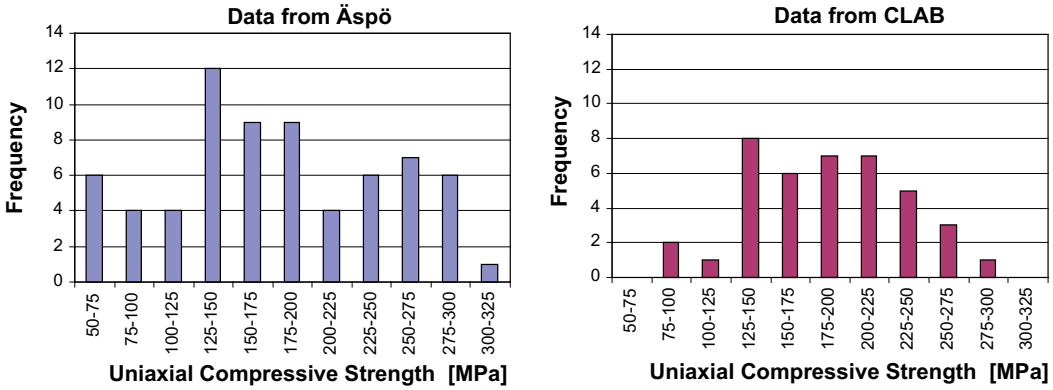

Figure 2-1. *Frequency distributions of the uniaxial compressive strength of all samples available from Äspö and CLAB. The rock types were not specified in the sources.*

2.1.1 Crack initiation stress

The crack initiation stress σ_{ci} was calculated according to /Martin and Chandler 1994/. For samples of granite to monzodiorite, the values in Table 2-4 and the frequency distribution in Figure 2-3 apply. As for the uniaxial compressive strength, differences in the statistics are observed between samples from KLX02 and KLX04 (Table 2-5).

Table 2-4. The crack initiation stress σ_{ci} from uniaxial compressive tests performed on intact rock samples from KLX02 and KLX04.

Rock type	Number of samples	Minimum σ_{ci} [MPa]	Mean σ_{ci} [MPa]	Frequent σ_{ci} [MPa]	Maximum σ_{ci} [MPa]	σ_{ci}'s Standard deviation [MPa]
Granite to monzodiorite	29[1)]	32.0	95.8	100.0	126.5	20.7

[1)] Results are not reported in SICADA for 1 test on a sample from KLX02.

Table 2-5. Comparison of the crack initiation stress from uniaxial compressive tests obtained for samples from borehole KLX02 and KLX04.

Rock type	Number of samples	Minimum σ_{ci} [MPa]	Mean σ_{ci} [MPa]	Frequent σ_{ci} [MPa]	Maximum σ_{ci} [MPa]	σ_{ci}'s Standard deviation [MPa]
Granite to monzo-diorite in KLX02	14[1)]	82.0	105.3	105.0	126.5	12.0
Granite to monzo-diorite in KLX04	15	32.0	86.2	98.0	112.5	23.5

[1)] Results are not reported in SICADA for 1 test on a sample from KLX02.

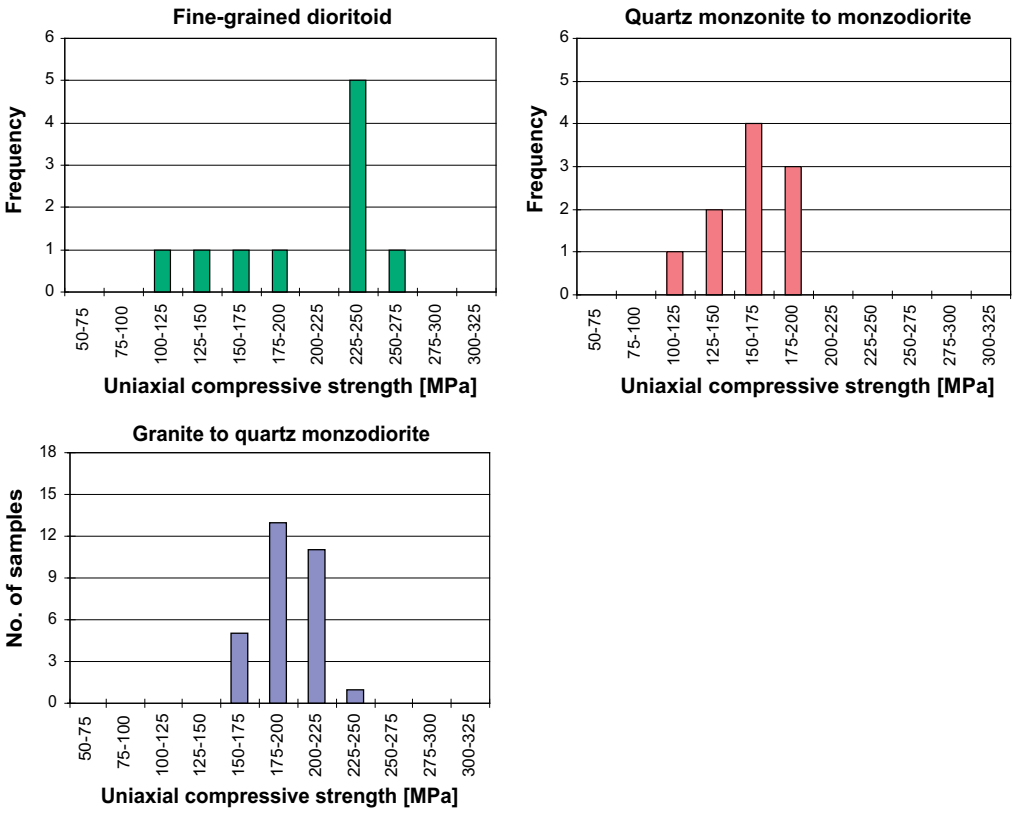

Figure 2-2. *Frequency distributions of the uniaxial compressive strength of the samples of fine-grained dioritoid, quartz monzonite to monzodiorite and granite to quartz monzodiorite from borehole KSH01A, KSH02A, KLX02 and KLX04.*

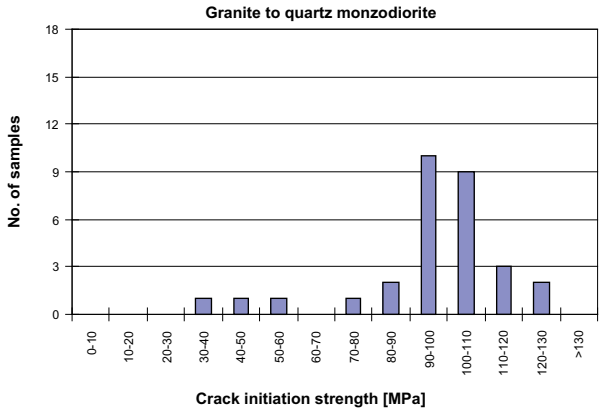

Figure 2-3. *Crack initiation stress for the granite to monzodiorite from the uniaxial compression testing of samples from borehole KLX02 and KLX04.*

2.1.2 Correlation between uniaxial compressive strength and crack initiation stress

The values of the crack initiation stress in Section 2.1.1 can be plotted against the uniaxial compressive strength in Section 2.1 so that Figure 2-4 can be obtained. This figure shows that there is a clear correlation between the two values that can be approximated with a linear trend. The slope of such trend is 0.5.

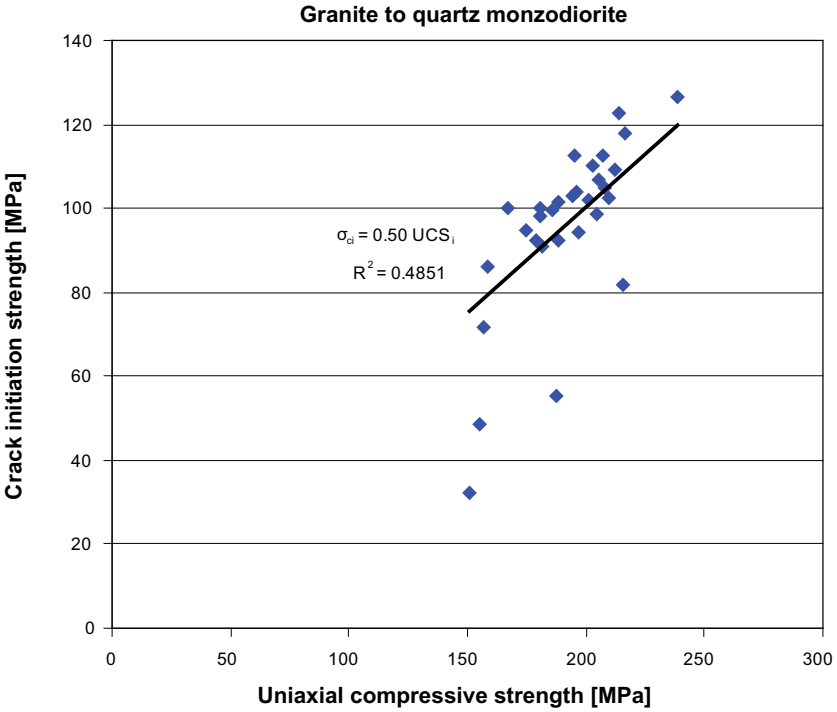

Figure 2-4. *Uniaxial compressive strength versus crack initiation stress for the granite to monzodiorite of the samples from borehole KLX02 and KLX04.*

2.2 Triaxial compressive strength

Laboratory tests of triaxial compressive strength were carried out at the SP Laboratory (Swedish National Testing and Research Institute) on samples from borehole KSH01A, KSH02A and KLX04 /Jacobsson 2004fgh/. In the following analyses, the results of triaxial testing are considered together with the results of uniaxial testing.

For each main rock type (fine-grained dioritoid, quartz monzonite to monzodiorite, granite to quartz monzodiorite), the triaxial results were analysed together with the correspondent results of the uniaxial compressive tests. The laboratory results on intact rock samples were interpolated with the Hoek and Brown's Failure Criterion /Hoek et al. 2002/.

$$\sigma'_1 = \sigma'_3 + UCS_T \left(m_i \frac{\sigma'_3}{UCS_T} + 1 \right)^{0.5} \quad (1)$$

where σ'_1 and σ'_3 are the maximum and minimum principal stress and m_i is a strength parameter typical for each rock type. $UCSi_T$ is obtained by matching the uniaxial and triaxial test results and thus slightly differs from UCSi in Section 2.1.

When analysing the laboratory results, the intact rock parameters in Table 2-6 are obtained. Although obtained in a slightly different way, the results of the UCSi are in rather good agreement with the values in obtained on uniaxial tests only (Table 2-2).

The Coulomb's linear approximations of the Hoek and Brown's Criterion were also calculated for a certain stress interval (0 to 15 MPa, Table 2-7). These linear approximations are shown in Figure 2-5, Figure 2-6 and Figure 2-7 for the fine-grained dioritoid, quartz monzonite to monzodiorite, granite to quartz monzodiorite, respectively. The Hoek and Brown's Criterion also provides an estimation of the tensile strength of the intact rock that can be compared with the laboratory results in Section 2.3. The statistics for the samples containing sealed fractures are also reported.

Five samples of quartz monzonite to monzodiorite were also tested in triaxial compression conditions at the HUT Laboratory /Eloranta 2004b/ under confining pressures of 2, 7 and 10 MPa. These results are in good agreement with the SP Laboratory results but were not included in Table 2-6 and Table 2-7.

Table 2-6. Parameters for the Hoek & Brown's Criterion based on the results of uniaxial and triaxial tests performed on intact rock samples from borehole KSH01A, KSH02A, KLX02 and KLX04.

Rock type	Number of samples	Minimum USC_T [MPa]	mi	Mean $UCSi_T$ [MPa]	mi	Maximum $UCSi_T$ [MPa]	mi
Fine-grained dioritoid[1)]	16	118.5	15.0	207.3	13.7	296.1	13.2
Quartz monzonite to monzodiorite[1)]	15	123.4	32.6	160.1	30.6	196.8	29.3
Granite to quartz monzodiorite	44	152	16.6	192	18.9	235	19.7
Sealed fractures in intact rock[1)]	11	55.0	19.8	122.2	16.5	189.4	15.5

[1)] Data reported in Simpevarp SDM version 1.2 /SKB 2005/.

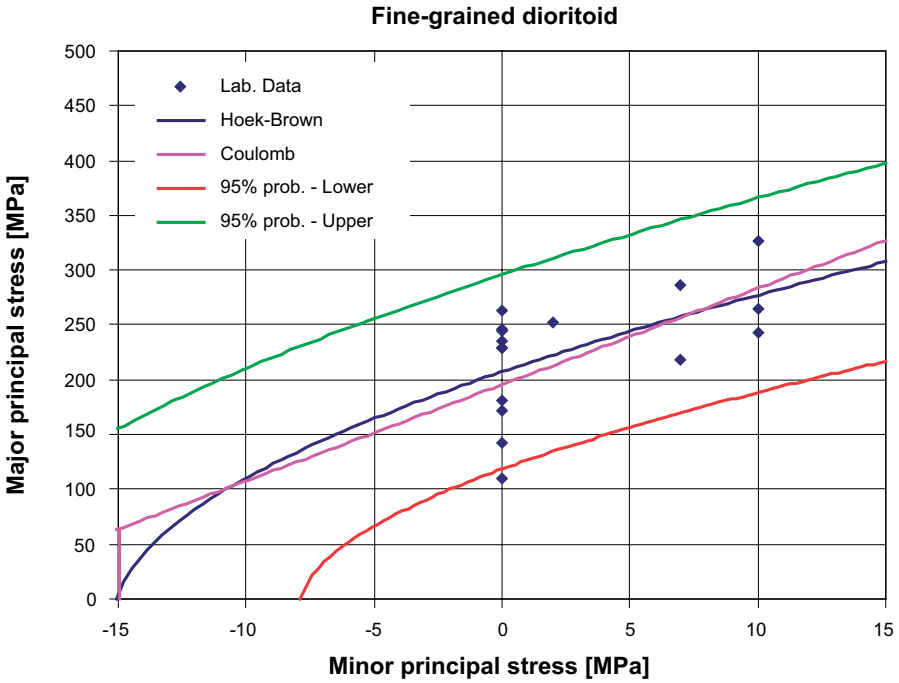

Figure 2-5. *Hoek & Brown's and Coulomb's failure envelopes from uniaxial and triaxial tests for the fine-grained dioritoid. Data reported in Simpevarp SDM version 1.2 /SKB 2005/.*

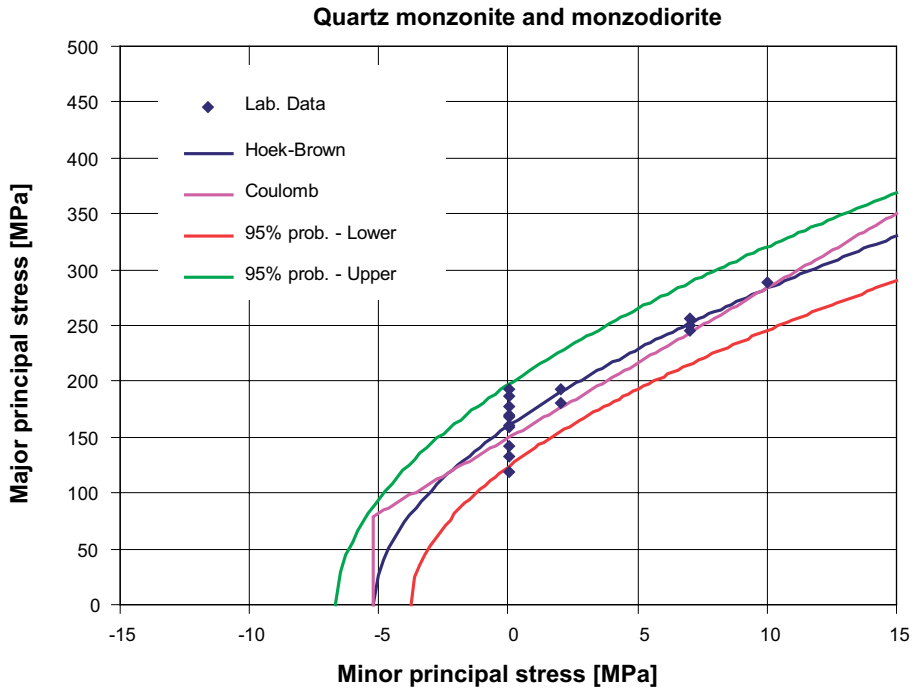

Figure 2-6. *Hoek & Brown's and Coulomb's failure envelopes from uniaxial and triaxial tests for the samples of quartz monzonite to monzodiorite. Data reported in Simpevarp SDM version 1.2 /SKB 2005/.*

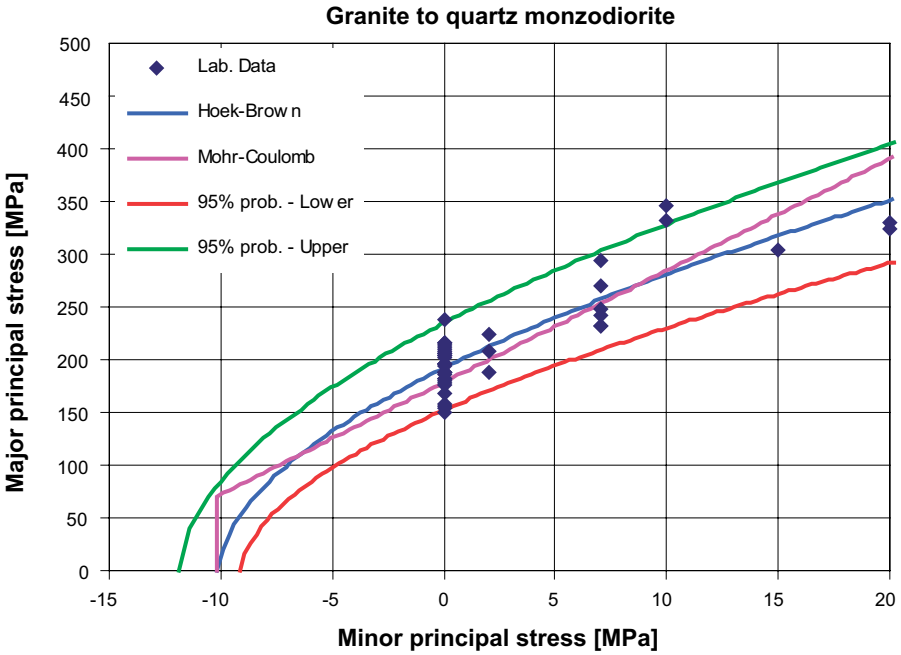

Figure 2-7. *Hoek & Brown's and Coulomb's failure envelopes from uniaxial and triaxial tests for the samples of granite to quartz monzodiorite.*

Table 2-7. Parameters for the Coulomb's criterion based on the results of uniaxial and triaxial tests performed on intact rock samples from borehole KSH01A, KSH02A, KLX02 and KLX04.

Rock type	Number of samples	Minimum c' [MPa]	φ' [°]	Mean c' [MPa]	φ' [°]	Maximum c' [MPa]	φ' [°]
Fine-grained dioritoid[1)]	16	19.3	51.2	33.0	52.7	47.1	53.5
Quartz monzonite to monzodiorite[1)]	16	16.5	58.7	20.3	59.5	24.3	60.1
Granite to quartz monzodiorite	44	23.2	53.5	27.4	55.9	32.3	57.1
Sealed fractures in intact rock[1)]	11	10.1	49.3	19.2	52.3	29.0	53.7

[1)] Data already reported in Simpevarp SDM version 1.2 /SKB 2005/.
The values of the cohesion and friction angle are obtained for a confinement stress between 0 and 15 MPa.

2.3 Indirect tensile strength

Indirect tensile tests were conducted on 143 core samples at the SP Laboratory (KSH01A, KSH02A, KLX02 and KLX04 /Jacobsson 2004ijkl/).

Table 2-8 contains the statistics of the test results for the fine-grained dioritoid, quartz monzonite to monzodiorite, granite to quartz monzodiorite, respectively. Figure 2-8 also shows the frequency distributions of the indirect tensile strength for each of the main rock types. Statistics for the samples containing sealed fractures are also reported.

Table 2-8. Summary of the results of indirect tensile tests performed on intact rock sampled from borehole KSH01A, KSH02A, KLX02 and KLX04.

Rock type	Number of samples	Minimum TS [MPa]	Mean TS [MPa]	Frequent TS MPa]	Maximum TS [MPa]	TS Standard deviation [MPa]
Fine-grained dioritoid[1)]	24	14	19	19	24	2
Quartz monzonite to monzodiorite[1)]	18	12	18	17	24	4
Granite to quartz monzodiorite	60	9.3	13.0	13.1	16.4	1.5
Sealed fractures in intact rock[1)]	10	9	14	15	22	5

[1)] Data already reported in Simpevarp SDM version 1.2 /SKB 2005/.

Five samples of quartz monzonite to monzodiorite were tested in indirect tensile conditions at the HUT Laboratory /Eloranta 2004c/. The results are in agreement with the SP Laboratory results but were not included in Table 2-8.

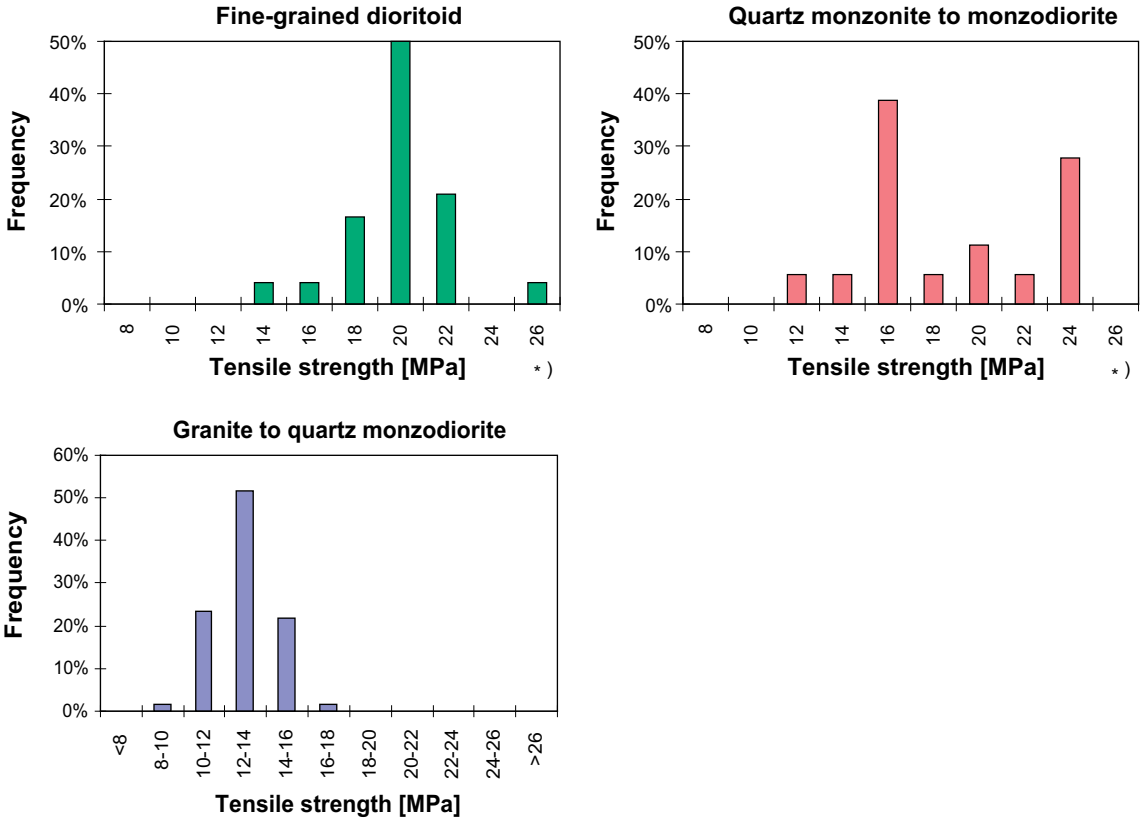

Figure 2-8. *Frequency distribution of the indirect tensile strength of the samples of fine-grained dioritoid and quartz monzonite to monzodiorite. *) Data already reported in Simpevarp SDM version 1.2 /SKB 2005/.*

2.4 Young's modulus

Based on the stress-strain curves obtained for the tests reported in Section 2.1 and 2.2, the deformation modulus of the intact rock could be obtained.

2.4.1 Uniaxial loading

Table 2-9 presents a summary of the deformability results from the uniaxial compression tests. The same data are also shown as histogram for the granite to quartz monzodiorite in Figure 2-9. For the other rock types, no new laboratory results are available compared to Simpevarp SDM version 1.2 /SKB 2005/, therefore their statistics are unchanged in Table 2-9. The Young's modulus of the samples of intact fine-grained dioritoid is lower than for the samples containing sealed fractures.

Table 2-9. Summary of the results of Young's modulus from uniaxial compressive tests performed on intact rock samples from borehole KSH01A, KSH02A, KLX02 and KLX04.

Rock type	Number of samples	Minimum E [GPa]	Mean E [GPa]	Frequent E [GPa]	Maximum E [GPa]	E Standard deviation [GPa]
Fine-grained dioritoid[1)]	10	78	85	83	101	7
Quartz monzonite to monzodiorite[1)]	10	69	78	81	86	7
Granite to quartz monzodiorite	29[2)]	61	72	71	89	5
Fine-grained dioritoid with sealed fractures[1)]	4	83	91	89	104	10

[1)] Data already reported in Simpevarp SDM version 1.2 /SKB 2005/.
[2)] Results are not reported in SICADA for 1 test on a sample from KLX02.

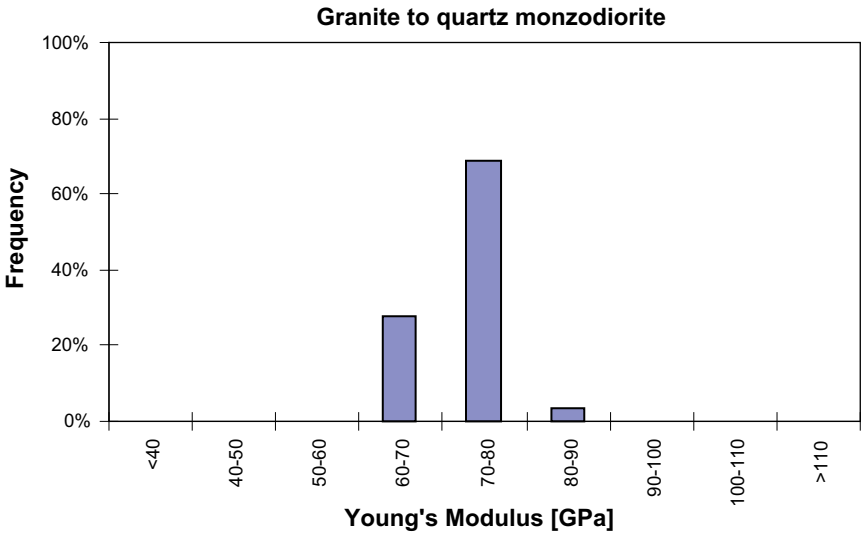

Figure 2-9. *Frequency distributions of the Young's modulus of the granite to quartz monzodiorite from tests for Laxemar 1.2.*

2.4.2 Triaxial loading

Even for the triaxial tests, all the new samples were taken from granite to quartz monzodiorite, therefore these are the new values in Table 2-10 compared to Simpevarp SDM version 1.2 /SKB 2005/. Also in this case, the Young's modulus of the samples of intact rock is lower than for the samples containing sealed fractures.

Table 2-10. Summary of the results of Young's modulus from triaxial compressive tests performed on intact rock samples from borehole KSH01A, KSH02A, KLX02 and KLX04.

Rock type	Number of samples	Minimum E [GPa]	Mean E [GPa]	Frequent E [GPa]	Maximum E [GPa]	E Standard deviation [GPa]
Fine-grained dioritoid[1)]	6	69	78	79	87	6
Quartz monzonite to monzodiorite[1)]	6	69	77	77	91	8
Granite to quartz monzodiorite	14	61	70	70	76	4
Sealed fractures[1)]	5	75	81	83	88	5

[1)] Data already reported in Simpevarp SDM version 1.2 /SKB 2005/.

2.5 Poisson's ratio

Also the Poisson's ratio can independently be obtained from the stress-strain curves of the tests reported in Section 2.1, uniaxial conditions, and Section 2.2, triaxial conditions, respectively.

2.5.1 Uniaxial loading

From the uniaxial compression tests, the statistics of the Poisson's ration in Table 2-11 can be obtained.

Table 2-11. Summary of the results of Poisson's ratio from uniaxial compressive tests performed on intact rock sampled from borehole KSH01A, KSH02A, KLX02 and KLX04.

Rock type	Number of samples	Minimum ν [–]	Mean ν [–]	Frequent ν [–]	Maximum ν [–]	ν Standard deviation [–]
Fine-grained dioritoid[1)]	10	0.21	0.26	0.26	0.31	0.03
Quartz monzonite to monzodiorite[1)]	10	0.19	0.27	0.28	0.33	0.05
Granite to quartz monzodiorite	29[2)]	0.15	0.20	0.20	0.26	0.03
Fine-grained dioritoid with sealed fractures[1)]	4	0.18	0.24	0.24	0.31	0.07

[1)] Data already reported in Simpevarp SDM version 1.2 /SKB 2005/.
[2)] Results are not reported in SICADA for 1 test on a sample from KLX02.

2.5.2 Triaxial loading

From the triaxial compression tests, the statistics of the Poisson's ration in Table 2-11 can be obtained.

Table 2-12. Summary of the results of Poisson's ratio from triaxial compressive tests performed on intact rock sampled from borehole KSH01A, KSH02A, KLX02 and KLX04.

Rock type	Number of samples	Minimum ν [–]	Mean ν [–]	Frequent ν [–]	Maximum ν [–]	ν Standard deviation [–]
Fine-grained dioritoid[1)]	6	0.19	0.21	0.20	0.23	0.02
Quartz monzonite to monzodiorite[1)]	6	0.18	0.22	0.23	0.24	0.02
Granite to quartz monzodiorite	14	0.15	0.18	0.19	0.20	0.02
Sealed fractures	5	0.15	0.18	0.18	0.24	0.03

[1)] Data already reported in Simpevarp SDM version 1.2 /SKB 2005/.

3 Natural fractures

The strength and deformability of the natural rock fractures was determined in two ways:

1) By means of tilt tests where shearing is induced by the self-weight of the upper block when the fracture is progressively tilted.
2) By means of direct shear tests where shearing is induced by actuators that apply a load perpendicular and parallel to the fracture plane. Three different types of shear test techniques were used; these are referred to as: Shear I, Shear II and Shear III. The main differences between the different shear test techniques are explained in Section 3.2.

The samples of natural fractures were taken from boreholes KAV01, KSH01A, KSH02A, KLX02, and KLX04.

Direct shear tests were performed on altogether 54 fracture samples. These were taken from boreholes KLX02 and KLX04 /Jacobsson 2004mn/, KAV01 /Jacobsson 2005o/, KSH01A /Jacobsson 2005p, Chryssanthakis 2004e/ and KSH02A /Jacobsson 2005q/. Seven fracture samples from borehole KSH01A were tested by NGI and 47 samples were tested by the Swedish National Testing and Research Institute (SP). To examine how the clamping of rock specimens in the laboratory test apparatus may influence test results, three different techniques were used. The main difference between the different methods is the casting material and size of the steel holders, which are used to hold the specimen in the shear test apparatus.

Tilt tests were performed on 157 fracture samples, which were taken from all boreholes (KAV01, KSH01A, KSH02A, KLX02, and KLX04) /Chryssanthakis 2003, Chryssanthakis 2004abcd/. All tilt tests were performed by the Norwegian Geological Institute Laboratory (NGI).

The laboratory results are evaluated in terms of several different rock mechanics parameters that describe fracture strength and deformability. These parameters are summarized and analysed in the following sections. It is of interest to analyze if the different fracture sets from the Simpevarp and Laxemar site have different fracture strength and deformability. Therefore the fractures were grouped into fracture sets at the site by matching the reported fracture depth with the BOREMAP records in SICADA according to the Descrete Fracture Network DFN model of the site /Hermansson et al. 2005/ (Table 3-1; see also Appendix 2). However, as explained above, the parameters have been derived by different laboratory test methods, which may entail systematic differences in results. The objective is therefore to distinguish whether significant differences can be found in laboratory data, in terms of: 1) fracture sets, and 2) laboratory test methods.

Table 3-1. Orientation of the fracture sets at Simpevarp and Laxemar /Hermansson et al. 2005/.

Simpevarp			Laxemar		
Fracture set	Strike (right rule) [°]	Dip [°]	Fracture set	Strike (right rule) [°]	Dip [°]
S_A	158	86	S_A	150	84
S_B	280	90	S_B	105	89
S_C	033	89	S_C	022	86
S_d	183	28	S_d	264	08
S_f	063	66	S_e	247	75

3.1 Tilt tests

Tilt tests were carried out on 157 samples from boreholes KAV01, KSH01A, KSH02, KLX02, and KLX04 /Chryssanthakis 2003, Chryssanthakis 2004abcd/. The tilt tests are designed to suit the fracture parameter determination according to /Barton and Bandis 1990/. The shear strength of the fracture is a function of the normal stress σ_n as:

$$\tau = \sigma_n \tan\left[\Phi_b^{BB} + JRC \log\left(\frac{JCS}{\sigma_n}\right)\right] \quad (2)$$

JRC is Joint Roughness Coefficient that quantifies roughness, JCS is Joint Wall Compression Strength of the rock surfaces, and Φ_b^{BB} is basic friction angle on dry saw-cat surfaces, respectively. The residual friction angle Φ_r^{BB} is used instead of Φ_b^{BB} if the strength of wet surfaces is concerned. The index notation BB is used to emphasize that the parameters relate to the Barton-Bandis model, to differentiate them from parameters in the Mohr-Coulomb model, discussed later. /Barton and Bandis 1990/ also suggest truncating the strength envelope for low normal stresses as follows: τ/σ should always be smaller than 70° and, in this case, the envelope should go through the origin ($\sigma_n = \tau = 0$ MPa), in other words the cohesion is zero.

The JRC and JCS parameters are dependent on fracture length. The measured JRC_0 and JCS_0 values relate to fracture specimens of different lengths. Therefore, the measured values are normalised and extrapolated to values that relate to a standard fracture length of 100 mm, and hereafter referred to as JRC_{100} and JCS_{100} values.

The parameters of the Barton and Bandis's criterion are summarised in Table 3-2 for each borehole and for all the fractures. The parameters of the Barton and Bandis's for each fracture set are summarised in Table 3-3. The fracture sets are given according to the DFN model of the site /Hermansson et al. 2005/, see Table 3-1.

It can be observed that, independently on the fracture orientation and borehole, the fracture parameters do not noticeably change. Some of the tested samples were mapped as "sealed fractures" in BOREMAP maybe because of some mismatch in the reported sample depth.

Table 3-2. Summary of the results of tilt tests performed on rock fractures sampled from Borehole KAV01, KSH01A, KSH02, KLX02, and KLX04.

Borehole	Number of samples	Φ_b^{BB} [°]	Φ_r^{BB} [°]	JRC_{100} [–]	JCS_{100} [MPa]
KAV01	26	30.8 (0.8)	26.3 (2.2)	6.2 (1.6)	53.0 (13.2)
KSH01A	41	31.2 (2.6)	26.2 (3.1)	6.1 (1.2)	76.2 (25.7)
KSH02A	48	31.5 (1.6)	26.2 (3.4)	5.8 (1.4)	70.3 (25.7)
KLX02	24	31.4 (1.2)	25.4 (2.9)	6.7 (1.5)	63.3 (21.4)
KLX04	18	31.4 (1.0)	25.2 (2.3)	5.8 (1.8)	60.0 (19.4)
All fractures	157	31.3 (1.7)	26.0 (2.9)	6.1 (1.5)	66.7 (24)

The average values are indicated. The standard deviation is set between brackets.

Table 3-3. Summary of the results of tilt tests performed on rock fractures grouped in different fracture sets and from borehole KAV01, KSH01A, KSH02, KLX02, and KLX04.

Fracture set	Number of samples	Φ_b^{BB} [°]	Φ_r^{BB} [°]	JRC_{100} [–]	JCS_{100} [MPa]
S_A	26	31.4 (1.1)	25.9 (2.5)	6.51 (1.4)	65.8 (26)
S_B	23	30.9 (2.7)	26.1 (3.6)	6.11 (1.5)	71.1 (24)
S_C	21	31.1 (2.2)	26.1 (2.7)	6.41 (1.4)	69.8 (21)
S_d	66	31.3 (1.4)	25.8 (2.9)	5.85 (1.4)	64.1 (25)
S_ef	21	31.4 (1.5)	26.6 (3.1)	6.15 (1.8)	68.3 (21)
All fractures	157	31.3 (1.7)	26.0 (2.9)	6.11 (1.5)	66.7 (24)

The average values are indicated. The standard deviation is set between brackets.

For a certain level of stresses, or for a certain stress interval, the relation in Equation (2) can be linearly approximated to determine the peak friction angle and cohesion of the Mohr-Coulomb Strength Criterion in Equation (3) (Figure 3-1):

$$\tau = c_p^{MC} + \sigma_n \tan\left(\Phi_p^{MC}\right) \tag{3}$$

where c_p^{MC} and Φ_p^{MC} are peak cohesion and peak friction angle. Similarly, the residual cohesion and peak friction angle, c_r^{MC} respectively Φ_r^{MC}, can be fitted by the Mohr-Coulomb residual envelope. The determined Mohr-Coulomb model parameters are reported in Table 3-9 and Table 3-10.

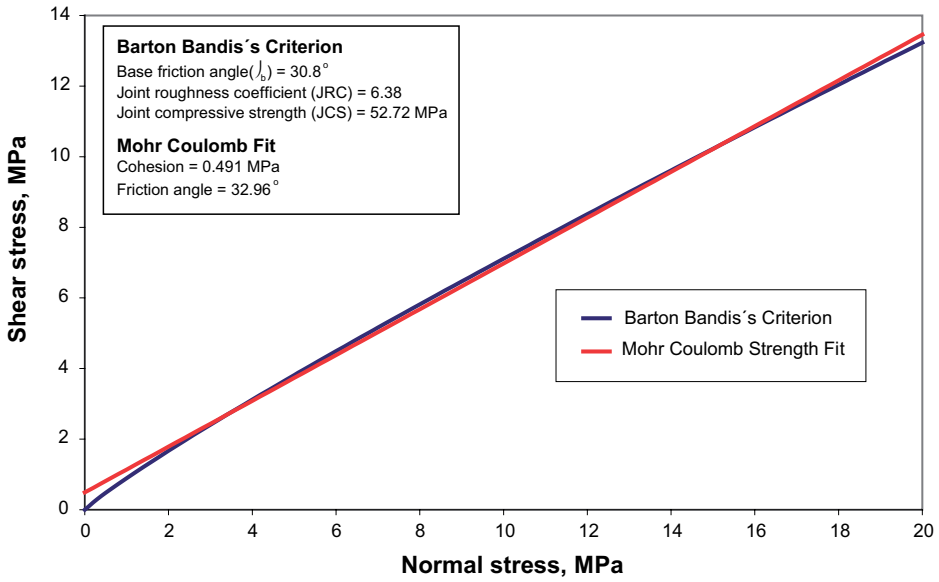

Figure 3-1. *Fitting of the Barton Bandis' Strength Criterion with the Mohr-Coulomb's Strength Criterion.*

3.2 Direct shear tests

Shear test results on natural fractures are obtained by means of three different methods. In the first method used (here referred to as Shear I), the rock specimens were clamped with cement casting with high stiffness. However, it was found that the rock specimens could slip in the cement casting. Therefore, the shear test laboratory set up was modified and epoxy was used instead as casting material. Epoxy casting reduced the problem of slipping of the rock specimen, but it has a too low stiffness. Therefore the holder device was reduced in diameter in order to avoid the effects of a soft casting material. Nineteen fracture samples from borehole KLX02 and KLX04 were tested with this modified approach at the SP laboratory (here referred to as Shear II). Furthermore, seven samples from borehole KSH01A were tested using epoxy casting at NGI (this data set is referred to as Shear III). The shear test results are summarized and analyzed in the following sections. The displacement curves were measured during normal loading and shearing so that the normal and shear stiffness of the samples could be determined. The shear tests were conducted under three levels of normal stress: 0.5, 5 and 20 MPa.

3.2.1 SP shear test results, cement casting (Shear I)

A set of 28 fracture samples from boreholes KSH01A, KSH02A and KAV01 were tested at the SP Laboratory /Jacobsson 2005opq/ based on ISRM standard from 1974. The specimens in this data set include granite to quartz monzodiorite (Ävrö granite), fine-grained dioritoid and quartz monzonite to monzodiorite.

In this shear test, the rock specimens were clamped into the specimen holder apparatus using a cement casting, which has a high stiffness. Owing to the high stiffness of the casting material, large holders could be used (a diameter of 152 mm). The benefit of large holders is that fracture core samples of different sizes and shapes can more easily be clamped into the device (i.e. with less cutting and trimming of the core specimens). Consequently, most of the available fracture area of a core sample could be shear tested by this approach (the fracture areas tested range from 20 to 52 cm^2). The drawback of this casting material is that that the rock specimens could slip during the shear test. Therefore other casting materials were used for comparison.

3.2.2 SP shear test results, epoxy casting (Shear II)

Another set of 19 fracture samples from boreholes KLX02 and KLX04 were also tested at the SP laboratory /Jacobsson 2004mn/ based on ISRM standard from 1974. The specimens in this data set exclusively comprise granite to quartz monzodiorite (Ävrö granite).

In these tests, the specimens were cast with a two-component epoxy that was mixed with quartz sand to increase its stiffness. The stiffness of the epoxy mix is lower than that of cement and therefore the holder size had to be reduced to a diameter of 80 mm. Consequently, the core specimens had to be cut to fit this smaller holder, such that the tested fracture areas range from 20 to 28 cm^2.

3.2.3 NGI shear test results, epoxy casting (Shear III)

A set of 7 fracture samples from borehole KSH01A was tested at the NGI Laboratory /Chryssanthakis 2004e/ based on ISRM standard for shear 7testing from 1981. The specimens in this data set include fine-grained dioritoid and quartz monzonite to monzodiorite.

In these tests, the specimens were cast with epoxy that was mixed with dolomite powder. For these tests, holders with a diameter of 80 mm had to be used and therefore the core specimens had to be cut, leading to reduced tested fracture areas.

3.3 Evaluation of the mechanical parameters

Deformability and stiffness of the fractures are parameters of concern and are presented in the following sections, where results from different testing techniques are compared.

3.4 Deformability

3.4.1 Stiffness

Before shearing, the samples were normally loaded to determine their normal stiffness. The secant normal stiffness of the fracture samples for normal stress between 0.5 and 10 MPa was evaluated for the second loading cycle. The shear stiffness was then determined as the secant stiffness between 0 MPa and half of the peak shear stress. Table 3-4 shows the summary statistics for the normal and shear stiffness obtained from the tests. Most of the fracture normal stiffness data from Shear I and II range between 50 and 250 MPa/mm, but also includes exceptionally high values (primarily Shear III data). Thus, if considered all together, the normal stiffness data appears to be skewed (e.g. somewhat lognormally distributed; see Appendix 2). In such cases the arithmetic mean is not very representative of a data set (Figure 3-2). Therefore, the arithmetic mean, median and geometric mean are reported in Table 3-5. For fracture stiffness, the geometric mean is closer to the median and, therefore, the geometric mean was considered a better representation of the data.

Table 3-4. Minimum, mean and maximum normal and shear stiffness for all the fracture samples tested with different methods.

Method	Minimum		Mean		Maximum		Standard deviation	
	k_n [MPa/mm]	k_s [MPa/mm]	k_n [MPa/mm]	k_s [MPa/mm]	k_n [MPa/mm]	k_s [MPa/mm]	k_n [MPa/mm]	k_s [MPa/mm]
Shear I	49.2	10.3	135.2	29.3	864.0	48.7	151.7	10.6
Shear II	150.1	18.3	237.3	41.4	513.7	66.6	78.7	11.6
Shear III	310.9	7.7	607.9	21.2	1,461	34.1	393.8	8.7
All samples	49.2	7.7	232.4	32.5	1,461	66.6	234.5	12.7

Shear I method: data from boreholes KAV01, KSH01A, and KSH02.
Shear II method: data from boreholes KLX02 and KLX04.
Shear III method: data from borehole KSH01A.

Table 3-5. Arithmetic mean, median and geometric mean normal and shear stiffness for all the fracture samples tested with different methods.

Method	Arithmetic mean		Median		Geometric mean	
	k_n [MPa/mm]	k_s [MPa/mm]	k_n [MPa/mm]	k_s [MPa/mm]	k_n [MPa/mm]	k_s [MPa/mm]
Shear I	135.2	29.3	101.5	30.0	107.8	27.1
Shear II	237.3	41.4	224.4	41.3	228.2	39.6
Shear III	607.9	21.2	431.0	21.9	534.3	19.4
All samples	232.4	32.5	175.8	34.3	172.7	29.7

Shear I method: data from boreholes KAV01, KSH01A, and KSH02.
Shear II method: data from boreholes KLX02 and KLX04.
Shear III method: data from borehole KSH01A.

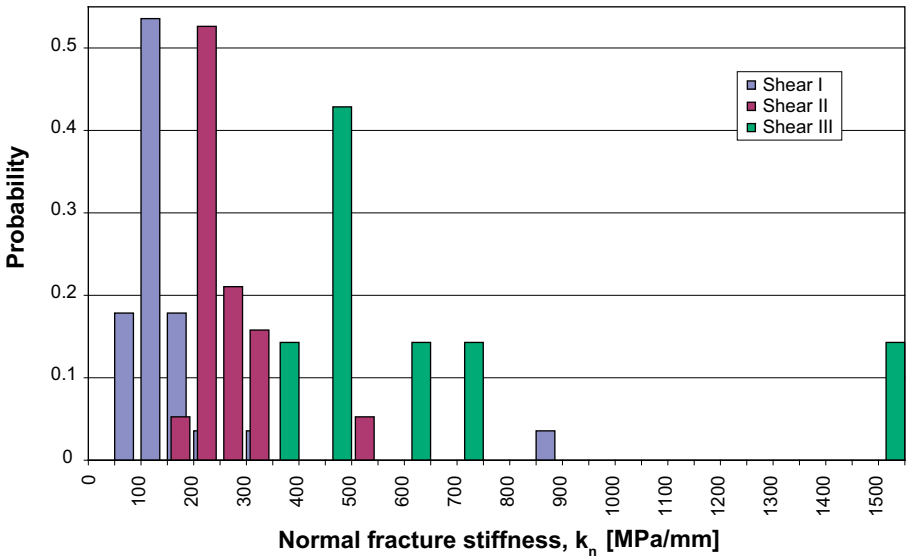

Figure 3-2. *Frequency distributions of the normal stiffness of the fractures tested according to method Shear I, Shear II and Shear III.*

3.4.2 Dilation

The dilation angle was evaluated from the tests for Shear I and Shear II (see also Appendix 2). Table 3-6, Table 3-7 and Table 3-8 show the summary statistics for the dilation angle for shear tests with normal stress 0.5, 5.0 and 20.0 MPa.

Table 3-6. Dilation angle at normal stress 0.5 MPa evaluated for all tests in Shear I and Shear II.

Method	Number of samples	Minimum dilation angle [°]	Mean dilation angle [°]	Maximum dilation angle [°]	Standard deviation of dilation angle [°]
Shear I	28	6.7	15.6	29.4	5.5
Shear II	19	3.6	15.9	28.9	7.6

Table 3-7. Dilation angle at normal stress 5 MPa evaluated for all tests in Shear I and Shear II.

Method	Number of samples	Minimum dilation angle [°]	Mean dilation angle [°]	Maximum dilation angle [°]	Standard deviation of dilation angle [°]
Shear I	28	0.3	3.8	8.9	2.3
Shear II	19	1.2	8.5	15.5	3.9

Table 3-8. Dilation angle at normal stress 20 MPa evaluated for all tests in Shear I and Shear II.

Method	Number of samples	Minimum dilation angle [°]	Mean dilation angle [°]	Maximum dilation angle [°]	Standard deviation of dilation angle [°]
Shear I	28	0.0	1.3	5.2	1.4
Shear II	19	0.7	4.0	9.3	2.2

3.5 Strength

The mechanical properties of the fractures obtained from the tilt tests were already presented in Section 3.1.

In the direct shear tests, the strength envelopes of the natural fractures were rather linear so that they suited the fitting with the Coulomb's Criterion (e.g. Figure 3-3). Furthermore, peak and residual conditions could be considered. In dry conditions, the average peak and residual friction angle of all the samples were 33.8 and 29.5°, respectively. The average cohesion of the samples was 0.54 and 0.41 MPa in peak and residual conditions, respectively. Table 3-9 and Table 3-10 summarise the experimental results in terms of minimum, mean and maximum cohesion and friction angles.

The statistical parameters obtained from the three different laboratory test techniques on natural fractures are compared in Table 3-9. Distributions of the data are shown as histograms in Appendix 2.

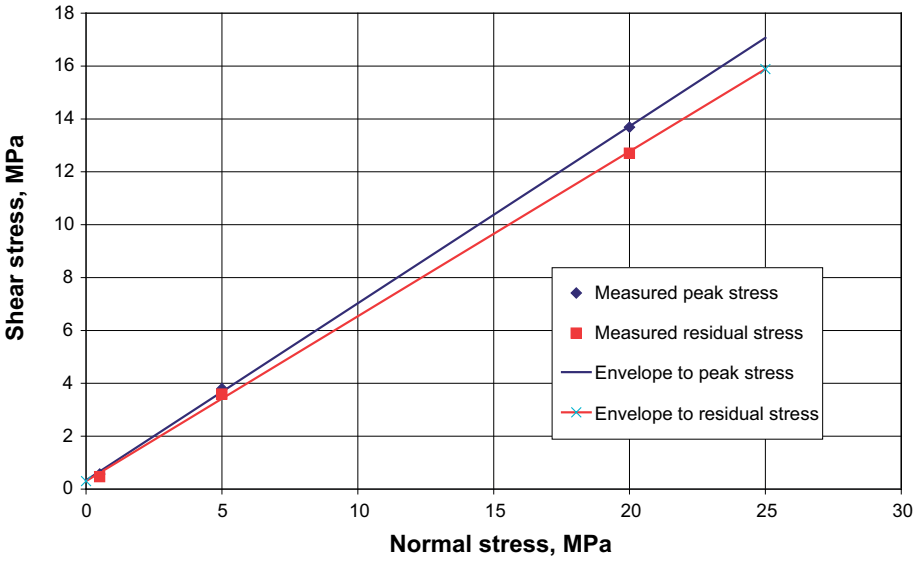

Figure 3-3. *Peak shear and residual strength according to the Coulomb's Criterion for fracture sample KLX02-117-1.*

Table 3-9. Comparison of the results obtained from different testing techniques and laboratories: cohesion and friction angle of the peak envelope of Coulomb's Criterion. All tests samples are considered (boreholes KAV01, KSH01A, KSH02A, KLX02, and KLX04).

Laboratory test method	Number of samples	Mean		Standard deviation		Minimum		Maximum	
		c_p^{MC} [MPa]	Φ_p^{MC} [°]	c_p^{MC} [MPa]	Φ_p^{MC} [°]	c_p^{MC} [MPa]	Φ_p^{MC} [°]	c_p^{MC} [MPa]	Φ_p^{MC} [°]
Tilt test[1)] (KAV01, KSH01A, KSH02A, KLX02, and KLX04)	157	0.48	33.7	0.13	1.8	0.24	31.5	0.75	35.8
Shear I method (KAV01, KSH01A, and KSH02)	28	0.51	32	0.35	4.2	0.07	23.9	1.66	40.7
Shear II method (KLX02 and KLX04)	19	0.82	36.6	0.37	3.0	0.26	31.2	1.56	40.8
Shear III method (KSH01A)	7	1.1	35.4	0.18	3.8	0.89	30.2	1.36	40.3

[1)] The values for tilt test are obtained from the Barton-Bandis' Criterion for normal stresses between 0.5 and 20 MPa.

Table 3-10. Comparison of the results obtained from different testing techniques and laboratories: cohesion and friction angle of the residual envelope of Coulomb's Criterion. All tests samples are considered (boreholes KAV01, KSH01A, KSH02A, KLX02, and KLX04).

Laboratory test method	Number of samples	Mean		Standard deviation		Minimum		Maximum	
		c_r^{MC} [MPa]	Φ_r^{MC} [°]	c_r^{MC} [MPa]	Φ_r^{MC} [°]	c_r^{MC} [MPa]	Φ_r^{MC} [°]	c_r^{MC} [MPa]	Φ_r^{MC} [°]
Tilt test[1)] (KAV01, KSH01A, KSH02A, KLX02, and KLX04)	157	0.43	28.5	0.11	3.3	0.23	22.4	0.61	32.7
Shear I method (KAV01, KSH01A, and KSH02)	28	0.33	30.9	0.27	4.7	0.00	21.5	1.00	40.9
Shear II method (KLX02 and KLX04)	19	0.36	34.0	0.12	3.3	0.18	27.5	0.62	39.5
Shear III method (KSH01A)	7	0.60	34.2	0.12	3.1	0.43	30.4	0.77	37.7

[1)] The values for tilt test are obtained from the Barton-Bandis' Criterion for normal stresses between 0.5 and 20 MPa.

3.5.1 Correlation between friction angle and cohesion

The possibility of correlation between the peak cohesion and friction angle of the natural fractures was evaluated for the different sets of laboratory results (Figure 3-4). The Simpevarp and Laxemar data obtained from the tilt test and the shear test show no correlation between the peak friction angle and the peak cohesion.

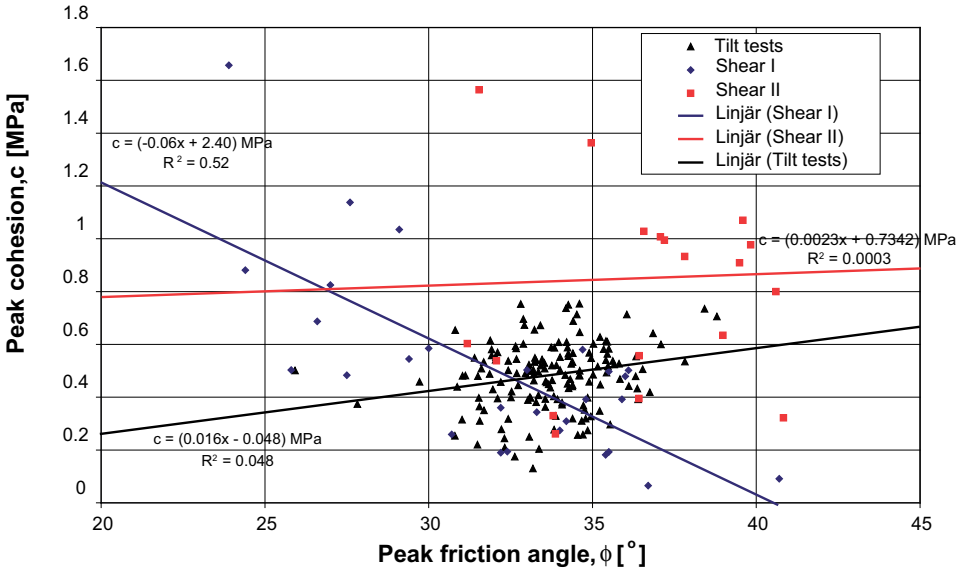

Figure 3-4. *Correlations between the peak friction angle and cohesion obtained with different testing techniques and sample sets.*

3.6 Statistical inference tests on fracture data

The strength and deformability data comprise several rock mechanics parameters. These have been derived from three different laboratory test methods, which may entail systematic differences in results. The primary interest is to analyze if different fracture sets have significant differences in fracture strength and deformability. The objective is therefore to distinguish whether significant differences can be found in laboratory data, in terms of: 1) fracture sets, and 2) laboratory test methods.

The parameters studied are the Mohr-Coulomb model parameters (c_p^{MC}, Φ_p^{MC}, c_r^{MC}, Φ_r^{MC}) and the Barton-Bandis model parameters (Φ_b^{BB}, Φ_r^{BB}, JRC_{100}, JCS_{100}). To clarify the statistical analyses, the data is referred to as x_{ij}, where x is the parameter studied, i is laboratory testing method used (Tilt, Shear I, and Shear II methods; see Section 3.1 and 3.2), and j is its fracture set (S_A, S_B, S_C, S_d, or S_ef). The fracture sets are defined in Tables 6-1 and 6-2 /Hermansson et al. 2005/. In this study, sets S_e (in Simpevarp) and S_f (in Laxemar) have been combined into a set 'S_ef', because they have similar orientation.

The total number of samples is 211 and most of the data come from tilt tests (Table 3-11). The chance of finding significant differences in statistical tests improves with larger sample sizes. However, grouping the data that do not belong to a homogeneous population may lead to incorrect inference.

The four different laboratory test methods appear to comprise rather unbiased samples of the different fracture sets (Figure 3-5). This signifies that the data can be grouped and compared, either in terms of laboratory test methods, or by fracture sets, irrespectively of risking large sampling bias. However, the modified shear method (Shear II) involves somewhat more S_A fractures, than to S_B fractures, and the original Shear method (Shear I) is applied to relatively more S_e fractures than to S_B fractures (Figure 3-5).

Therefore, with respect to the number of data available, the following analyses are considered possible:

1) Analyzing influence of laboratory tests method for all fractures, regardless of fracture sets, i.e. comparing x_i, for all j combined.
2) Analyzing differences between fracture sets for tilt test data alone.

The reason for excluding all shear test data in alternative 2) is that, if the laboratory test methods entail systematic differences in results, it may be erroneous to group different types of laboratory data as one homogeneous population. The reason for not analyzing the influence of fracture set for the two types of shear test data (as done for tilt data in alternative 2) is that much less data are available from these testing methods (Table 3-11).

Table 3-11. Sample sizes classified by test methods and fracture sets.

Set *j*\Method *i*	Tilt[1)]	Shear I[2)]	Shear II[3)]	Shear III[2)]	All methods
S_A[1)]	26	5	6	1	38
S_B[1)]	23	2	1	1	27
S_C[1)]	21	3	2	2	28
S_d[1)]	66	12	8	3	89
S_e[2)]	12	6	0	0	18
S_f[3)]	9	0	2	0	11
All fractures	157	28	19	7	211

[1)] From Boreholes KAV01, KSH01A, and KSH02 in Simpevarp, and KLX02 and KLX04 in Laxemar.
[2)] From Boreholes KAV01, KSH01A, and KSH02 in Simpevarp.
[3)] From Boreholes KLX02 and KLX04 in Laxemar.

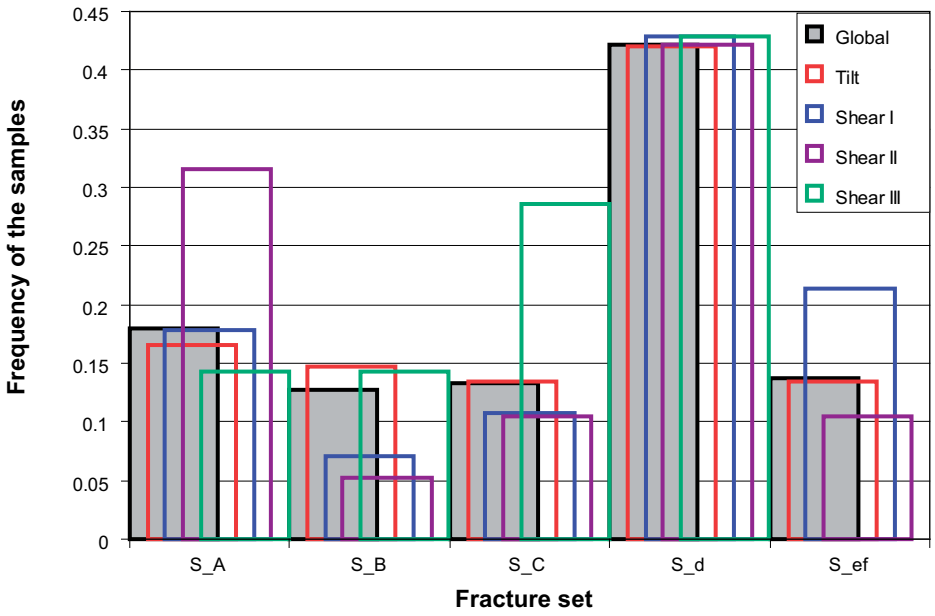

Figure 3-5. *Frequency of the samples grouped in fracture sets. "Global" refers to the total data set, regardless of testing method.*

3.6.1 Statistical tests

The following three types of parametric tests were used: i) *t*-test, for pair-wise sample mean comparison, ii) *F*-test, for pair-wise sample variance comparison, and iii) ANOVA (Analysis of variance) e.g. /Davis 2002/. These are all parametric tests, which require that the underlying distributions of data are normal. Normality can be tested by various methods, including probability plots, Chi-squared, and Kolmogorov-Smirnov tests. In this study, normality was only estimated roughly by visual inspections of the data plotted as histograms (Figure 3-6, Figure 3-7, Figure 3-8, Figure 3-9). Yet, another requirement for these tests is that the sample variances and sample sizes should not be too different from each other.

If the underlying distributions prove not to be normal, non-parametric tests must be used. Therefore, the Mann-Whitney test is also used for pair-wise sample mean comparisons of sample medians (as alternative to the *t*-test) e.g. /Davis 2002/. The drawback of many non-parametric tests is that they generally require large sample sizes to be powerful. The tests use a significance level $\alpha = 0.05$ (Type I error; the risk of erroneously rejecting a true null-hypothesis). The risk of the statistical tests not being powerful enough to reveal a true significant difference between data sets (Type II error) is not addressed in this study. The inference tests are finally reported in terms of *p*-values, which are defined as the smallest level of significance at which the null hypothesis would be rejected for a specific test (Table 3-12 to Table 3-18). In other words, a low *p*-value (i.e. $p < 0.05$) means that two data sets are likely to be significantly different, in terms of the specific test used.

t-test: pair-wise comparison of sample means

The t-test is used to test if there is a significant difference in mean values of two data sets. The two data sets are assumed to belong to two populations that are normally distributed and have unknown and unequal variances:

$$x_1 \sim N(\mu_1, \sigma_1^2) \text{ and } x_2 \sim N(\mu_2, \sigma_2^2) \quad (4)$$

The population mean values are estimated by the sample means ($\mu_1 \approx \bar{x}_1$ and $\mu_2 \approx \bar{x}_1$) and population variances are estimated by sample variances ($\sigma_1 \approx s_1$ and $\sigma_2 \approx s_2$).

Two hypotheses are set up: the null-hypothesis and the alternative hypothesis:

$$H_0 : \mu_1 - \mu_2 = \delta \text{ and } H_1 : \mu_1 - \mu_2 \neq \delta; \quad \delta \tag{5}$$

The test statistics used for a two-sided t-test at significance level $\alpha = 0.05$ is:

$$t = \frac{(\bar{x}_1 - \bar{x}_2 - \delta)}{\sqrt{(s_1^2 / n_1 + s_2^2 / n_2)}} \tag{6}$$

Then, the hypothesis H_{A0} can be rejected at significance level $\alpha = 0.05$, if:

$$|t| \geq \frac{w_1 t_1 + w_2 t_2}{w_1 + w_2} \tag{7}$$

where:

$$w_1 = s_1^2 / n_1 \text{ and } w_2 = s_2^2 / n_1 \tag{8}$$

$$t_1 = t_{1-\alpha/2, n_1 - 1} = t_{0.975, n_1 - 1} \text{ and } t_2 = t_{1-\alpha/2, n_2 - 1} = t_{0.975, n_2 - 1} \tag{9}$$

The two data sets must have 'similar' variance, if the number of data $n < 30$. Also, the number of available data of the two data sets should not differ too much.

F-test: pair-wise comparison of sample variances

The *F*-test is used to test if there is a significant difference in variance of two data sets. As above, two hypotheses are set up: the null-hypothesis and the alternative hypothesis:

$$\begin{aligned} H_0 &: \sigma_1^2 = \sigma_2^2 \\ H_1 &: \sigma_1^2 \neq \sigma_2^2 \end{aligned} \tag{10}$$

In this case, the test statistics used for a one-sided F-test at significance level $\alpha = 0.05$ is:

$$F_c = s_1^2 / s_2^2; \quad s_1^2 > s_2^2 \tag{11}$$

where F_c is F-distributed with $n_1 - 1$ and $n_2 - 1$ degrees of freedom. The null hypothesis H_0 is therefore rejected if:

$$F_c > F_{1-\alpha, n_1 - 1, n_2 - 1} \tag{12}$$

ANOVA: simultaneous analysis of variance

The *t*- and *F*-tests can only infer differences between two data sets at a time. The present data set can be divided into several different groups (fracture sets and laboratory test methods). Thus, the *t*- and *F*-tests require many pair-wise test combinations, either between a global group and a sub-group, or between two sub-groups. The benefit of the ANOVA test is that it can compare sample mean values of several different sub-groups at the time. The one-way ANOVA test uses the null hypothesis that assumes that there is no difference

between any of the sub-groups being compared. Then it uses the F-test statistics to compare whether the ratio (variance between groups/variance within sample groups) exceeds its critical value for rejecting its null hypothesis. The drawback is that it can only reject or accept the null hypothesis that all sub-groups share the same mean; it cannot infer if a particular group is different.

Mann-Whitney: pair-wise comparison of sample medians

The Mann-Whitney test is a non-parametric equivalence of the t-test, which tests the hypothesis that two samples have equal medians. Thus, the method is useful when the underlying distribution of a sample cannot be assumed to be normal. The two data sets are first combined. Each data value is then ranked by its value relative to others in the combined data set. Next, the ranks of combined data set are transferred back to the two original data sets. Thus, if both data sets reflect the same underlying population, the ranks would be more or less uniformly distributed between the two data sets. The test statistics used is the sum of ranks in the smaller sample set, Wx. For data sets larger than 7, Wx tends to follow a normal distribution. In such cases, it can be converted to the standard score, z (i.e. by subtracting its expected mean and dividing by its expected standard deviation) and evaluated by a two-tailed N-test (i.e. cumulative value of a standardized normal distribution, N(0,1)).

3.6.2 Comparison of the different laboratory techniques on natural fractures

Statistical inference tests were used to evaluate the influence that different laboratory test techniques may have on results. The four data sets compared are: tilt data (referred to as Tilt), and the three types of shear data (referred to as Shear I, Shear II and Shear III). The fracture properties studied are primarily the Mohr-Coulomb model parameters: peak cohesion c_p, peak friction angle Φ_p, residual cohesion c_r, and residual friction angle Φ_r. In this inference test, the data are only grouped in terms of laboratory testing technique, i.e. no distinction was made regarding fracture sets ($\overline{x}_i = \Sigma_j x_{ij}/n_j$).

The distributions of x_i were plotted as histograms to examine normality, which is required for parametric tests (Figure 3-6; Figure 3-7). In particular, Shear I appears to be more skewed than is expected for normally distributed data (Figure 3-7). However, if all three types of shear data are combined to form a larger data set, the distributions appear much more normal (Figure 3-6). Therefore the tilt test data was first compared to the grouped Shear data. The results of the *t*-tests (H_{A0}: $\mu_{Tilt} = \mu_{Shear}$), *F*-tests (H_{B0}: $\sigma_{Tilt} = \sigma_{Shear}$) and Mann-Whitney tests yield significant differences for all parameters, with the only exception of average peak friction angle (Table 3-12). Pair-wise Mann-Whitney tests are also made between tilt test data and each of the three types of shear tests (Table 3-14). The reason for this is that, in case the three types of shear tests are significantly different (as examined below), it may be erroneous to combine them into one group.

Table 3-12. Inference tests on laboratory test methods. Tilt test data and combined shear data.

	Average, $\bar{x}_i$					Standard Deviation, s_i			
	n_i	c_p^{MC}	Φ_p^{MC}	c_r^{MC}	Φ_r^{MC}	c_p^{MC}	Φ_p^{MC}	c_r^{MC}	Φ_r^{MC}
Tilt test data	157	0.48	33.73	0.43	28.47	0.13	1.76	0.11	3.33
All Shear data	54	0.69	34.03	0.38	32.40	0.40	4.34	0.23	4.28

Statistical inference between tilt test and all shear data (rejection risk)	c_p^{MC}	Φ_p^{MC}	c_r^{MC}	Φ_r^{MC}
t-test: HA0	0.01[1)]	0.87	0.02[1)]	0.0[3)]
F-test: HB0	0.0[3)]	0.0[3)]	0.0[3)]	0.01[2)]
Mann-Whitney test	0.00[2)]	0.12	0.00[2)]	0.00[3)]

[1)] significance level α = 0.05
[2)] significance level α = 0.01
[3)] significance level α = 0.001

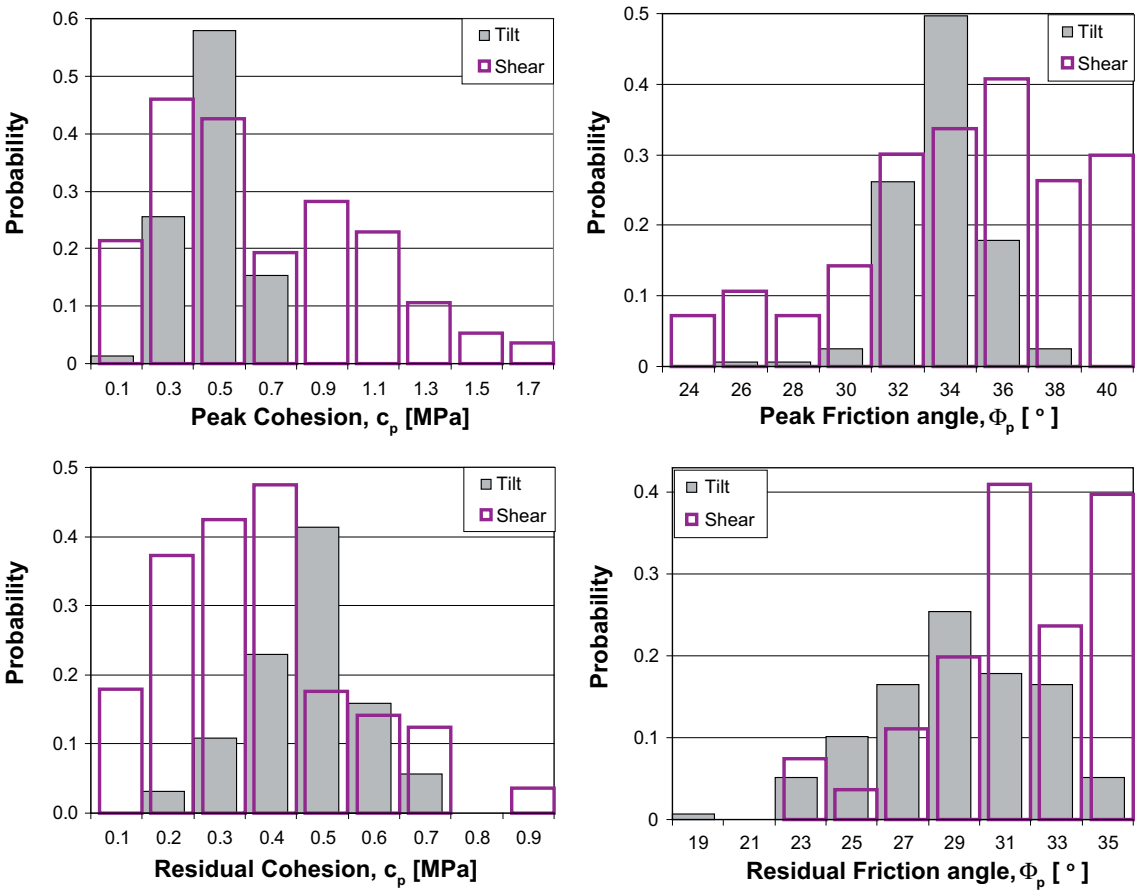

Figure 3-6. *Exploring normality in parameter distributions of tilt test data and shear test data. The tilt test data appears normally distributed.*

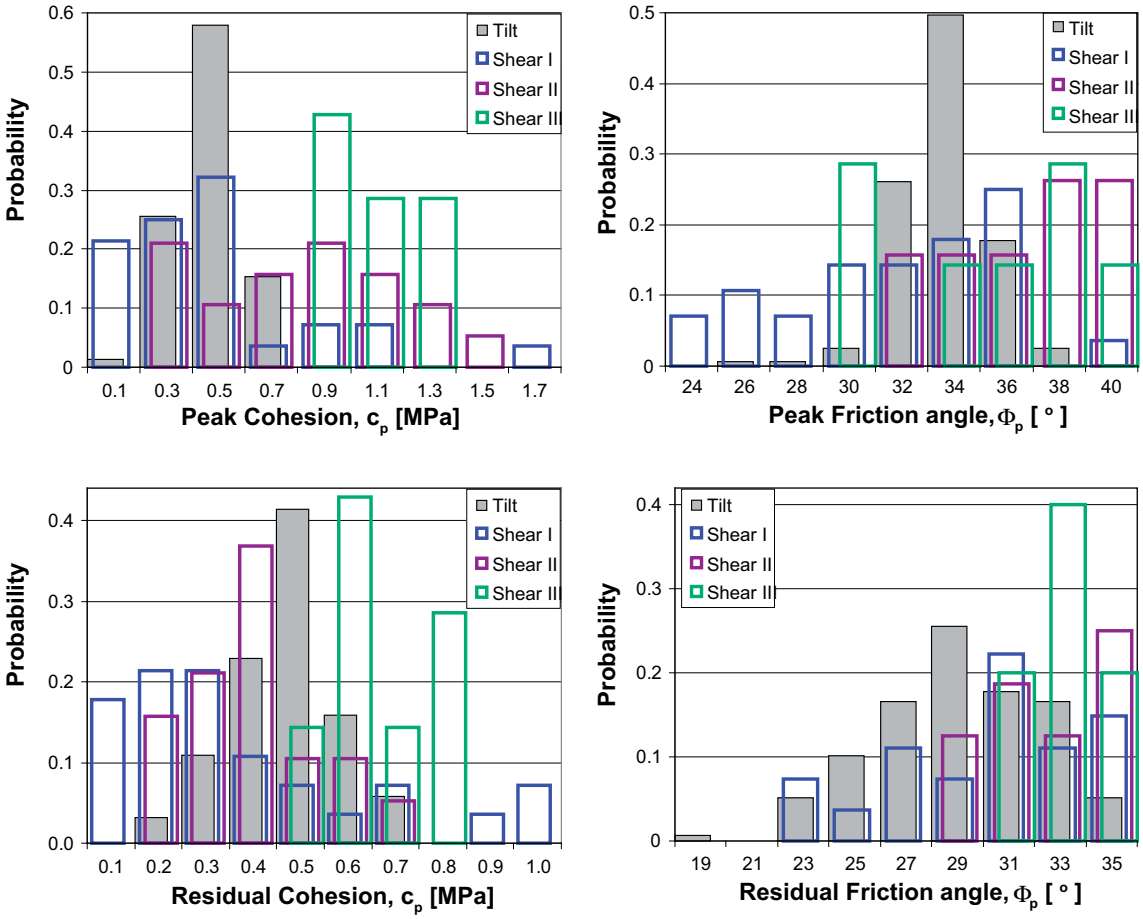

Figure 3-7. *Exploring normality in parameter distributions obtained by tilt test, Shear I, Shear II, and Shear III laboratory test methods. The different types of shear data do not appear normally distributed.*

Table 3-13. Pair-wise Mann-Whitney tests on laboratory test methods; tilt test data compared to each of the three different types of shear data.

Tilt test data vs	n_i	c_p^{MC}	Φ_p^{MC}	c_r^{MC}	Φ_r^{MC}
Shear I	28	0.30	0.10	0.0[3)]	0.0[2)]
Shear II	19	0.0[3)]	0.0[3)]	0.0[2)]	0.0[3)]
Shear III	7	0.0[3)]	0.14	0.0[2)]	0.0[3)]

[1)] significance level α = 0.05
[2)] significance level α = 0.01
[3)] significance level α = 0.001

Table 3-14. Pair-wise inference tests on the three types of shear test laboratory methods: Shear I, Shear II, Shear III data.

Average, $\bar{x}_i$	n_i	c_p^{MC}	Φ_p^{MC}	c_r^{MC}	Φ_r^{MC}	k_n	k_s
Shear I	28	0.51	31.95	0.33	30.86	135.2	29.28
Shear II	19	0.82	36.61	0.36	33.99	237.3	41.37
Shear III	7	1.10	35.36	0.60	34.21	607.9	21.20
Standard Deviation, s_i	n_i	c_p^{MC}	Φ_p^{MC}	c_r^{MC}	Φ_r^{MC}	k_n	k_s
Shear I	28	0.35	4.24	0.27	4.67	151.7	10.55
Shear II	19	0.37	3.01	0.12	3.26	78.68	11.63
Shear III	7	0.18	3.84	0.12	3.06	393.8	8.72
Pairwise Mann-Whitney tests, rejection risk H0: mi1 = mi2		c_p^{MC}	Φ_p^{MC}	c_r^{MC}	Φ_r^{MC}	k_n	k_s
Shear I vs II		0.0[2)]	0.0[3)]	0.16	0.01[1)]	0.0[3)]	0.0[3)]
Shear II vs III		0.04	0.20	0.0[3)]	0.40	0.0[3)]	0.0[3)]
Shear I vs III		0.0[3)]	0.053	0.0[2)]	0.057	0.0[3)]	0.076

[1)] significance level α = 0.05
[2)] significance level α = 0.01
[3)] significance level α = 0.001

Having inferred significant differences between the tilt test data and the grouped shear data, the next step was to test if there are also significant differences between the three types of shear data. The data from the three shear tests were compared pair-wise, similarly as was done above (Table 3-12). The parameter distributions of the different types of shear data appear to deviate from normality (Figure 3-7). Therefore, only the non-parametric Mann-Whitney test was used.

The tests reveal significant differences in results from the three different laboratory methods (Table 3-14). In these analyses, it should be remembered that that the three types of shear data sets contain somewhat different proportions of set S_A, S_B, and S_ef fractures (Figure 3-5). The potential differences between fracture sets are examined below.

3.6.3 Comparing fracture set properties: Mohr-Coulomb model parameters

To avoid erroneous grouping of different laboratory data types, only the tilt test data set was used to analyse the differences between fractures of different sets. The reason for selecting the tilt test data set is that it is the largest homogeneous data set (Table 3-11). Too few data are available for pursuing similar studies on individual shear data sets. In this section, the fracture set properties are compared in terms of Mohr-Coulomb model parameters. An analogous study, in terms of Barton-Bandis model parameters, is given in the following section. As above, the distributions of $x_{Tilt,j}$ were plotted as histograms to examine normality (Figure 3-8).

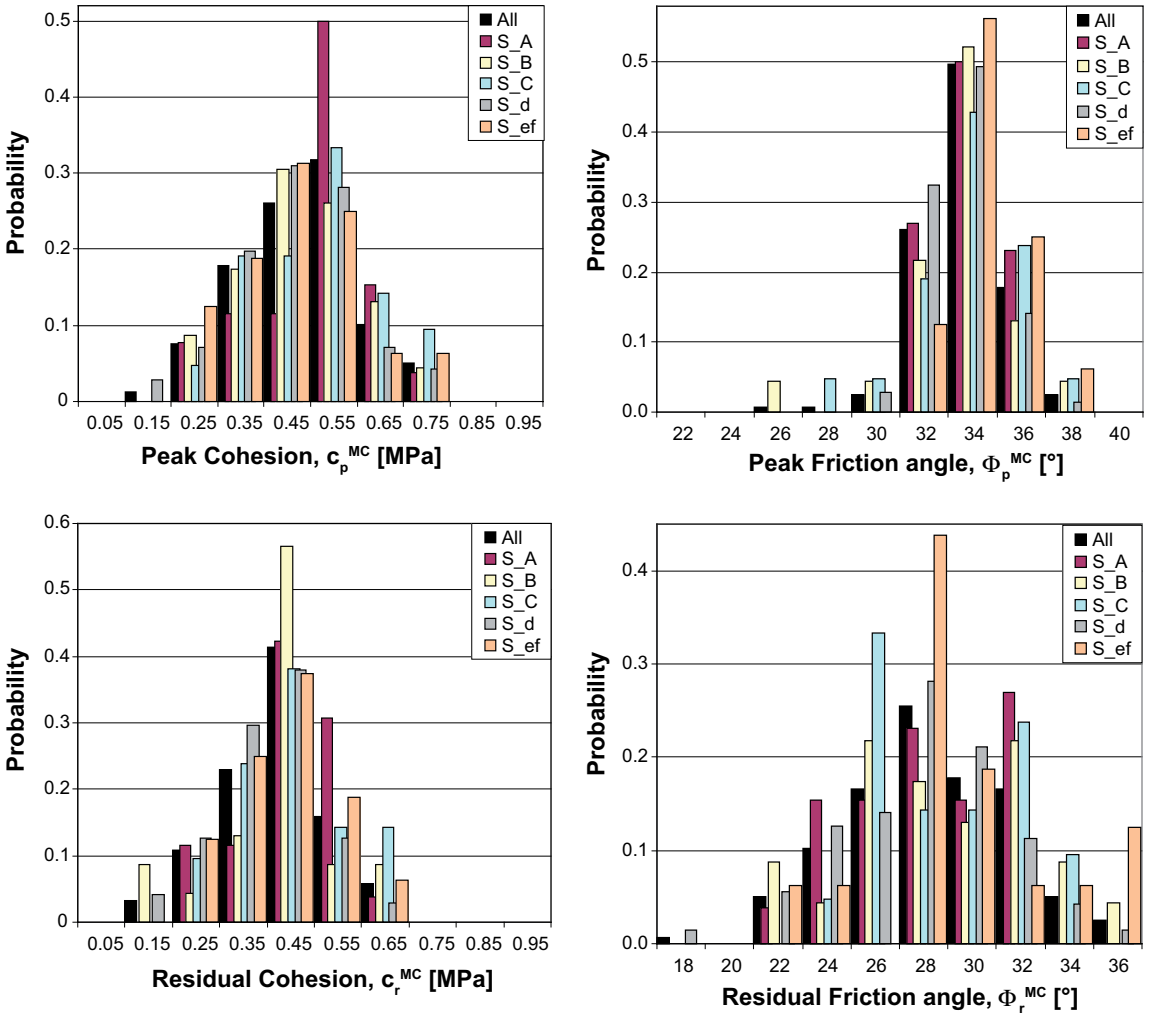

Figure 3-8. *Exploring normality of Mohr-Coulomb model parameter distributions in the tilt test data set.*

The ANOVA test is first used for simultaneous comparisons between the individual fracture sets. No significant differences are found between the fracture sets by the ANOVA-test (Table 3-15). Next, all tilt test data are combined to form a reference data set, x_{all}, which contains data from all fracture sets. The properties of each individual fracture set are then compared to this reference data set, by means of *t*-tests (H_{A0}: $\mu_j = \mu_{all}$) and *F*-tests (H_{B0}: $\sigma_j = \sigma_{all}$). No significant differences are found between the fracture sets. The only exception being variance in peak friction angle (Table 3-15).

Next, the properties of the individual fracture sets were pair-wise compared, by means of *t*-tests (H_0: $\mu_{j1} = \mu_{j2}$), Mann-Whitney tests(H_0: $m_{j1} = m_{j2}$) and *F*-tests (H_0: $\sigma_{j1} = \sigma_{j2}$). A significant difference in mean cohesion was found between sets S_A and S_d (Table 3-16). Furthermore, the significant difference in peak friction angle variance (found in Table 3-15) is differentiated, in terms of which sets differ significantly from another (Table 3-16).

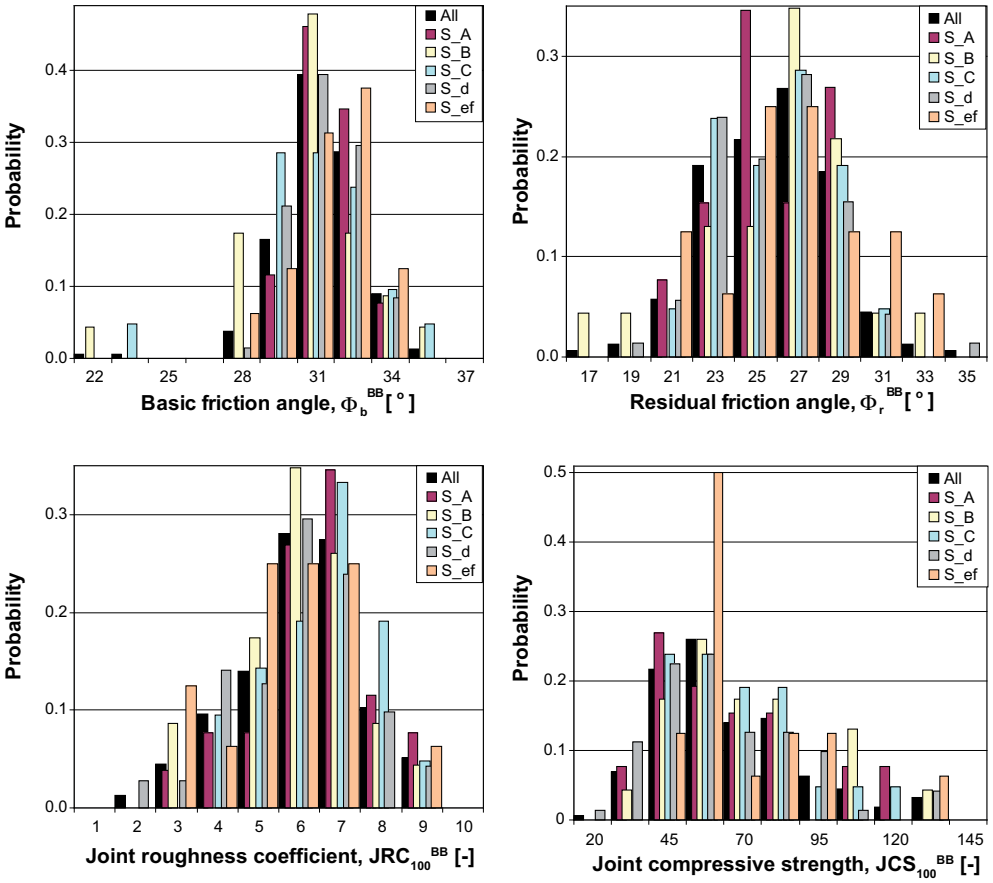

Figure 3-9. *Exploring normality of the Barton-Bandis model parameter distributions in the tilt test data set.*

Table 3-15. Inference tests on fracture set properties of the Mohr-Coulomb model; pair-wise tests between individual fracture set, x_j, and total data set, x_{all}.

	Average, $\overline{x}_j$					t-test; risk of rejecting H_0			
	n_j	c_p^{MC}	Φ_p^{MC}	c_r^{MC}	Φ_r^{MC}	c_p^{MC}	Φ_p^{MC}	c_r^{MC}	Φ_r^{MC}
S_A	26	0.52	33.9	0.45	28.4	0.17	0.49	0.19	0.91
S_B	23	0.48	33.6	0.43	28.8	0.98	0.80	0.84	0.66
S_C	21	0.51	33.9	0.45	28.9	0.37	0.81	0.28	0.25
S_d	66	0.46	33.5	0.40	28.0	0.16	0.43	0.11	0.33
S_ef	21	0.49	34.1	0.44	29.2	0.82	0.33	0.75	0.34
All	157	0.48	33.7	0.43	28.5				
ANOVA test; risk of rejecting H_0						0.22[1)]	0.71[1)]	0.15[1)]	0.54[1)]
	Standard Deviation, S_j					**F-test: risk of rejecting H_0**			
	n_j	c_p^{MC}	Φ_p^{MC}	c_r^{MC}	Φ_r^{MC}	c_p^{MC}	Φ_p^{MC}	c_r^{MC}	Φ_r^{MC}
S_A	26	0.12	1.3	0.10	3.1	0.12	0.03[2)]	0.28	0.32
S_B	23	0.13	2.4	0.11	3.7	0.28	0.01[2)]	0.37	0.21
S_C	21	0.13	2.3	0.10	2.9	0.46	0.04[2)]	0.52	0.25
S_d	66	0.12	1.5	0.10	3.4	0.45	0.11	0.26	0.39
S_ef	21	0.15	1.5	0.13	3.3	0.38	0.22	0.11	0.45
All	157	0.1	1.8	0.1	3.3				

[1)] ANOVA test
[2)] significance level α = 0.05.

Table 3-16. Inference tests on fracture set properties of the Mohr-Coulomb model: pair-wise tests between individual fracture sets, x_{j1} and x_{j2}.

t-test of sample means; risk of rejecting H_0: $\mu_{j1} = \mu_{j2}$									
c_p^{MC}	**S_B**	**S_C**	**S_d**	**S_ef**	**Φ_p^{MC}**	**S_B**	**S_C**	**S_d**	**S_ef**
S_A	0.30	0.80	0.03[1)]	0.49	S_A	0.55	0.90	0.23	0.71
S_B		0.48	0.43	0.84	S_B		0.71	0.93	0.42
S_C			0.11	0.66	S_C			0.56	0.71
S_d				0.37	S_d				0.17
c_r^{MC}	**S_B**	**S_C**	**S_d**	**S_ef**	**Φ_r^{MC}**	**S_B**	**S_C**	**S_d**	**S_ef**
S_A	0.46	0.99	0.03[1)]	0.60	S_A	0.65	0.54	0.58	0.39
S_B		0.51	0.27	0.90	S_B		0.93	0.34	0.73
S_C			0.06	0.63	S_C			0.22	0.77
S_d				0.28	S_d				0.15
Mann-Whitney test of sample medians; risk of rejecting H_0: $m_{j1} = m_{j2}$									
c_p^{MC}	**S_B**	**S_C**	**S_d**	**S_ef**	**Φ_p^{MC}**	**S_B**	**S_C**	**S_d**	**S_ef**
S_A	0.95	0.65	0.03[1)]	0.12	S_A	0.66	0.90	0.23	0.66
S_B		0.44	0.54	0.75	S_B		0.92	0.51	0.49
S_C			0.19	0.35	S_C			0.51	0.56
S_d				0.96	S_d				0.16
c_r^{MC}	**S_B**	**S_C**	**S_d**	**S_ef**	**Φ_r^{MC}**	**S_B**	**S_C**	**S_d**	**S_ef**
S_A	0.21	0.72	0.03[1)]	0.15	S_A	0.62	0.70	0.65	0.43
S_B		0.58	0.35	0.53	S_B		0.90	0.35	0.73
S_C			0.14	0.29	S_C			0.33	0.78
S_d				0.91	S_d				0.33
F-test of sample variance; risk of rejecting H_0: $\sigma_{j1} = \sigma_{j2}$									
c_p^{MC}	**S_B**	**S_C**	**S_d**	**S_ef**	**Φ_p^{MC}**	**S_B**	**S_C**	**S_d**	**S_ef**
S_A	0.37	0.38	0.46	0.13	S_A	0.0[2)]	0.0[2)]	0.16	0.21
S_B		0.49	0.31	0.22	S_B		0.41	0.0[2)]	0.02[1)]
S_C			0.33	0.22	S_C			0.01[2)]	0.03[1)]
S_d				0.07	S_d				0.49
c_r^{MC}	**S_B**	**S_C**	**S_d**	**S_ef**	**Φ_r^{MC}**	**S_B**	**S_C**	**S_d**	**S_ef**
S_A	0.24	0.32	0.44	0.08	S_A	0.17	0.41	0.28	0.33
S_B		0.42	0.24	0.25	S_B		0.13	0.28	0.31
S_C			0.34	0.20	S_C			0.22	0.27
S_d				0.06	S_d				0.48

[1)] significance level α = 0.05
[2)] significance level α = 0.01

3.6.4 Comparing fracture set properties: Barton-Bandis model parameters

In this section, fracture set properties are compared in terms of Barton-Bandis model parameters (analogous to the approach above). By visual inspection, only the distribution of joint compressive strength, JCS_{100}, appears to deviate particularly from normality. For consistency, it is treated with the same tests as in the previous section, although results from the parametric *t*- and *F*-tests should be treated with caution.

Significant differences in mean basic friction angle are found between sets S_A and S_d. However, the difference in median basic friction angle between sets S_A and S_d is not significant, which may imply that the non-parametric test is inappropriate in this case. Significant differences in variance of basic friction angle are also found between sets.

Table 3-17. Inference tests on fracture set properties of the Barton-Bandis model in Equation (2): pair-wise tests between individual fracture set, x_j, and total data set, x_{all}.

	Average, $\overline{x}_j$					t-test; risk of rejecting H_0			
	n_j	Φ_b^{BB}	Φ_r^{BB}	JRC_{100}	JCS_{100}	Φ_b^{BB}	Φ_r^{BB}	JRC_{100}	JCS_{100}
S_A	26	31.4	25.9	6.51	65.8	0.51	0.85	0.19	0.87
S_B	23	30.9	26.1	6.11	71.1	0.51	0.87	1.00	0.43
S_C	21	31.1	26.1	6.41	69.8	0.76	0.83	0.36	0.54
S_d	66	31.3	25.8	5.85	64.1	0.77	0.60	0.21	0.47
S_ef	21	31.4	26.6	6.15	68.3	0.64	0.44	0.93	0.75
All	157	31.3	26.0	6.11	66.7				
ANOVA test; risk of rejecting H_0						0.77[1)]	0.86[1)]	0.29[1)]	0.73[1)]
	Standard Deviation, s_j					t-test; risk of rejecting H_0			
	n_j	Φ_b^{BB}	Φ_r^{BB}	JRC_{100}	JCS_{100}	Φ_b^{BB}	Φ_r^{BB}	JRC_{100}	JCS_{100}
S_A	26	1.09	2.5	1.40	26.2	0.0[3)]	0.16	0.41	0.25
S_B	23	2.69	3.6	1.46	24.3	0.0[4)]	0.09	0.52	0.42
S_C	21	2.21	2.7	1.37	21.1	0.05	0.35	0.37	0.27
S_d	66	1.42	2.9	1.42	24.9	0.03[2)]	0.50	0.38	0.34
S_ef	21	1.48	3.1	1.75	20.8	0.21	0.31	0.12	0.24
All	157	1.73	2.9	1.5	23.9				

[1)] ANOVA test
[2)] Significance level α = 0,05
[3)] Significance level α = 0,01
[4)] Significance level α = 0,001

Table 3-18. Inference tests on fracture set properties of the Barton-Bandis model; pair-wise tests between individual fracture sets, x_{j1} and x_{j2}.

t-test of sample means; risk of rejecting H_0: $\mu_{j1} = \mu_{j2}$									
Φ_b^{BB}	**S_B**	**S_C**	**S_d**	**S_ef**	**Φ_r^{BB}**	**S_B**	**S_C**	**S_d**	**S_ef**
S_A	0.36	0.54	0.71	1.00	S_A	0.79	0.76	0.84	0.43
S_B		0.76	0.45	0.40	S_B		0.99	0.67	0.67
S_C			0.67	0.58	S_C			0.60	0.63
S_d				0.78	S_d				0.31
JRC_{100}	**S_B**	**S_C**	**S_d**	**S_ef**	**JCS_{100}**	**S_B**	**S_C**	**S_d**	**S_ef**
S_A	0.33	0.81	0.04[1)]	0.44	S_A	0.47	0.57	0.77	0.72
S_B		0.49	0.46	0.94	S_B		0.85	0.25	0.68
S_C			0.11	0.59	S_C			0.31	0.82
S_d				0.48	S_d				0.45
Mann-Whitney test of sample medians; risk of rejecting H_0: $m_{j1} = m_{j2}$									
Φ_b^{BB}	**S_B**	**S_C**	**S_d**	**S_ef**	**Φ_r^{BB}**	**S_B**	**S_C**	**S_d**	**S_ef**
S_A	0.79	0.74	0.65	0.61	S_A	0.55	0.86	0.07	0.41
S_B		0.79	0.93	0.39	S_B		0.93	0.36	0.71
S_C			1.00	0.56	S_C			0.58	0.56
S_d				0.41	S_d				0.27
JRC_{100}	**S_B**	**S_C**	**S_d**	**S_ef**	**JCS_{100}**	**S_B**	**S_C**	**S_d**	**S_ef**
S_A	0.31	0.86	0.07	0.10	S_A	0.35	0.40	0.89	0.34
S_B		0.47	0.55	0.48	S_B		0.98	0.19	0.85
S_C			0.18	0.23	S_C			0.23	0.99
S_d				0.75	S_d				0.32
F-test of sample variance; risk of rejecting H_0: $\sigma_{j1} = \sigma_{j2}$									
Φ_b^{BB}	**S_B**	**S_C**	**S_d**	**S_ef**	**Φ_r^{BB}**	**S_B**	**S_C**	**S_d**	**S_ef**
S_A	0.0[3)]	0.0[3)]	0.07	0.07	S_A	0.04[1)]	0.34	0.18	0.13
S_B		0.19	0.0[3)]	0.0**	S_B		0.11	0.11	0.29
S_C			0.0[2)]	0.04	S_C			0.36	0.25
S_d				0.38	S_d				0.32
JRC_{100}	**S_B**	**S_C**	**S_d**	**S_ef**	**JCS_{100}**	**S_B**	**S_C**	**S_d**	**S_ef**
S_A	0.92	0.46	0.49	0.14	S_A	0.37	0.16	0.36	0.15
S_B		0.39	0.41	0.21	S_B		0.26	0.47	0.24
S_C			0.45	0.14	S_C			0.21	0.47
S_d				0.10	S_d				0.18

[1)] significance level α = 0.05
[2)] significance level α = 0.01
[3)] significance level α = 0.001

3.7 Discussion

Natural fractures were tested according to four different techniques (tilt tests and Shear I, II and III) and by two laboratories (SP and NGI). Tilt tests show that the average JRC_{100} of the fractures is on average around 6 while the basic friction angle is around 31°. The joint wall strength of the fractures JCS_{100} seems to be rather high (around 65 MPa).

The normal stiffness of the fractures was obtained from the normal loading tests. However, the stiffness obtained from the NGI Laboratory results is much higher than that obtained by the SP Laboratory. The average NGI result is 607 MPa/mm, while the SP average results are 135 and 237 MPa/mm, for Shear I and Shear II, respectively. These differences, even tough the natural variability of the experimental results, indicates significant differences in results from different testing procedures at the two laboratories.

The direct shear also returned the strength of the natural fractures. The average peak cohesion of all the samples tested by the SP Laboratory was 0.5 and 0.8 MPa for Shear I and Shear II, respectively, and 32° and 37° respectively for peak friction angle. The same parameters determined from the NGI shear tests were slightly higher and equal to 1.1 MPa and 35°. However, these figures do not consider the fact that the fractures in each test batch (Shear I, II and III) belong to different fracture sets and thus should not be grouped disregarding the orientation.

When the tilt tests were re-analysed in terms of peak cohesion and friction angle, the values of 0.5 MPa and 34°, respectively, were obtained. The tilt test data set was also examined in terms of fracture set properties. The overall conclusion is that the differences between fracture sets are found to be small.

From the shear tests (Shear I, II and III), also the shear stiffness at half the peak shear strength could be determined. Average values of 29–41 MPa/mm and 22 MPa/mm were respectively obtained from the SP and NGI Laboratory, respectively.

4 Conclusions

This report contain a summary of all primary data on intact rock and fractures available for rock mechanics analyses at the time of the data freeze for Laxemar Site Descriptive Model version 1.2 (31st October 2004). For intact rock, only samples of granite to quartz monzodiorite (Ävrö granite) from borehole KLX02 and KLX04 were added to the data set. For the rock fractures, samples from borehole KLX02 and KLX04 were added to the dataset.

Thus, for the rock types quartz monzonite to monzodiorite and fine-grained dioritoid, the same mechanical properties as for Simpevarp SDM version 1.2 apply /SKB 2005/. For the samples of granite to quartz monzodiorite, differences were observed between the results from samples in borehole KLX02 and KLX04. In general, the mechanical properties of the samples from the second borehole are lower (e.g. 11% for the uniaxial compressive strength).

The samples containing sealed fractures and tested in uniaxial and triaxial conditions exhibit a Young's modulus higher than for the samples without any fractures.

Testing of fractures involved tilt testing and direct shear testing. For fracture testing, new samples were collected on all fracture sets. Therefore, the statistics of the mechanical properties for each fracture set could be updated.

Because the same mechanical parameters could be determined by means of two different testing methods, and for the same method, with different sample preparation techniques (i.e. Tilt, Shear I, Shear II, Shear III described in this report), the comparison of the different sets of laboratory results was carried out.

From the tilt tests of the fractures, it was inferred that all the fracture sets seem to have the same mechanical properties independently of the set orientation. The only significant difference was observed for the basic friction angle between set S_A and S_d. The average peak friction angle for the Coulomb's Criterion of the fracture sets varies between 33.6° and 34.1°, while the average cohesion ranges between 0.46 and 0.52 MPa, respectively. The average of the Coulomb's residual cohesion and friction angle varies in the ranges 28.0°–29.2° and 0.40–0.45 MPa, respectively. On the other hand, the direct shear testing results were too few to enable the comparison of different fracture sets.

From the direct shear tests of the fractures, it was observed that differences could be observed between the statistics of a certain parameter (e.g. peak cohesion) obtained by means of the three different sample preparation techniques. Furthermore, significant differences were observed between the parameters obtained from the tilt tests and the same parameters obtained from the direct shear tests.

Major differences were obtained for the normal stiffness of the fractures determined by NGI Laboratory (Shear III) compared to the results obtained by SP Laboratory (Shear I and II). The fracture stiffness for normal stresses between 0.5 and 10 MPa ranges between 311 and 1,461 MPa/mm for Shear III method, while it varies between 49 and 864 MPa/mm for Shear I and II methods.

Recent laboratory experiments on samples from Laxemar (KLX03A and KLX06A) also show that the fracture stiffness depend on the testing technique due to a new testing technique. This testing technique is gaining credit /Jacobsson and Flansbjer 2005ab/ and gives fracture stiffness results very similar to the Shear III results. This implies higher stiffness values than those obtained from Shear I and II methods reported in this report.

The large differences between results obtained from laboratory test methods rise questions about the comparability of the laboratory tests. Therefore, considering the uncertainty in laboratory tests, the differences found between fracture sets appear to be less relevant. Among these four data sets, the SP results were chosen to represent the properties of the fractures at Oskarshamn, mainly because they were the most numerous and agreed well with the tilt tests. In particular, SP results for the fractures from borehole KLX02 and KLX04 would be representative for the Laxemar subarea.

5 References

Barton N, Bandis SC, 1990. Review of predictive capabilities of JRC-JCS model in engineering practice, Proc. Int. Symp. Rock Joints, Loen, Norway (eds. Barton N & Stephansson O), Balkema: Rotterdam, p. 603–10.

Chryssanthakis P, 2003. Oskarshamn site investigation – Borehole: KSH01A. Results of tilt testing, SKB P-03-107, Svensk Kärnbränslehantering AB.

Chryssanthakis P, 2004a. Oskarshamn site investigation – Borehole: KSH02. Results of tilt testing, SKB P-04-10, Svensk Kärnbränslehantering AB.

Chryssanthakis P, 2004b. Oskarshamn site investigation – Borehole: KAV01. Results of tilt testing, SKB P-04-42, Svensk Kärnbränslehantering AB.

Chryssanthakis P, 2004c. Oskarshamn site investigation – Borehole: KLX04A. Tilt testing, SKB P-04-265, Svensk Kärnbränslehantering AB.

Chryssanthakis P, 2004d. Oskarshamn site investigation – Borehole: KLX02. Results of tilt testing, SKB P-04-44, Svensk Kärnbränslehantering AB.

Chryssanthakis P, 2004e. Oskarshamn site investigation – Drillle: KSH01A. The normal stress and shear tests on joints. SKB P-04-185, Svensk Kärnbränslehantering AB.

Davis JC, 2002. Statistics and data analysis in geology – 3rd ed. John Whiley & Sons, Inc. New York.

Eloranta P, 2004a. Oskarshamn site investigation – Drill hole KSH01A. Uniaxial compression test (HUT), SKB P-04-182, Svensk Kärnbränslehantering AB.

Eloranta P, 2004b. Oskarshamn site investigation – Drill hole KSH01A. Triaxial compression test (HUT), , SKB P-04-183, Svensk Kärnbränslehantering AB.

Eloranta P, 2004c. Oskarshamn site investigation – Drill hole KSH01A: Indirect tensile strength test (HUT), SKB P-04-184, Svensk Kärnbränslehantering AB.

Hoek E, Carranza-Torres C, Corkum B, 2002. The Hoek-Brown Failure Criterion – 2002 Edition. 5th North American Rock Mechanics Symposium and 17th Tunneling Association of Canada Conference: NARMS-TAC, p.267–271.

Hermansson J, Forsberg O, Fox A, La Pointe P, 2005. Preliminary site description, Laxemar subarea – version 1.2, Statistical model of fractures and deformation zones, SKB R-05-45, Svensk Kärnbränslehantering AB.

Jacobsson L, 2004a. Oskarshamn site investigation – Drill hole KSH01A – Uniaxial compression test of intact rock, SKB P-04-207, Svensk Kärnbränslehantering AB.

Jacobsson L, 2004b. Oskarshamn site investigation – Drill hole KSH02A – Uniaxial compression test of intact rock, SKB P-04-209, Svensk Kärnbränslehantering AB.

Jacobsson L, 2004c. Oskarshamn site investigation – Borehole KLX02 – Uniaxial compression test of intact rock, SKB P-04-255, Svensk Kärnbränslehantering AB.

Jacobsson L, 2004d. Oskarshamn site investigation – Borehole KLX04A – Uniaxial compression test of intact rock, SKB P-04-261, Svensk Kärnbränslehantering AB.

Jacobsson L, 2004f. Oskarshamn site investigation – Drill hole KSH01A. Triaxial compression test of intact rock, SKB P-04-208, Svensk Kärnbränslehantering AB.

Jacobsson L, 2004g. Oskarshamn site investigation Drill hole KSH02A. Triaxial compression test of intact rock, SKB P-04-210, Svensk Kärnbränslehantering AB.

Jacobsson L, 2004h. Oskarshamn site investigation – Borehole KLX04A Triaxial compression test of intact rock, SKB P-04-262, Svensk Kärnbränslehantering AB.

Jacobsson L, 2004i. Oskarshamn site investigation – Drill hole KSH01A. Indirect tensile strength test., SKB P-04-62, Svensk Kärnbränslehantering AB.

Jacobsson L, 2004j. Oskarshamn site investigation – Drill hole KSH02. Indirect tensile strenght test., SKB P-04-63, Svensk Kärnbränslehantering AB.

Jacobsson L 2004k. Oskarshamn site investigation – Drill hole KLX02. Indirect tensile strength test, SKB P-04-256, Svensk Kärnbränslehantering AB.

Jacobsson L, 2004l. Oskarshamn site investigation – Drill hole KLX04A: Indirect tensile strength test, SKB P-04-263, Svensk Kärnbränslehantering AB.

Jacobsson L, 2004m. Oskarshamn site investigation – Borehole KLX02 Normal stress and shear tests on joints, SKB P-04-257, Svensk Kärnbränslehantering AB.

Jacobsson L, 2004n. Laxemar site investigation – Borehole KLX04A Normal stress and shear tests on joints, SKB P-04-264, Svensk Kärnbränslehantering AB.

Jacobsson L, 2005o. Oskarshamn site investigation – Drill hole KAV01 Normal loading and shear tests on joints, SKB P-05-05, Svensk Kärnbränslehantering AB.

Jacobsson L, 2005p. Oskarshamn site investigation – Drill hole KSH01A Normal loading and shear tests on joints, SKB P-05-06, Svensk Kärnbränslehantering AB.

Jacobsson L, 2005q. Oskarshamn site investigation – Drill hole KSH02A Normal loading and shear tests on joints, SKB P-05-07, Svensk Kärnbränslehantering AB.

Jacobsson L, Flansbjer M, 2005a. Oskarshamn site investigation – Borehole KLX03A. Normal loading and shear tests on joints, SKB P-05-92, Svensk Kärnbränslehantering AB.

Jacobsson L, Flansbjer M, 2005b. Oskarshamn site investigation – Borehole KLX06A. Normal loading and shear tests on joints, SKB P-05-146, Svensk Kärnbränslehantering AB.

Martin CD, Chandler NA, 1994. The progressive fracture of Lac du Bonnet granite. International Journal Rock Mechanics Mining Science & Geomechanics Abstracts, 31(6):643–659.

SKB, 2004. Preliminary site description Simpevarp area – version 1.1, SKB R-04-25, Svensk Kärnbränslehantering AB.

SKB, 2005. Simpevarp subarea – version 1.2 – Preliminary site description, SKB R-05-08, Svensk Kärnbränslehantering AB.

Appendix 1

Intact rock

A.1.1 Variation of the uniaxial compressive strength of the granite to quartz monzodiorite with depth

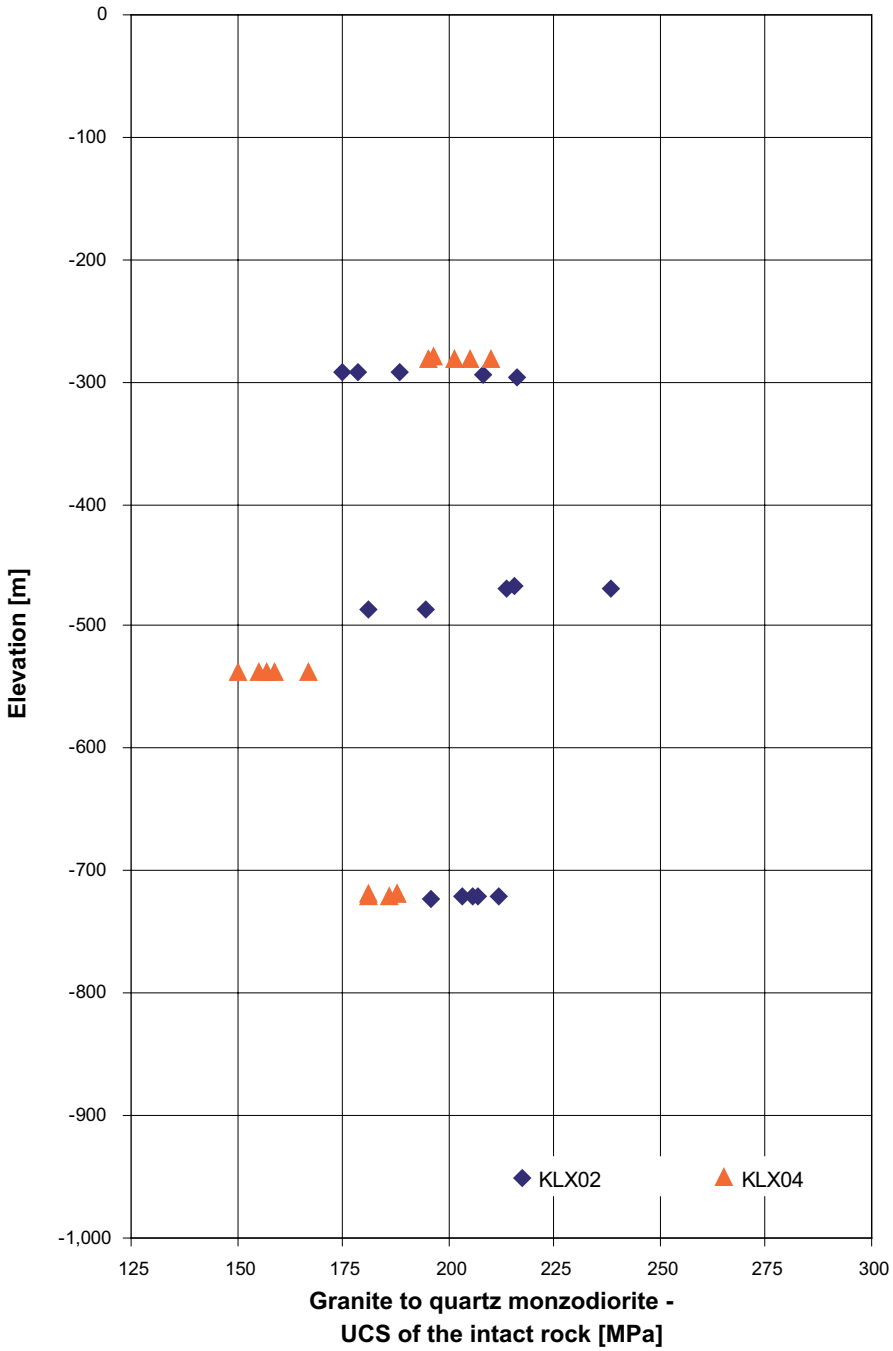

A.1.2 Variation of the Young's modulus of the granite to quartz monzodiorite with depth

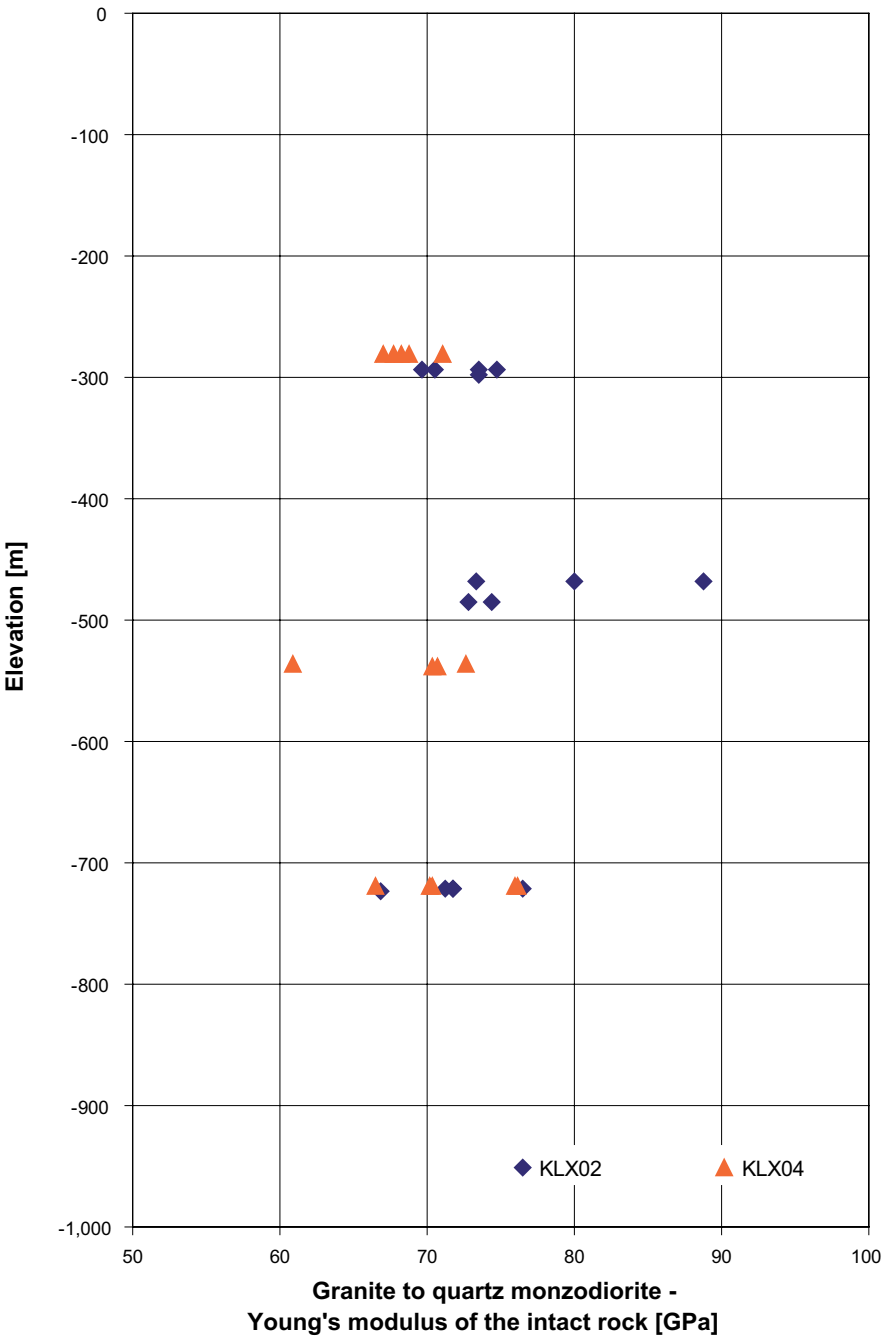

A.1.3 Variation of the Poisson's ratio of the granite to quartz monzodiorite with depth

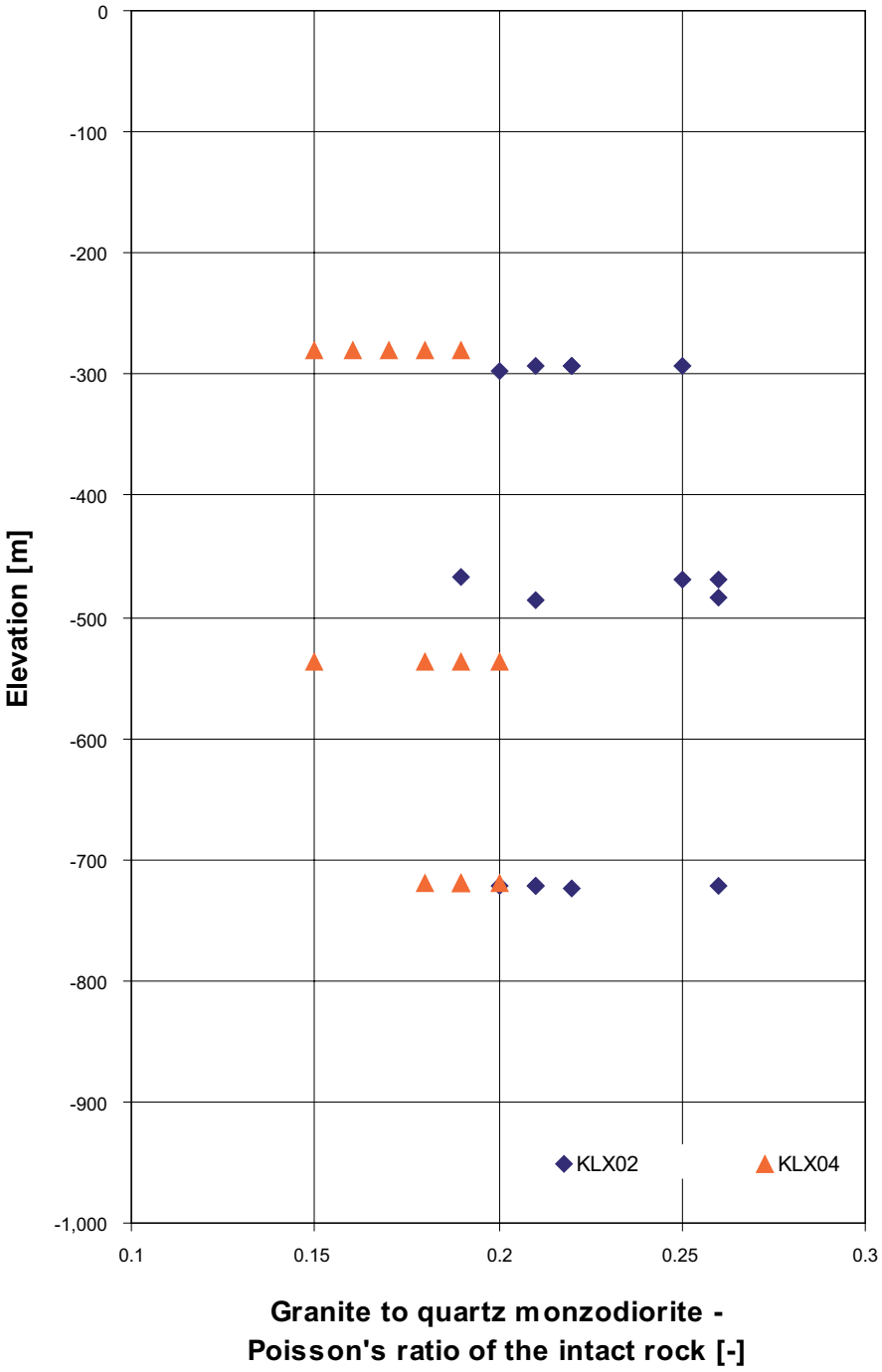

Appendix 2

Natural fractures

A.2.1 Laboratory test methods – Mohr-Coulomb's parameters

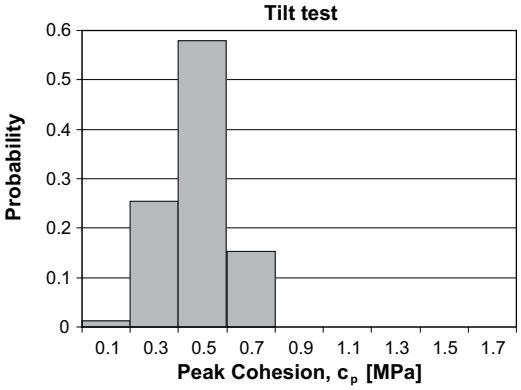

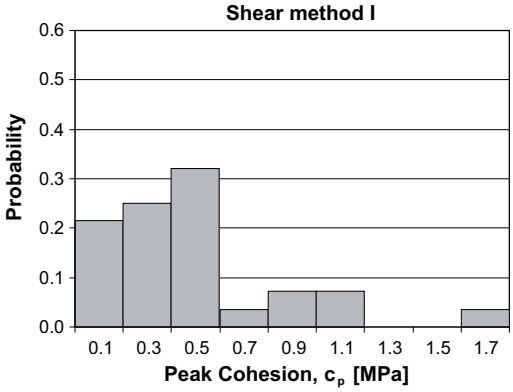

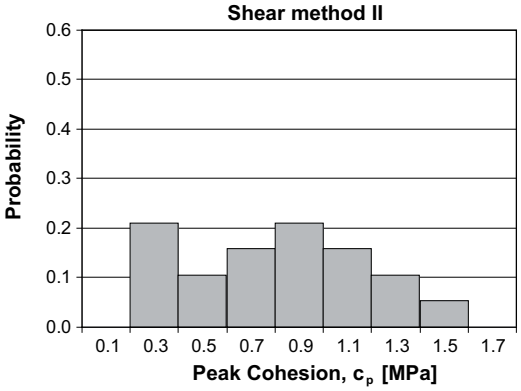

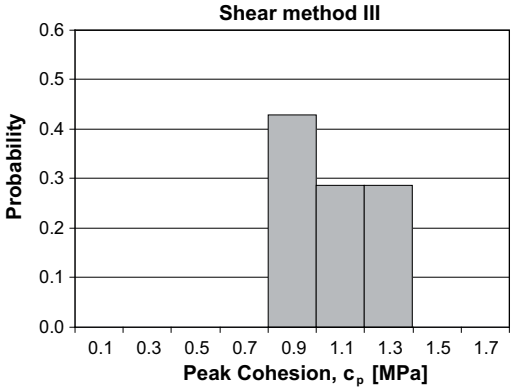

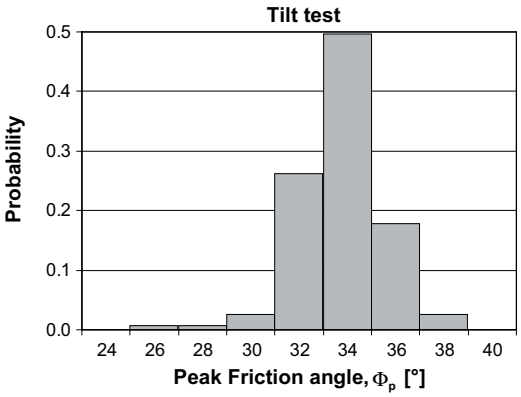

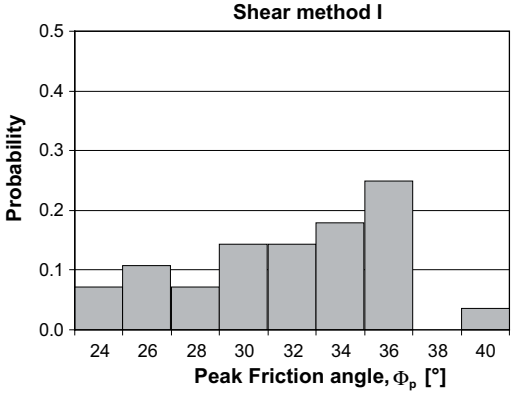

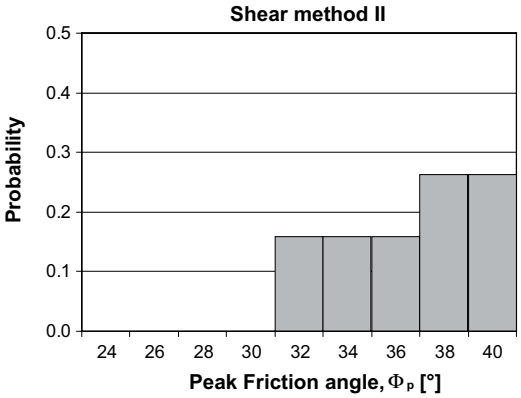

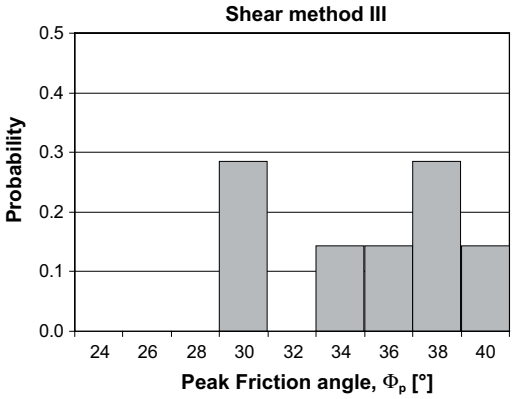

Laboratory test methods – Mohr-Coulomb's parameters

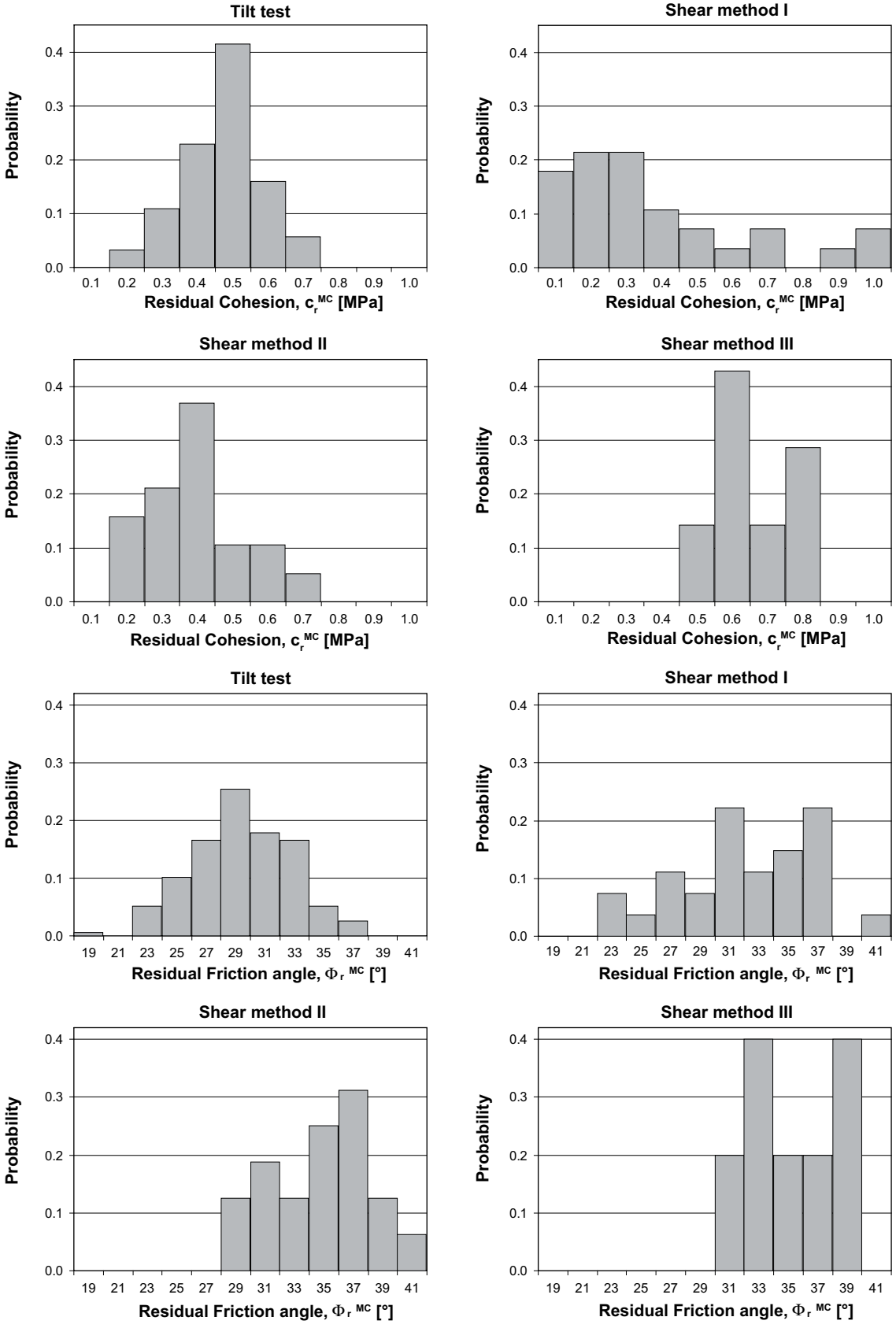

A.2.2 Normal loading and shear tests – fracture stiffness

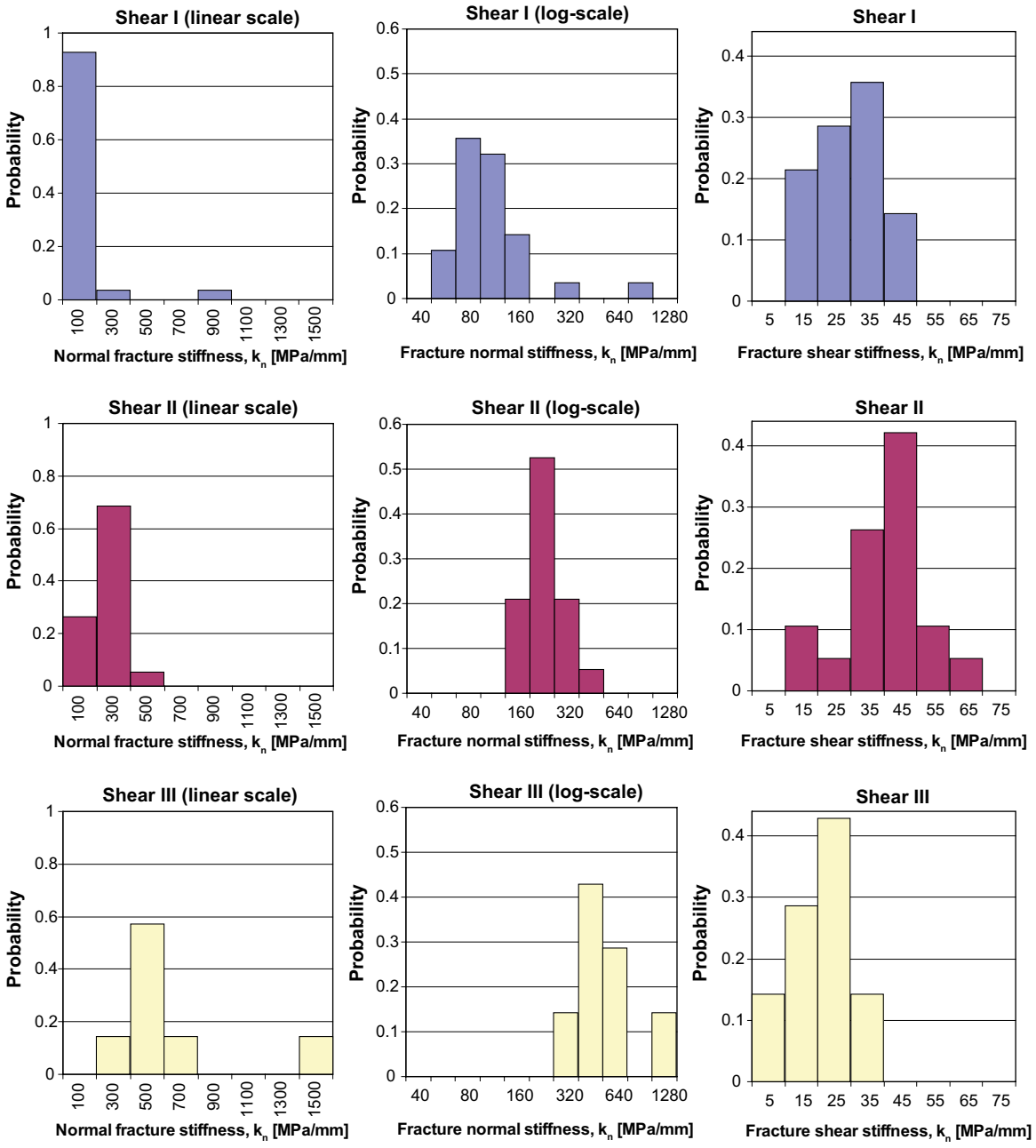

Note: Linear and logarithmic binning scales compared in normal stiffness histograms.

A.2.3 Tilt tests – Mohr-Coulomb's parameters for each fracture set

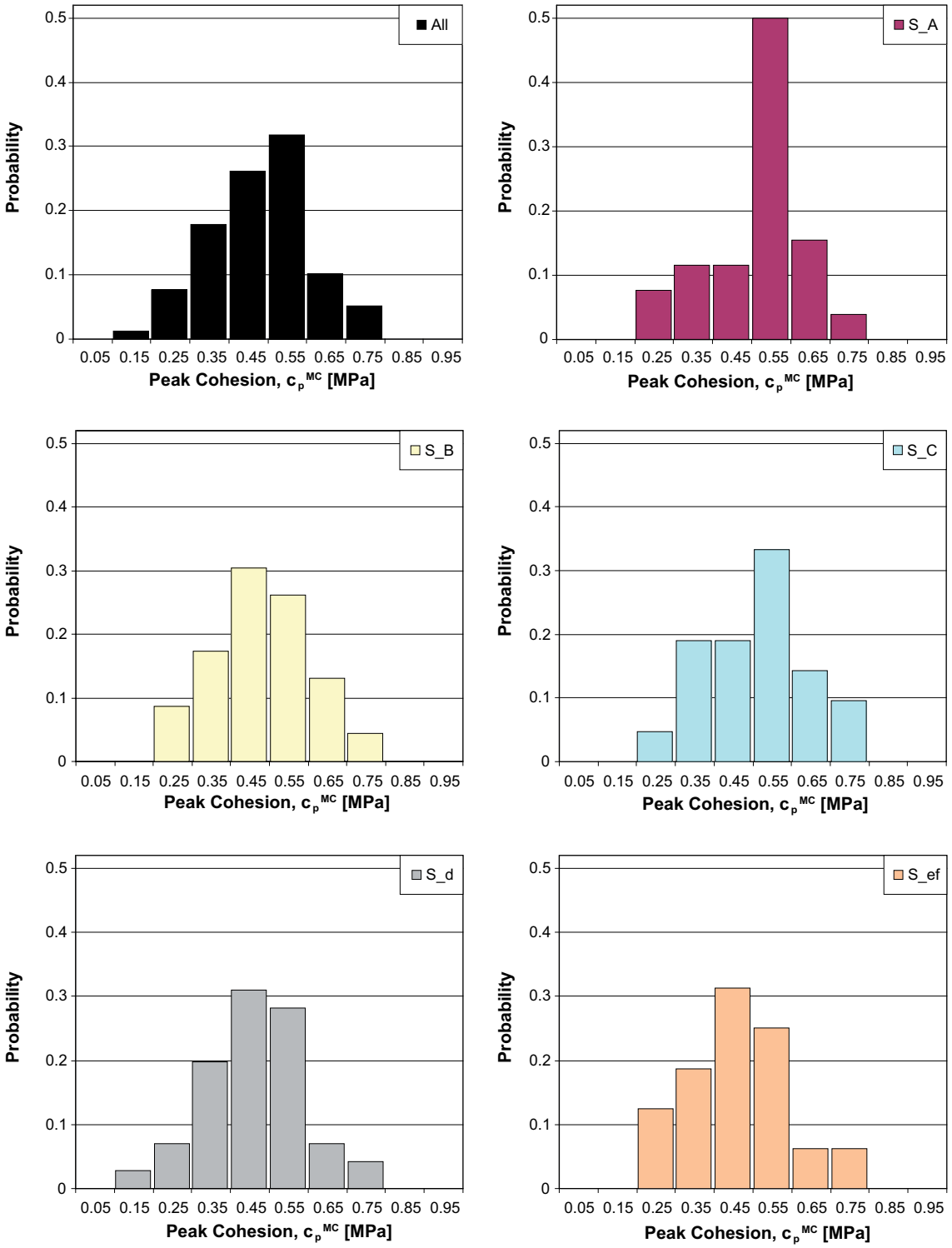

Mohr-Coulomb's peak cohesion for all Tilt data. The fractures are grouped into fracture sets.

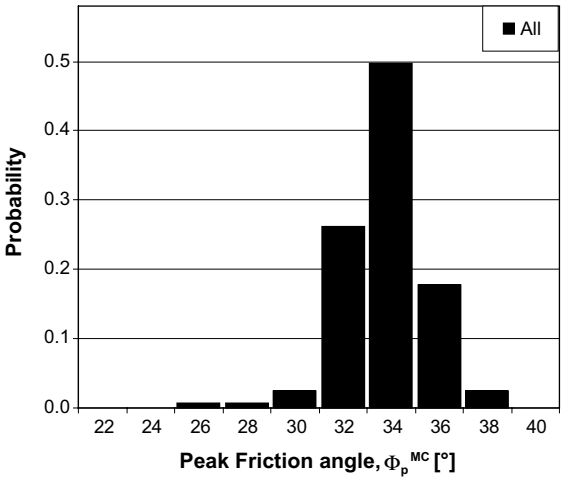

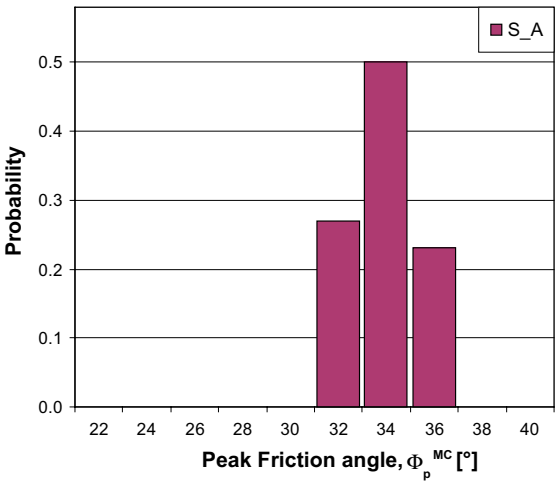

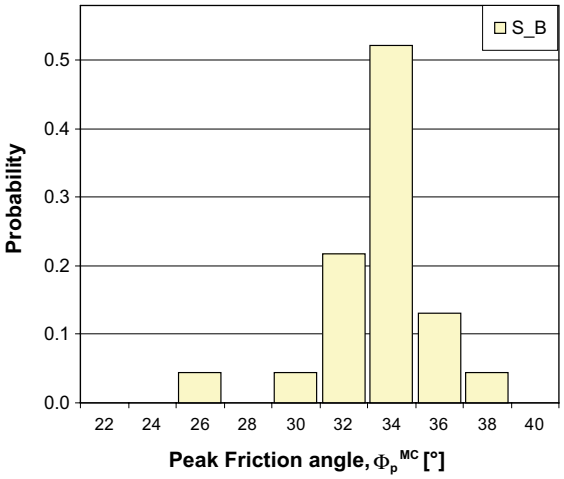

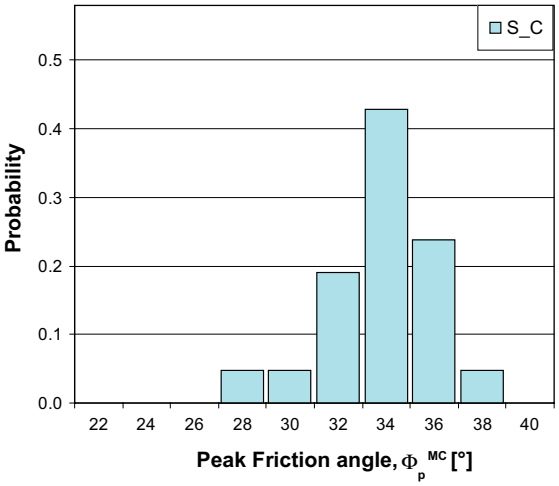

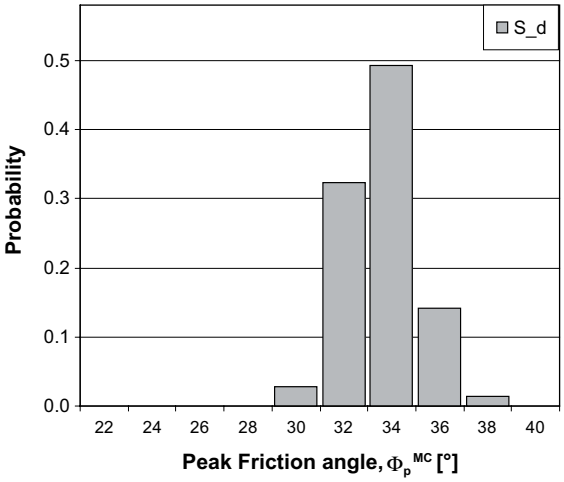

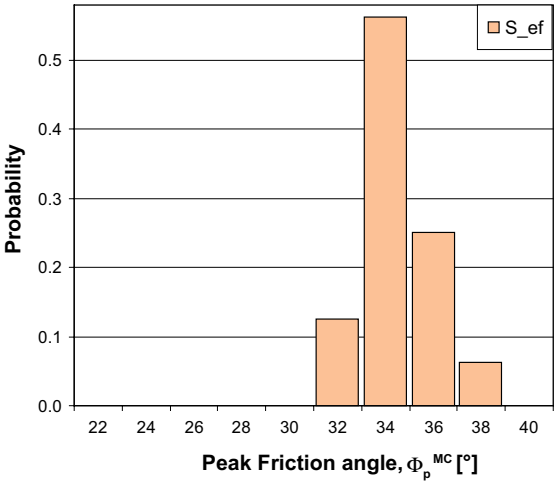

Mohr-Coulomb's peak friction angle for all Tilt data. The fractures are grouped into fracture sets.

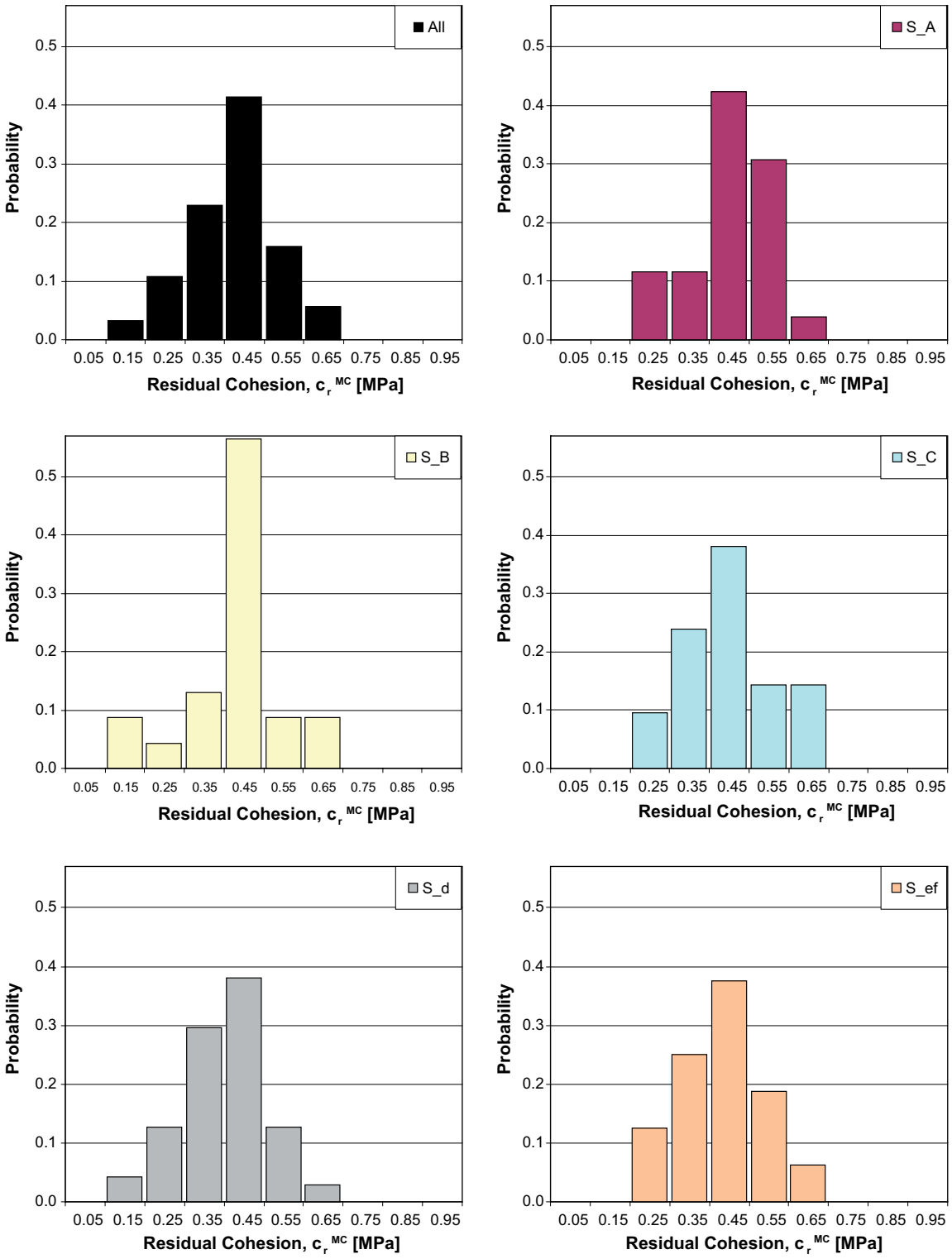

Mohr-Coulomb's residual cohesion for all Tilt data. The fractures are grouped into fracture sets.

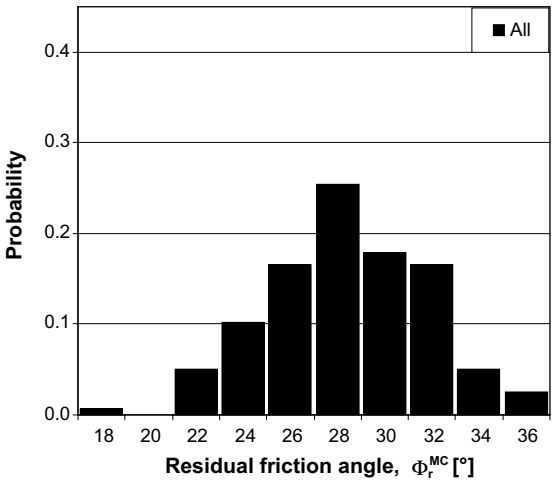

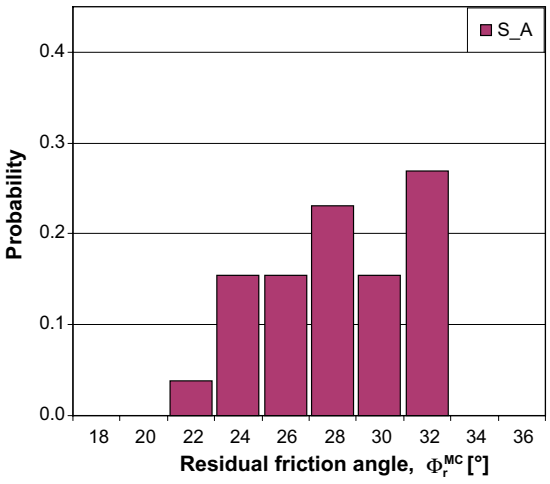

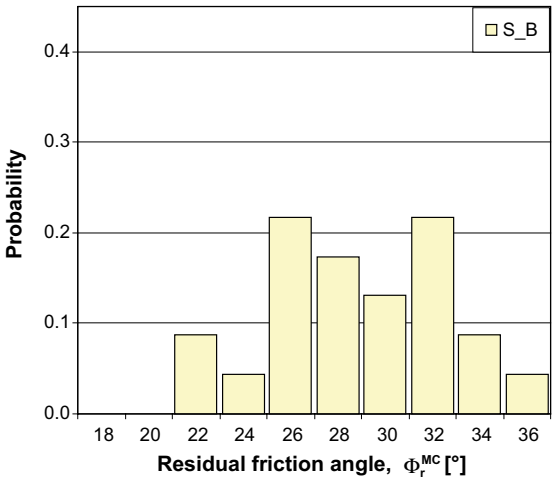

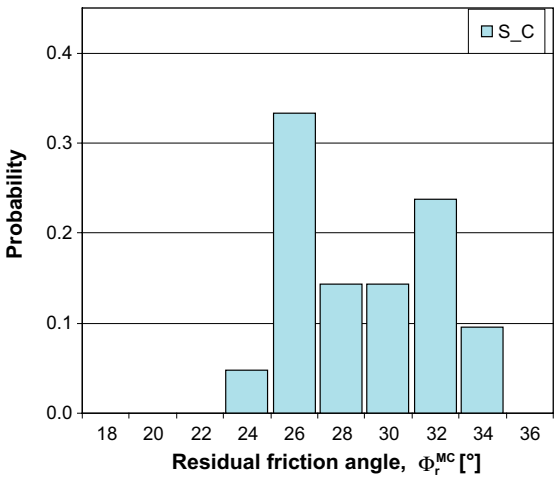

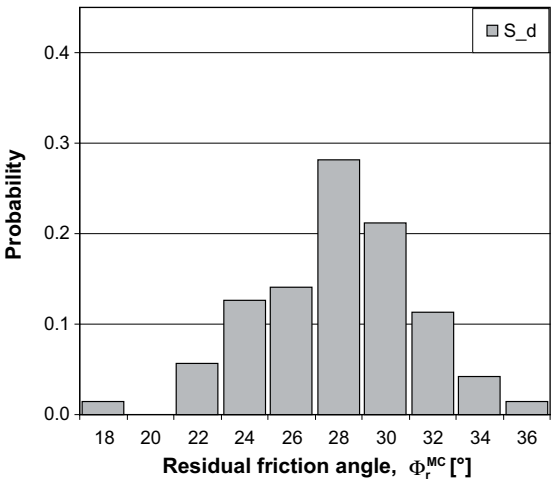

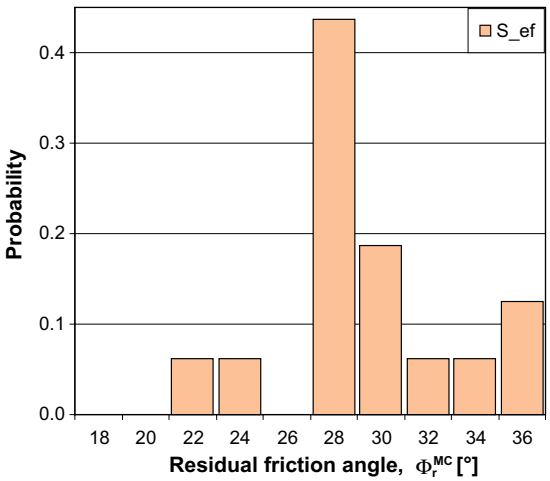

A.2.4 Tilt tests – Barton-Bandis' parameters for each fracture set

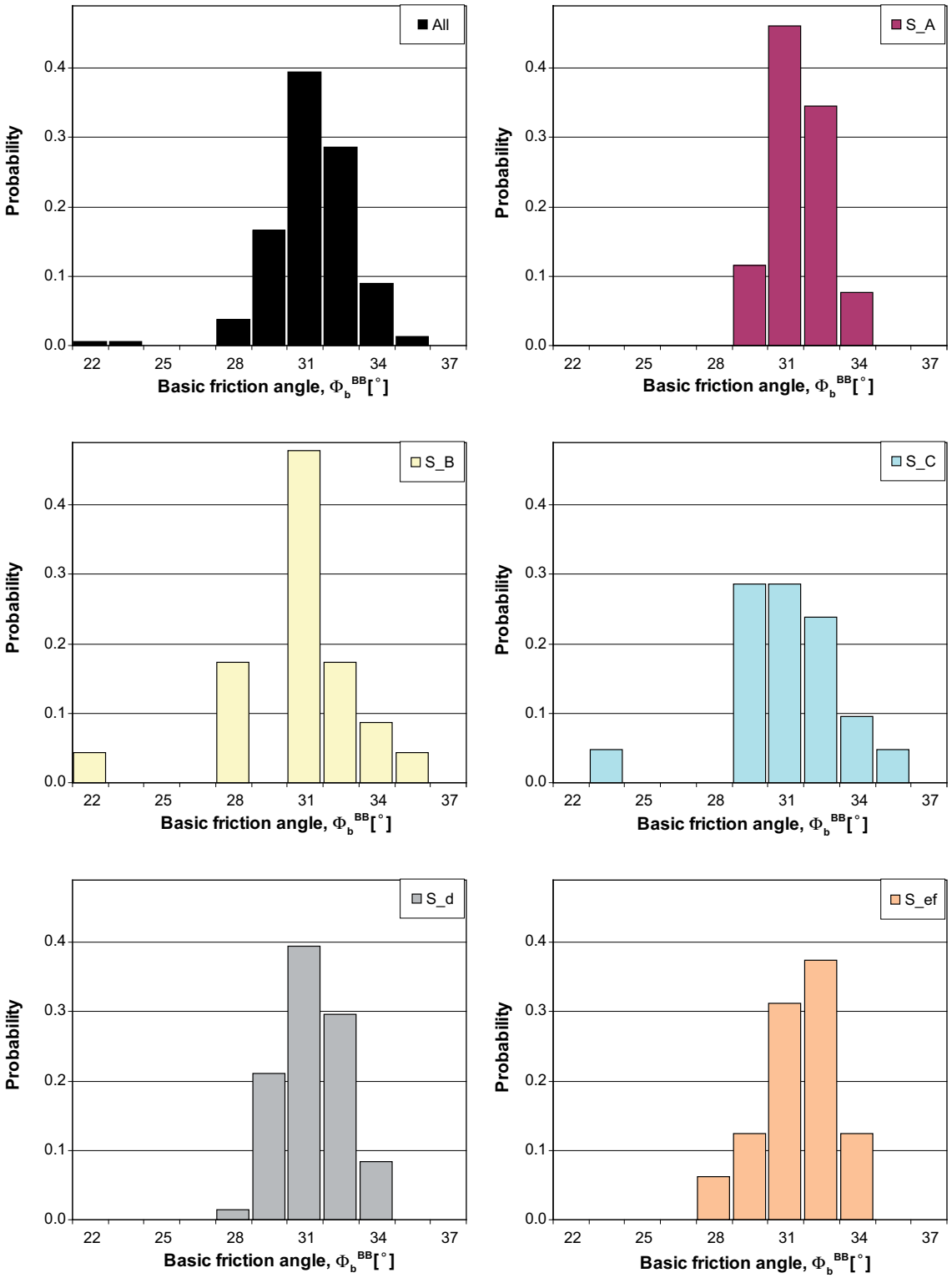

Barton-Bandis' basic friction angle for all Tilt data. The fractures are grouped into fracture sets.

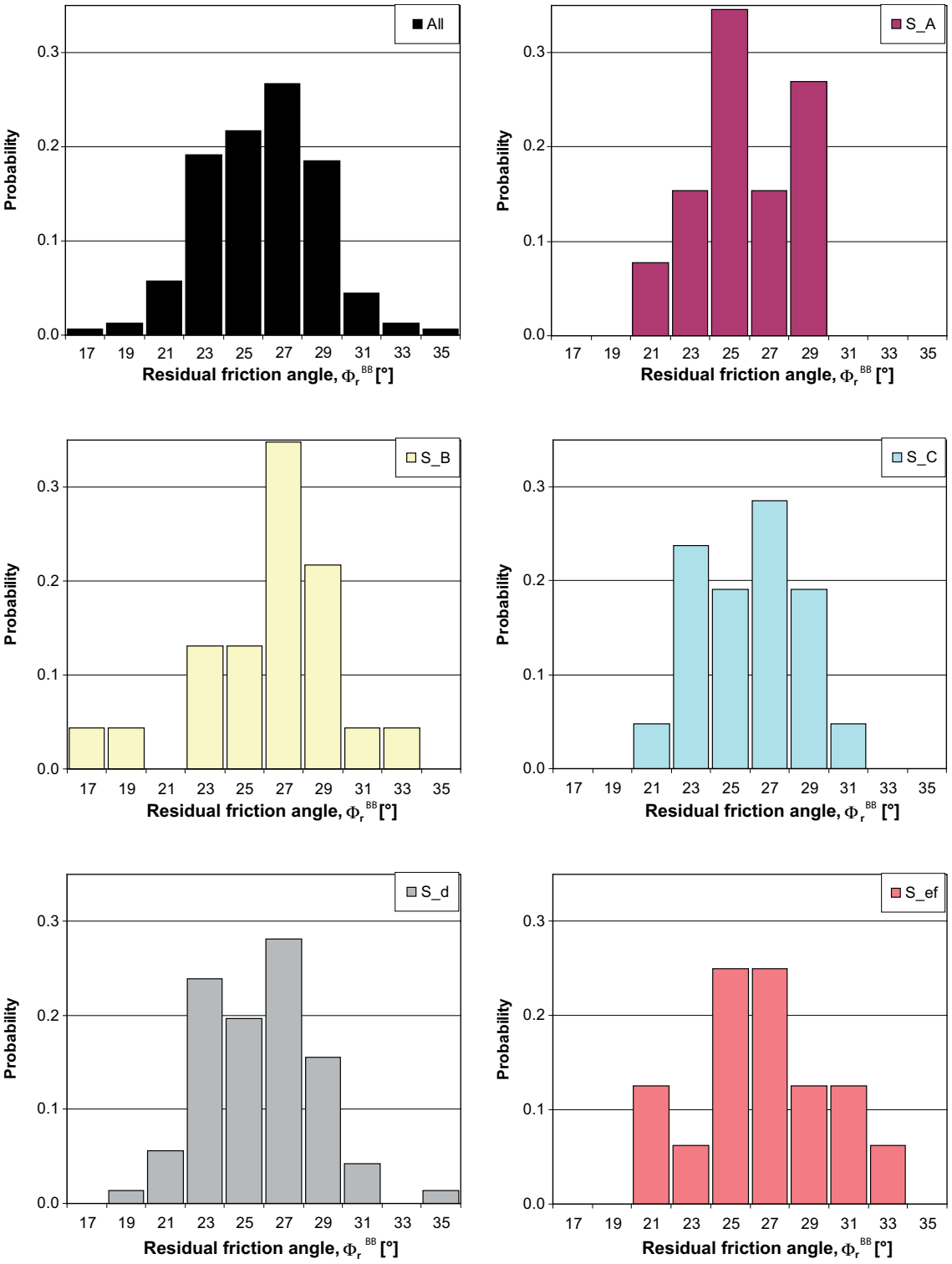

Barton-Bandis' residual friction angle for all Tilt data. The fractures are grouped into fracture sets.

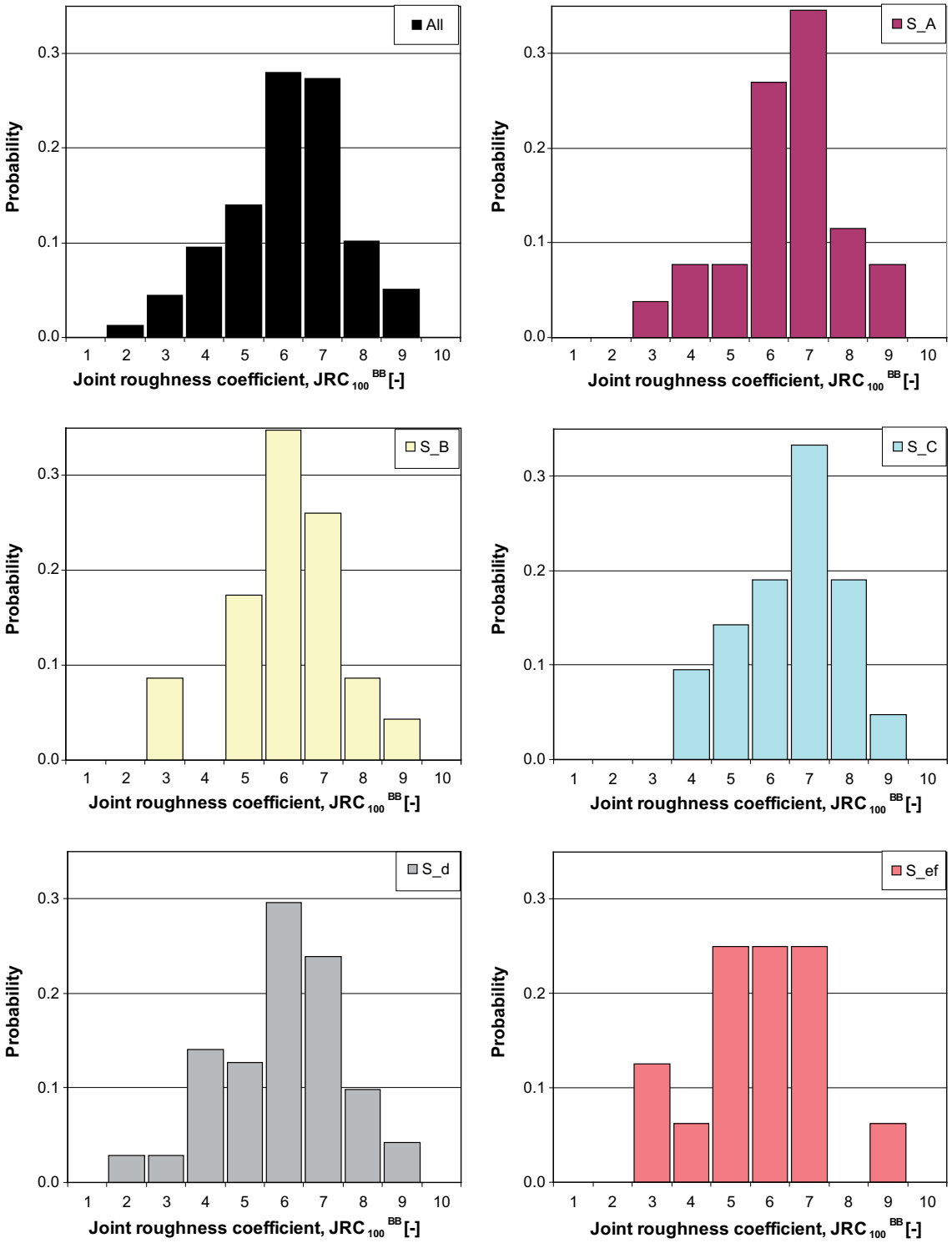

Barton-Bandis' joint roughness coefficient JRC_{100} for all Tilt data. The fractures are grouped into fracture sets.

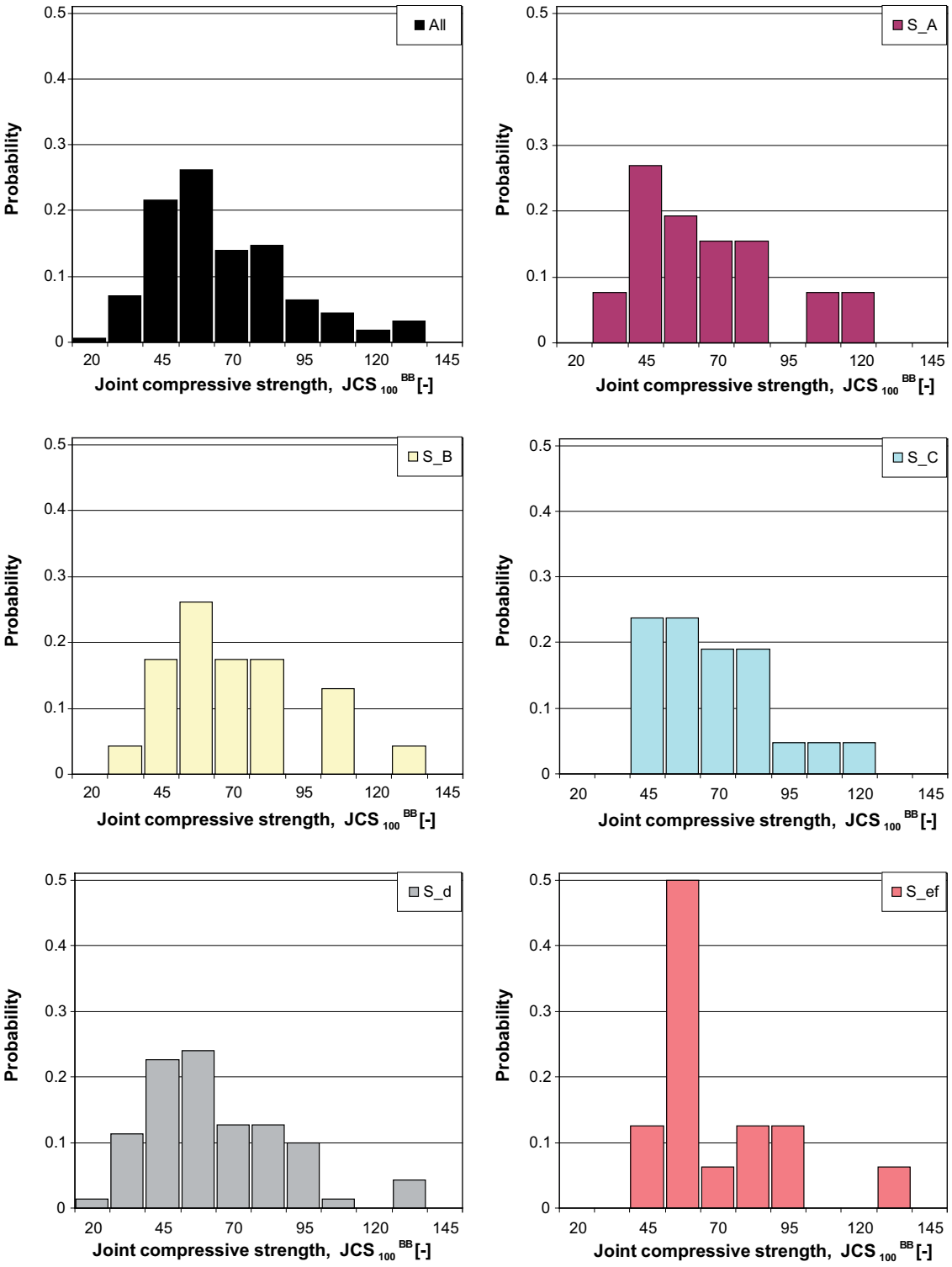

A.2.5 Tilt tests – Variation with depth of the Mohr-Coulomb's parameters

Peak and residual values for cohesion and friction angle from tilt tests. The fractures are grouped per fracture sets.

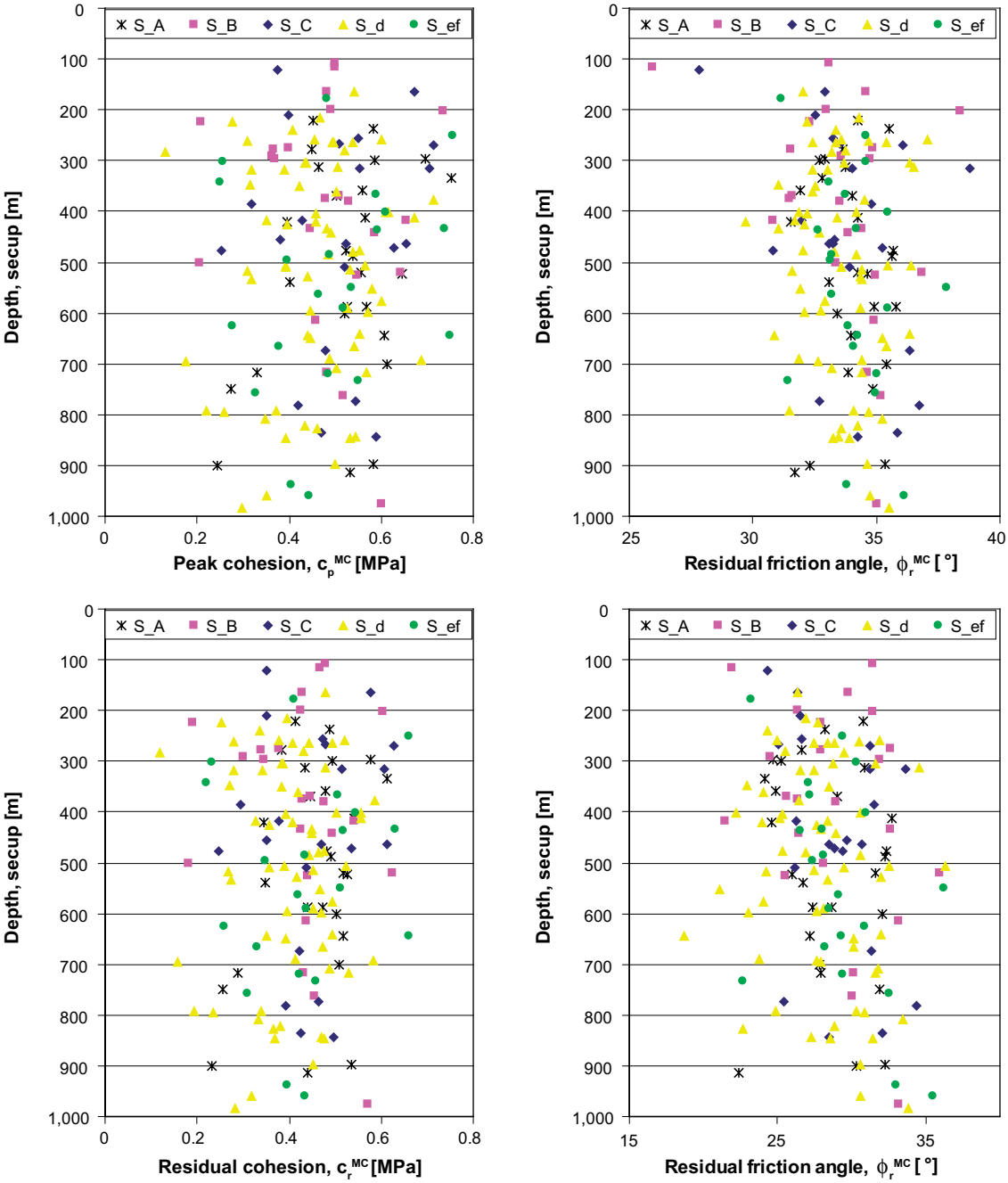

A.2.6 Shear tests – Variation with depth of the Mohr-Coulomb's parameters

Peak and residual values for cohesion and friction angle from shear tests. The data are grouped per test method.

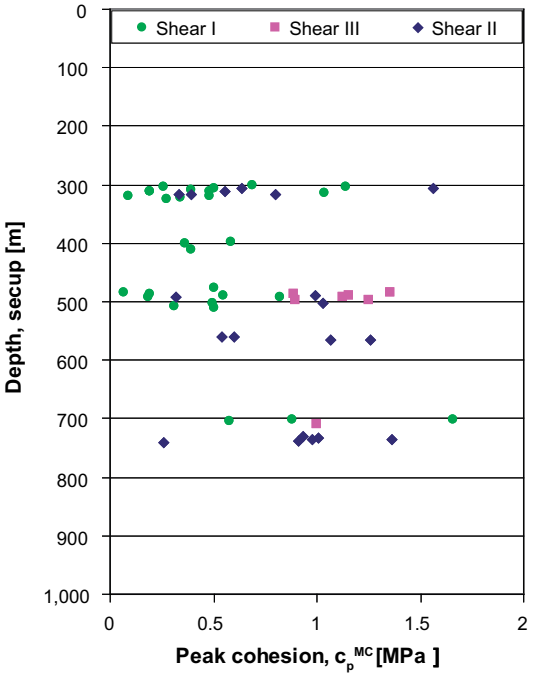

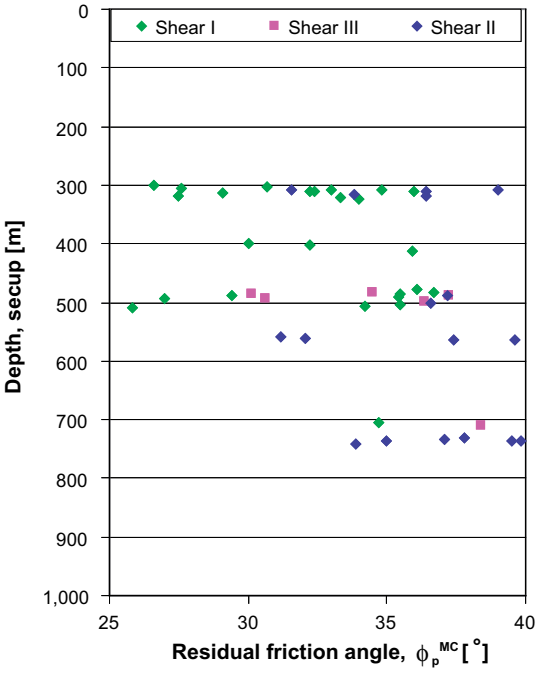

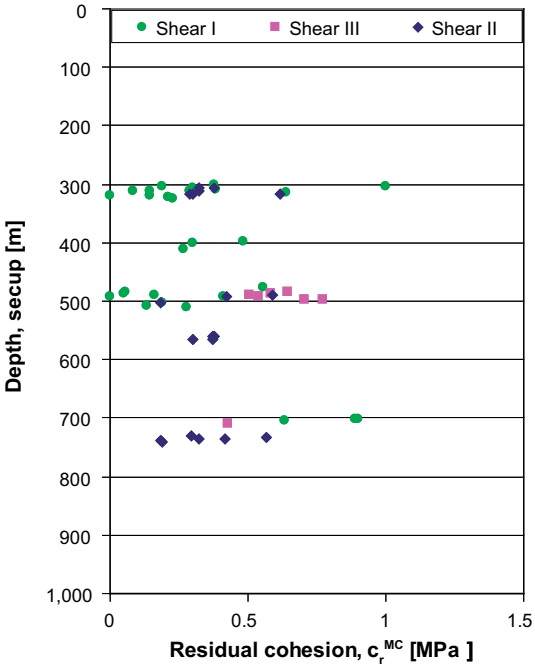

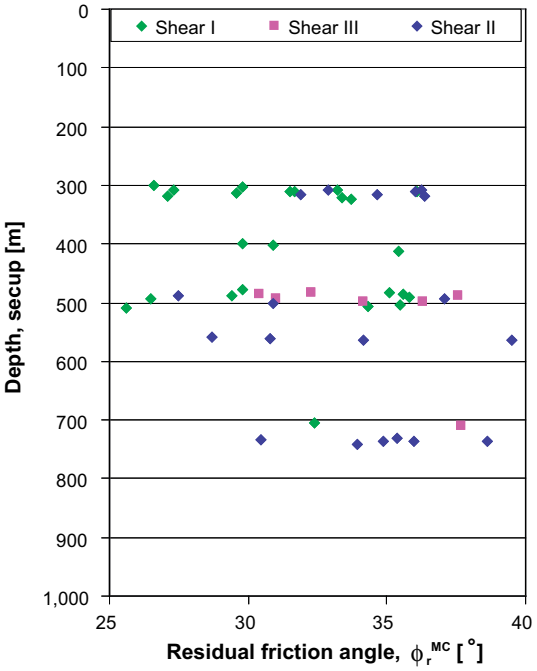

A.2.7 Shear tests – Variation with depth of the normal and shear stiffness

Fracture normal and shear stiffness, derived from normal loading and shear tests. The data are grouped per test method.

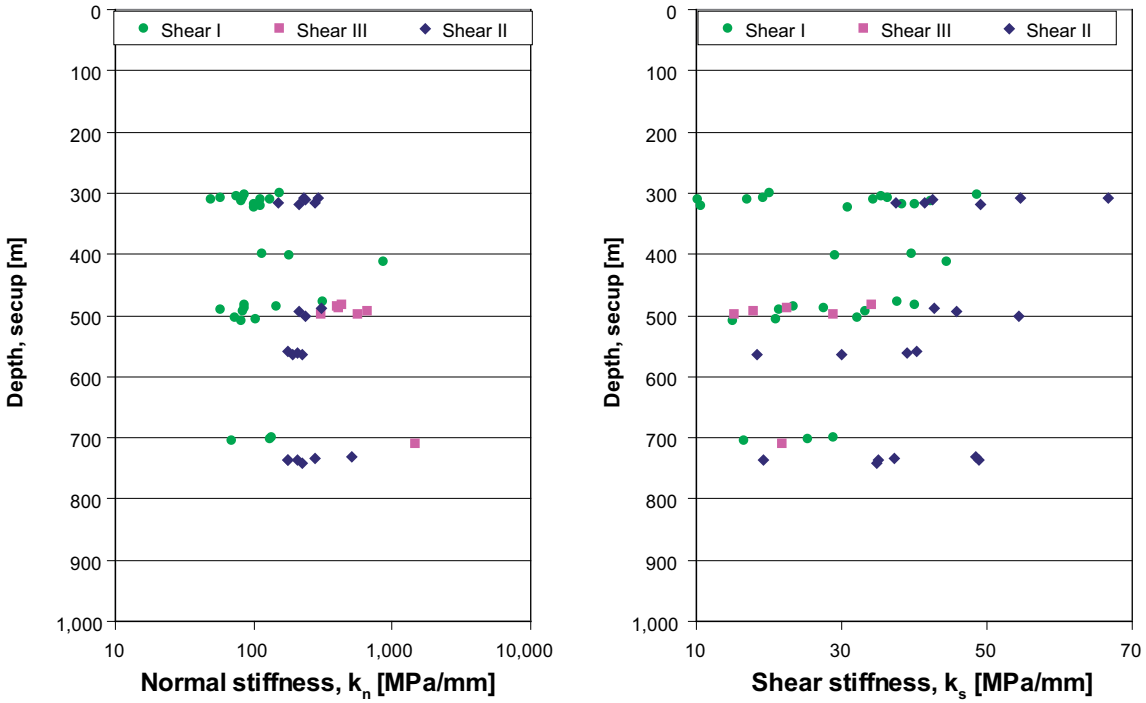

A.2.8 Shear I (SP Laboratory, cement casting) – Coulomb's parameters and stiffness from normal load and shear tests

Mechanical properties of fractures evaluated from laboratory tests (boreholes KAV01, KSH01A, and KSH02A).

Test sample	Peak cohesion c_p^{MC} [MPa]	Peak friction angle φ_p^{MC} [°]	Residual cohesion c_p^{MC} [MPa]	Residual friction angle φ_p^{MC} [°]	Normal stiffness K_n [MPa/mm]	Shear stiffness K_s [MPa/mm]
KSH01A-117-1	0.687	26.6	0.377	26.6	154.5	20.2
KSH01A-117-2	1.138	27.6	1.001	24	75.7	35.6
KSH01A-117-3	0.503	33	0.301	33.2	84.8	36.4
KSH01A-117-4	0.194	32.4	0.085	31.7	113.3	34.4
KSH01A-117-5	0.479	36	0.287	36.1	130.7	17
KSH01A-117-8	0.585	30	0.486	29.8	114.6	39.7
KSH01A-117-9	0.36	32.2	0.299	30.9	179.3	29.1
KSH01A-117-10	0.392	35.9	0.264	35.4	864	44.5
KSH01A-117-12	0.502	36.1	0.557	29.8	317.1	37.7
KSH01A-117-14	0.065	36.7	0.055	35.1	87.1	40.1
KSH01A-117-16	0.193	35.5	0.049	35.6	146.3	23.3
KSH01A-117-18	0.545	29.4	0.163	29.4	85.7	27.6
KSH01A-117-20	0.182	35.4	0	35.8	57.7	21.5
KSH01A-117-22	0.825	27	0.41	26.5	83.6	33.2
KSH01A-117-25	0.881	24.4	0.889	21.5	135.6	29
KSH01A-117-26	1.657	23.9	0.902	21.7	130.3	25.3
KSH01A-117-27	0.58	34.7	0.636	32.4	69.9	16.5

Test sample	Peak cohesion c_p^{MC} [MPa]	Peak friction angle φ_p^{MC} [°]	Residual cohesion c_p^{MC} [MPa]	Residual friction angle φ_p^{MC} [°]	Normal stiffness K_n [MPa/mm]	Shear stiffness K_s [MPa/mm]
KSH02A-117-1	0.19	32.2	0.145	31.5	49.2	10.3
KSH02A-117-2	1.035	29.1	0.637	29.6	80.9	42.3
KSH02A-117-4	0.091	40.7	0	40.9	109.4	40
KSH02A-117-5	0.483	27.5	0.147	27.1	101.1	38.4
KSH02A-117-6	0.343	33.3	0.212	33.4	113.4	10.6
KSH02A-117-7	0.274	34	0.226	33.7	101.9	30.9
KAV01-117-1	0.26	30.70	0.19	29.80	87	48.7
KAV01-117-2	0.39	34.80	0.38	27.30	57.9	19.3
KAV01-117-3	0.50	35.50	0.19	35.50	72.5	32.1
KAV01-117-4	0.31	34.20	0.14	34.30	102.3	20.9
KAV01-117-5	0.50	25.80	0.28	25.60	80.6	15.1

A.2.9 Shear I (SP Laboratory, cement casting) – Dilation angle from shear tests

Test sample	Dilation angle [°] at normal stress 0.5 MPa	Dilation angle [°] at normal stress 5 MPa	Dilation angle [°] at normal stress 20 MPa
KSH01A-117-1	18.4	3.9	–
KSH01A-117-2	17.7	8.9	–
KSH01A-117-3	18.4	3.3	–
KSH01A-117-4	19.1	–	–
KSH01A-117-5	18.8	3.6	2.4
KSH01A-117-8	12.0	6.9	0.8
KSH01A-117-9	10.5	3.4	1.1
KSH01A-117-10	16.8	3.1	0.2
KSH01A-117-12	18.9	6.6	1.4
KSH01A-117-14	7.9	0.6	1.5
KSH01A-117-16	19.4	1.2	0.2
KSH01A-117-18	23.7	4.7	0.0
KSH01A-117-20	12.5	4.5	2.2
KSH01A-117-22	16.8	4.1	0.0
KSH01A-117-25	15.0	4.9	0.0
KSH01A-117-26	27.0	6.0	0.0
KSH01A-117-27	11.7	3.3	0.3
KSH02A-117-1	6.7	1.5	1.8
KSH02A-117-2	18.0	1.5	0.0
KSH02A-117-4	15.0	5.3	5.2
KSH02A-117-5	16.0	7.3	1.0
KSH02A-117-6	29.4	2.0	1.9
KSH02A-117-7	7.8	0.3	1.2
KAV01-117-1	8.13	0.6	0.5
KAV01-117-2	14.0	3.45	3.6
KAV01-117-3	11.3	6.6	4.0
KAV01-117-4	11.6	2.0	1.0
KAV01-117-5	15.2	2.1	0.6

A.2.10 Shear II (SP Laboratory, epoxy casting) – Coulomb's parameters and stiffness from normal load and shear tests

Mechanical properties of fractures evaluated from laboratory tests (borehole KLX02 and KLX04)

Test sample	Peak cohesion c_p^{MC} [MPa]	Peak friction angle φ_p^{MC} [°]	Residual cohesion c_p^{MC} [MPa]	Residual friction angle φ_p^{MC} [°]	Normal stiffness K_n [MPa/mm]	Shear stiffness K_s [MPa/mm]
KLX04-117-1	1.56	31.54	0.32	32.90	288.64	54.51
KLX04-117-2	0.63	38.98	0.38	36.25	227.04	66.62
KLX04-117-5	0.56	36.43	0.32	36.04	235.88	42.57
KLX04-117-7	0.60	31.18	0.37	28.68	176.52	40.37
KLX04-117-8	0.54	32.07	0.38	30.80	204.52	39.08
KLX04-117-9	1.26	37.39	0.30	34.14	224.38	29.98
KLX04-117-10	1.07	39.59	0.37	39.50	191.25	18.30
KLX04-117-11	0.93	37.82	0.29	35.37	513.68	48.40
KLX04-117-13	1.01	37.08	0.56	30.46	276.86	37.32
KLX04-117-12	1.36	34.96	0.42	35.97	175.58	19.30
KLX02-117-1	0.33	33.80	0.30	31.89	274.07	37.50
KLX02-117-2	0.80	40.60	0.62	34.67	150.13	41.34
KLX02-117-3	0.40	36.42	0.29	36.34	211.30	49.16
KLX02-117-4	1.00	37.20	0.59	27.49	305.29	42.65
KLX02-117-5	0.32	40.83	0.42	37.09	213.14	45.75
KLX02-117-6	1.03	36.57	0.18	30.89	235.59	54.30
KLX02-117-8	0.98	39.83	0.32	34.86	204.06	35.10
KLX02-117-9	0.91	39.49	0.18	38.60	175.96	48.95
KLX02-117-10	0.26	33.87	0.19	33.92	224.63	34.81

A.2.11 Shear II (SP Laboratory, epoxy casting) – Dilation angle from shear tests

Test sample	Dilation angle [°] at normal stress 0.5 MPa	Dilation angle [°] at normal stress 5 MPa	Dilation angle [°] at normal stress 20 MPa
KLX04-117-1	28.9	9.6	3.2
KLX04-117-2	21.1	7.6	3.7
KLX04-117-5	13.9	9.8	2.4
KLX04-117-7	11.24	5.3	2.0
KLX04-117-8	8.3	4.1	0.7
KLX04-117-9	19.0	1.2	3.4
KLX04-117-10	19.3	11.3	3.1
KLX04-117-11	21.3	15.5	9.3
KLX04-117-13	24.5	11.9	2.1
KLX04-117-12	24.1	13.8	7.8
KLX02-117-1	4.4	5.5	3.8
KLX02-117-2	19.4	12.4	6.5
KLX02-117-3	5.9	3.5	1.7

Test sample	Dilation angle [°] at normal stress 0.5 MPa	Dilation angle [°] at normal stress 5 MPa	Dilation angle [°] at normal stress 20 MPa
KLX02-117-4	19.7	10.1	4.9
KLX02-117-5	3.6	7.0	4.8
KLX02-117-6	12.9	8.0	4.9
KLX02-117-8	19.1	11.8	6.0
KLX02-117-9	19.8	8.4	3.2
KLX02-117-10	5.5	3.7	2.4

A.2.12 Shear III (NGI Laboratory, epoxy casting) – Coulomb's parameters and stiffness from normal load and shear tests

Mechanical properties of fractures evaluated from laboratory tests (borehole KSH01A)

Test sample	Peak cohesion c_p^{MC} [MPa]	Peak friction angle φ_p^{MC} [°]	Residual cohesion c_p^{MC} [MPa]	Residual friction angle φ_p^{MC} [°]	Normal stiffness K_n [MPa/mm]	Shear stiffness K_s [MPa/mm]
KSH01A-117-28	0.9973	38.38	0.4271	37.69	1,461.2	21.9
KSH01A-117-13	1.358	34.48	0.646	32.29	431	34.1
KSH01A-117-15	0.89	30.15	0.585	30.42	406.7	7.7
KSH01A-117-17	1.158	37.24	0.503	37.6	413.6	22.6
KSH01A-117-19	1.124	30.63	0.537	31.01	663	17.9
KSH01A-117-21	1.25	36.37	0.708	34.15	310.9	15.3
KSH01A-117-23	0.896	40.29	0.771	36.31	568.9	28.9

A.2.13 Tilt test data (NGI Laboratory) – Coulomb's parameters

Mechanical properties of fractures evaluated from laboratory tests (borehole KAV01)

Borehole	Secup (unadjusted)	Peak cohesion c_p^{MC} [MPa]	Peak friction angle φ_p^{MC} [°]	Residual cohesion c_p^{MC} [MPa]	Residual friction angle φ_p^{MC} [°]	Fracture set
KAV01	198.637	0.491	32.96	0.424	26.37	B
KAV01	210.977	0.399	32.51	0.35	26.52	C
KAV01	223.325	0.209	32.32	0.19	27.93	B
KAV01	224.121	0.278	32.22	0.253	27.73	d
KAV01	254.841	0.549	33.24	0.472	26.65	C
KAV01	277.069	0.365	31.55	0.338	27.95	B
KAV01	295.383	0.696	32.89	0.577	24.73	A
KAV01	297.923	0.585	32.67	0.495	25.2	A
KAV01	373.847	0.48	31.5	0.429	26.31	B
KAV01	312.815	0.464	33.77	0.433	30.87	A
KAV01	411.733	0.565	34.26	0.542	32.67	A
KAV01	357.221	0.558	31.92	0.479	24.84	A
KAV01	436.089	0.593	32.65	0.516	26.57	e
KAV01	416.767	0.35	31.69	0.326	28.4	d
KAV01	464.275	0.655	33.23	0.613	30.64	C

Borehole	Secup (unadjusted)	Peak cohesion c_p^{MC} [MPa]	Peak friction angle φ_p^{MC} [°]	Residual cohesion c_p^{MC} [MPa]	Residual friction angle φ_p^{MC} [°]	Fracture set
KAV01	434.624	0.481	31.03	0.449	27.93	d
KAV01	520.173	0.555	34.26	0.518	31.57	A
KAV01	476.288	0.254	30.8	0.246	29.4	C
KAV01	564.191	0.463	33.21	0.42	29.12	e
KAV01	516.820	0.31	31.56	0.268	24.27	d
KAV01	602.269	0.52	33.42	0.502	32.03	A
KAV01	577.760	0.602	32.89	0.495	24.03	d
KAV01	643.283	0.75	34.26	0.66	29.29	e
KAV01	625.830	0.277	33.83	0.258	30.84	e
KAV01	716.899	0.567	34.4	0.528	31.6	d
KAV01	710.070	0.504	33.19	0.487	31.8	d

Mechanical properties of fractures evaluated from laboratory tests (borehole KLX02)

Borehole	Secup (unadjusted)	Peak cohesion c_p^{MC} [MPa]	Peak friction angle φ_p^{MC} [°]	Residual cohesion c_p^{MC} [MPa]	Residual friction angle φ_p^{MC} [°]	Fracture set
KLX02	249.509	0.754	34.6	0.66	29.43	f
KLX02	263.279	0.537	32.43	0.493	28.84	d
KLX02	334.677	0.753	32.81	0.613	24.16	A
KLX02	300.767	0.257	34.55	0.233	30.35	f
KLX02	366.251	0.589	33.74	0.505	27.17	f
KLX02	402.149	0.615	31.88	0.502	22.22	d
KLX02	441.827	0.587	33.84	0.495	26.47	B
KLX02	413.051	0.672	33.41	0.556	25.15	d
KLX02	472.459	0.628	35.23	0.535	28.85	C
KLX02	487.360	0.537	35.62	0.491	32.23	A
KLX02	540.303	0.4	33.09	0.347	26.7	A
KLX02	521.869	0.646	34.61	0.526	25.94	A
KLX02	615.733	0.458	34.9	0.438	33.2	B
KLX02	598.041	0.57	32.1	0.47	23.02	d
KLX02	665.916	0.379	34.07	0.331	28.17	f
KLX02	720.600	0.485	35.02	0.423	29.43	f
KLX02	700.233	0.613	35.41	0.509	27.83	A
KLX02	758.498	0.327	34.95	0.308	32.56	f
KLX02	772.851	0.544	32.68	0.463	25.4	C
KLX02	821.599	0.434	34.27	0.382	28.88	d
KLX02	914.417	0.533	31.68	0.44	22.41	A
KLX02	844.623	0.588	34.24	0.498	28.46	C
KLX02	975.635	0.602	35.03	0.572	33.13	B
KLX02	936.741	0.403	33.82	0.395	33.02	F

Mechanical properties of fractures evaluated from laboratory tests (borehole KLX04)

Borehole	Secup (unadjusted)	Peak cohesion c_p^{MC} [MPa]	Peak friction angle φ_p^{MC} [°]	Residual cohesion c_p^{MC} [MPa]	Residual friction angle φ_p^{MC} [°]	Fracture set
KLX04	236.791	0.583	35.5	0.487	28.22	A
KLX04	257.961	0.456	33.6	0.377	24.92	d
KLX04	239.249	0.407	33.35	0.336	24.36	d
KLX04	267.459	0.508	33.54	0.479	25.06	C
KLX04	314.644	0.552	34.01	0.515	31.22	C
KLX04	281.840	0.13	33.18	0.12	29.48	d
KLX04	268.975	0.713	36.05	0.627	31.27	C
KLX04	343.353	0.25	33.07	0.22	27.07	f
KLX04	348.124	0.315	31.02	0.27	22.93	d
KLX04	400.311	0.61	35.45	0.543	30.97	f
KLX04	404.687	0.457	32.2	0.394	25.31	d
KLX04	425.599	0.395	32.1	0.358	27.6	d
KLX04	464.275	0.523	33.06	0.469	28.47	C
KLX04	500.152	0.204	33.37	0.182	28.07	B
KLX04	527.120	0.441	34.38	0.415	31.98	d
KLX04	509.152	0.521	33.9	0.436	26.12	C
KLX04	552.708	0.581	31.92	0.466	21.06	d
KLX04	591.299	0.526	34.35	0.453	28.06	d

Mechanical properties of fractures evaluated from laboratory tests (borehole KSH01)

Borehole	Secup (unadjusted)	Peak cohesion c_p^{MC} [MPa]	Peak friction angle φ_p^{MC} [°]	Residual cohesion c_p^{MC} [MPa]	Residual friction angle φ_p^{MC} [°]	Fracture set
KSH01A	115.621	0.501	25.92	0.466	21.93	B
KSH01A	107.911	0.499	33.09	0.478	31.4	B
KSH01A	122.209	0.374	27.82	0.35	24.32	C
KSH01A	165.347	0.673	32.92	0.577	26.35	C
KSH01A	164.816	0.482	34.59	0.429	29.8	B
KSH01A	165.531	0.542	32.04	0.478	26.36	d
KSH01A	178.449	0.482	31.12	0.411	23.24	e
KSH01A	221.601	0.451	34.24	0.414	30.75	A
KSH01A	216.176	0.468	34.32	0.395	26.93	d
KSH01A	201.988	0.735	38.42	0.604	31.46	B
KSH01A	259.451	0.6	37.09	0.521	31.91	d
KSH01A	261.769	0.31	34.67	0.281	30.48	d
KSH01A	262.924	0.493	35.43	0.407	27.45	d
KSH01A	317.628	0.389	33.03	0.343	27.44	d
KSH01A	304.711	0.433	36.37	0.383	31.58	d
KSH01A	317.787	0.318	32.43	0.281	26.53	d
KSH01A	349.441	0.421	32.53	0.384	28.44	d
KSH01A	385.543	0.319	34.79	0.294	31.5	C
KSH01A	376.607	0.713	34.52	0.587	26.46	d

Borehole	Secup (unadjusted)	Peak cohesion c_p^{MC} [MPa]	Peak friction angle φ_p^{MC} [°]	Residual cohesion c_p^{MC} [MPa]	Residual friction angle φ_p^{MC} [°]	Fracture set
KSH01A	380.569	0.53	33.53	0.475	28.94	B
KSH01A	441.683	0.49	32.69	0.448	28.9	d
KSH01A	421.516	0.397	31.53	0.344	24.64	A
KSH01A	401.653	0.609	34.21	0.556	30.63	d
KSH01A	433.122	0.446	34.39	0.426	32.59	B
KSH01A	485.083	0.488	33.21	0.433	28.12	e
KSH01A	433.454	0.737	34.19	0.631	28.03	e
KSH01A	549.724	0.535	37.82	0.511	36.23	e
KSH01A	515.276	0.533	34.39	0.452	27.41	d
KSH01A	454.798	0.381	33.28	0.35	29.69	C
KSH01A	650.259	0.447	35.24	0.394	30.15	d
KSH01A	595.955	0.445	32.73	0.397	27.64	d
KSH01A	480.080	0.539	33.28	0.465	26.9	d
KSH01A	672.612	0.479	36.32	0.421	31.33	C
KSH01A	665.882	0.54	35.41	0.472	30.12	d
KSH01A	507.603	0.564	35.45	0.522	32.56	d
KSH01A	781.407	0.419	36.75	0.392	34.35	C
KSH01A	761.963	0.516	35.16	0.455	30.08	B
KSH01A	749.537	0.274	34.85	0.255	31.85	A
KSH01A	807.572	0.348	35.22	0.332	33.42	d
KSH01A	827.512	0.46	33.57	0.366	22.69	d
KSH01A	836.562	0.469	35.84	0.425	32.05	C

Mechanical properties of fractures evaluated from laboratory tests (borehole KSH02A)

Borehole	Secup (unadjusted)	Peak cohesion c_p^{MC} [MPa]	Peak friction angle φ_p^{MC} [°]	Residual cohesion c_p^{MC} [MPa]	Residual friction angle φ_p^{MC} [°]	Fracture set
KSH02A	273.628	0.398	34.85	0.377	32.65	B
KSH02A	291.463	0.363	33.56	0.3	24.47	B
KSH02A	263.901	0.496	33.35	0.442	28.36	d
KSH02A	277.450	0.449	33.66	0.383	26.58	A
KSH02A	297.748	0.368	34.72	0.344	31.92	B
KSH02A	280.510	0.52	33.76	0.432	25.48	d
KSH02A	315.090	0.706	38.8	0.607	33.62	C
KSH02A	311.340	0.506	36.53	0.479	34.54	d
KSH02A	303.830	0.436	33.71	0.388	28.72	d
KSH02A	368.185	0.508	31.61	0.446	25.63	B
KSH02A	369.665	0.503	34.01	0.446	29.02	A
KSH02A	360.500	0.502	32.43	0.42	24.05	d
KSH02A	419.125	0.654	30.81	0.54	21.45	B
KSH02A	418.972	0.429	31.96	0.379	26.27	C
KSH02A	420.970	0.458	29.72	0.408	23.94	d
KSH02A	495.342	0.397	33.11	0.349	27.32	e

Borehole	Secup (unadjusted)	Peak cohesion c_p^{MC} [MPa]	Peak friction angle φ_p^{MC} [°]	Residual cohesion c_p^{MC} [MPa]	Residual friction angle φ_p^{MC} [°]	Fracture set
KSH02A	507.669	0.392	36.39	0.391	36.29	d
KSH02A	478.082	0.552	32.05	0.477	25.37	d
KSH02A	478.379	0.524	35.66	0.481	32.37	A
KSH02A	485.621	0.484	34.17	0.443	30.58	d
KSH02A	509.800	0.393	33.56	0.357	29.47	d
KSH02A	519.278	0.642	36.85	0.626	35.96	B
KSH02A	525.315	0.548	34.96	0.44	25.49	B
KSH02A	533.860	0.319	34.39	0.274	28.34	d
KSH02A	587.341	0.527	35.81	0.441	28.62	A
KSH02A	587.341	0.568	34.9	0.474	27.32	A
KSH02A	590.162	0.517	35.47	0.436	28.49	e
KSH02A	642.081	0.554	36.33	0.493	31.94	d
KSH02A	645.128	0.608	33.97	0.517	27.19	A
KSH02A	642.910	0.439	30.87	0.351	18.69	d
KSH02A	691.615	0.688	34.41	0.582	27.64	d
KSH02A	689.639	0.488	31.86	0.412	23.78	d
KSH02A	695.091	0.175	32.63	0.158	27.94	d
KSH02A	732.274	0.549	31.4	0.458	22.63	e
KSH02A	716.535	0.329	33.88	0.287	27.89	A
KSH02A	716.285	0.482	34.61	0.431	30.12	B
KSH02A	792.309	0.372	34.07	0.34	30.27	d
KSH02A	791.475	0.22	31.49	0.193	24.89	d
KSH02A	794.140	0.258	34.71	0.236	30.91	d
KSH02A	845.115	0.533	33.23	0.477	28.55	d
KSH02A	844.070	0.543	33.46	0.47	27.28	d
KSH02A	845.385	0.392	33.93	0.369	31.44	d
KSH02A	896.688	0.582	35.34	0.536	32.25	A
KSH02A	897.303	0.5	34.61	0.453	30.62	d
KSH02A	899.787	0.244	32.31	0.233	30.31	A
KSH02A	959.621	0.352	34.76	0.318	30.57	d
KSH02A	960.762	0.442	36.11	0.435	35.51	e
KSH02A	983.210	0.296	35.54	0.284	33.84	d

A.2.14 Fracture set orientations

A detailed description of the derivation process for fracture sets is presented in /Hermansson et al. 2005/. The following tables summarize the chosen SDM Laxemar 1.2 fracture orientation model. These sets are based solely on univariate Fisher spherical probability distributions, and represent the ‘best fit’ to observed stereonet patterns. The distribution parameters were produced by entering amalgamated data from all outcrops in a particular subarea, applying a hard-sectored set division, and recording the results.

Table A2-1. Laxemar fracture set orientations. From /Hermansson et al. 2005/.

Set Name	Orientation Model	Mean Pole Trend	Mean Pole Plunge	Distribution Details Dispersion	Distribution Details Relative Intensity	Number of Fractures	K-S Statistic	% Significance
S_A	Univariate Fisher	338.1	4.5	13.06	28.28%	593	0.031	55.60%
S_B	Univariate Fisher	100.4	0.2	19.62	26.90%	564	0.058	10.70%
S_C	Univariate Fisher	212.9	0.9	10.46	29.47%	618	0.076	15.70%
S_d	Univariate Fisher	3.3	62.1	10.13	9.63%	202	0.021	99.70%
S_f	Univariate Fisher	243	24.4	23.52	5.72%	120	0.216	Not Significant

Table A2-2. Simpevarp fracture set orientations. From /Hermansson et al. 2005/.

Set Name	Orientation Model	Mean Pole Trend	Mean Pole Plunge	Distribution Details Dispersion	Distribution Details Relative Intensity	Number of Fractures	K-S Statistic	% Significance
S_A	Univariate Fisher	330.3	6.1	16.8	30.33%	1,190	0.091	Not Significant
S_B	Univariate Fisher	284.6	0.6	10.78	18.30%	718	0.076	0.02%
S_C	Univariate Fisher	201.8	3.7	14.6	31.12%	1,221	0.043	5.20%
S_d	Univariate Fisher	84.6	81.8	6.98	8.28%	325	0.053	6.90%
S_e	Univariate Fisher	67.1	15.5	11.73	11.98%	470	0.105	0.00%